United States Nuclear Regulatory Commission

Protecting People and the Environment

NUREG/CR-6988

Final Report — Evaluation of Chemical Effects Phenomena in Post-LOCA Coolant

Office of Nuclear Regulatory Research

This page intentionally left blank.

United States Nuclear Regulatory Commission

Protecting People and the Environment

NUREG/CR-6988

Final Report — Evaluation of Chemical Effects Phenomena in Post-LOCA Coolant

Manuscript Completed: December 2008
Date Published: March 2009

Prepared by
C.H. Delegard[1], M.R. Elmore[1], K.J. Geelhood[1], M.A. Lilga[1],
W.G. Luscher[1], G.T. MacLean[2], J.K. Magnuson[1], R.T. Pagh[1],
S.G. Pitman[1] and R.S. Wittman[1]

[1]Pacific Northwest National Laboratory
902 Battelle Boulevard
Richland, WA 99352

[2]Fluor Federal Services
120 Jadwin Avenue
Richland, WA 99352-3448

J.P. Burke, NRC Project Manager

NRC Job Code N6381

Office of Nuclear Regulatory Research

This page intentionally left blank.

ABSTRACT

During a loss-of-coolant accident (LOCA) in a pressurized water reactor (PWR), the integrity of the reactor coolant system is abruptly lost through a breach of the system pressure boundary. Remedial actions initiated automatically to limit the damage from the accident include 1) actuation of the containment spray system (CSS) for most plants to maintain containment building pressure below pre-established set points to prevent building damage and to scrub radioiodine from the containment air (minimizing offsite doses) and 2) actuation of the emergency core cooling system (ECCS) to provide an emergency supply of borated water from the refueling water storage tank to the core for cooling and to maintain the core subcritical. The reactor coolant, containment spray, and borated water injected by the ECCS drain to the floor of the containment building are collected by the recirculation sump with debris generated by the LOCA and latent debris pre-existing in the wetted parts of the containment building. Ultimately, the collected water is pumped from the sump, through a heat exchanger, into the reactor pressure vessel, and typically also, just after the rupture, through the containment spray nozzles in a recirculation loop. The recirculation flow encounters the sump strainer where solids may accumulate to block coolant flow or be ingested into the pump suction line to potentially damage the pump, irradiated fuel in the core, or other structures.

The Nuclear Regulatory Commission established Generic Safety Issue 191, “Assessment of Debris Accumulation on PWR Sump Performance”, to evaluate the effects of post-LOCA debris on the performance of the ECCS and CSS in recirculation mode at PWRs. Experimental testing and other studies have been completed to determine the impacts of cooling water composition, debris sources, and materials corrosion on the nature of the debris, presuming no fuel cladding failure. However, historical, ongoing, and planned testing and analysis studies were evaluated, and 10 further topics related to chemical effects were identified that deserve additional consideration.

The 10 topical areas are radiation effects (particularly on material corrosion), differences in concrete carbonation between tested systems and existing containment structures, effects of alloy variability between tested and actual materials, galvanic corrosion effects, biological fouling, co-precipitation, and other synergistic solids formation effects, inorganic agglomeration, crud release effects (types and quantities), retrograde solubility and solids deposition, and organic material impacts. Sufficient data or prior related studies were available to sufficiently address some of the questions raised in the 10 topic areas. However, within these 10 broad areas, topics meriting additional consideration also were identified and are the focus of this report.

The topic with the greatest perceived influence on ECCS performance is the interactions of organic materials (lubricants and coatings) with inorganic solids. The effects of radiolysis on redox potential and thus metal corrosion have the next most influence. Of similar influence are the effects of biological growth in the post-LOCA system and the impacts of dried borate salts on hot fuel cladding and reactor pressure vessel materials. Of lesser, but not insignificant, influence are galvanic corrosion, inorganic agglomeration, and crud release effects on increasing and altering solids delivered to the post-LOCA coolant. Changes in concrete carbonation and differences in alloy corrosion rates were judged to have minor impacts on ECCS functionality.

This page intentionally left blank.

FOREWORD

NRC Generic Letter 2004-02, "Potential Impact of Debris Blockage on Emergency Recirculation During Design Basis Accidents at Pressurized-Water Reactors" (GL), was issued in 2004. It requested pressurized-water reactor (PWR) licensees to perform an evaluation of the emergency core cooling system (ECCS) and containment spray system (CSS) recirculation functions in light of the information provided in the GL and, if appropriate, take additional actions to verify system functionality. It stated in part that "In addition to debris generated by jet forces from the pipe rupture, debris could be created by the chemical reaction between the materials in containment and the chemically reactive spray solutions used following a LOCA. These reactions might generate additional debris such as disbonded coatings and chemical precipitants." The Office of Nuclear Regulatory Research (RES) has sponsored several research activities to assess the potential significance of chemical effects on ECCS functionality as documented in Research Information Letter-0701.

The assessment of chemical effects on ECCS functionality has proven to be quite complex. Recognizing this complexity, RES conducted a phenomena identification and ranking table (PIRT) exercise in 2006 to provide a comprehensive evaluation of possible chemical effects in a post-LOCA containment environment. The PIRT was primarily focused on identifying phenomena that both may potentially affect ECCS functionality and also were not well understood within the context of the post-LOCA environment in light of recent and ongoing NRC and industry-sponsored research. The PIRT process first identified over 100 phenomena, 41 of which were judged to be highly significant by at least one PIRT team member. The staff then evaluated these 41 phenomena, and identified approximately 16 of these issues that are potentially deleterious to ECCS performance and merited additional analysis by the NRC to understand their significance. These issues were combined into the following 10 distinct topics: radiological effects, concrete carbonation, alloy corrosion, galvanic corrosion, biological fouling, co-precipitation and other synergistic phenomena, inorganic agglomeration, crud effects, retrograde solubility and solids deposition, and organic materials. These topics were further evaluated, as summarized in this report, using information available in the literature and by performing conservative calculations as appropriate. This more detailed evaluation identified several phenomena with knowledge gaps that could be studied further to have a more realistic understanding of ECCS performance following a LOCA. The phenomena evaluated in this report with the highest potential significance include synergistic solids formation between organics and inorganic solids, radiolytical effects, biological effects, and retrograde solubility. These effects are also highly plant-specific, and their significance is a function of parameters such as pH buffer, aluminum concentrations, insulation materials, containment cleanliness, quantity of unqualified coatings, and sump strainer submergence.

It is recognized that the licensees' evaluations of chemical effects in response to GL 2004-02 do not explicitly address the issues identified for additional consideration in this report. The licensee evaluations are intended to be simplified, yet conservative. Therefore, NRC staff plans to assess the impact of these remaining issues on ECCS performance. As part of this assessment, NRC staff will consider, as appropriate, plant-specific post-LOCA environments and conditions, results from additional vendor testing conducted since the conclusion of this scoping study, and additional evaluation to characterize the significance of these remaining issues with respect to the principal factors (e.g., particulate, chemical, and fiber concentrations) and conservatism that licensees have used to address GL 2004-02. The staff will document the disposition of these remaining issues upon completion of this assessment.

This page intentionally left blank.

TABLE OF CONTENTS

ABSTRACT iii

FOREWORD v

EXECUTIVE SUMMARY xi

ACKNOWLEDGMENTS xvii

ABBREVIATIONS AND ACRONYMS xix

1 INTRODUCTION 1

2 OVERVIEW OF THE 10 TOPICS OF STUDY IDENTIFIED IN THE PIRT 5

3 TOPIC 1—RADIATION EFFECTS 7

- **3.1** Solute Radiolysis Phenomena 8
- **3.2** Formation of H_2O_2 9
- **3.3** Formation of ClO_3^-, ClO^-, and HOCl 10
- **3.4** Formation of HNO_3 13
- **3.5** Formation of H^+ and H_2 13
- **3.6** Radiolysis of Sodium Metaborate 14
- **3.7** Mixed Potential Effects 14
- **3.8** Radiolysis of Solid Species 15
  - **3.8.1** Solid Silica Precipitates 16
  - **3.8.2** Degradation of Insulation Debris 17
- **3.9** Conclusions and Issues for Further Research 17

4 TOPIC 2—CARBONATION OF CONCRETE 19

- **4.1** Concrete Curing and Aging Chemistry 19
- **4.2** Concrete Carbonation Reactions 20
- **4.3** Measuring the Extent and Rate of Carbonation 21
- **4.4** Carbonation and the ICET Experiments 23
- **4.5** Conclusions 25

5 TOPIC 3—ALLOY CORROSION 27

- **5.1** Materials and Exposed Surfaces in Containment 27
- **5.2** Conditions of Coolant Solution 28
- **5.3** Conclusions 32

6 TOPIC 4—GALVANIC CORROSION 33

- **6.1** Galvanic Corrosion for the Copper–Carbon Steel Couple 33

6.2 Anodic Reversal 34
6.3 Conclusions 34

7 TOPIC 5—BIOLOGICAL FOULING 37
7.1 Biological Stressors 37
7.2 Microorganisms That May Survive in Post-LOCA Conditions 38
7.3 Conclusions 40
7.4 Issues for Further Research 41

8 TOPIC 6—CO-PRECIPITATION OR OTHER SYNERGISTIC SOLIDS FORMATION 43
8.1 Co-Precipitation 43
8.2 Synergistic Interactions of Organic Materials with Inorganic Solids 45
8.3 Conclusions 48

9 TOPIC 7—INORGANIC AGGLOMERATION 49
9.1 Behavior of Inorganic Solids 49
9.2 Organic Effects on Agglomeration 50
9.3 Conclusions 52

10 TOPIC 8—CRUD RELEASE EFFECTS 53
10.1 Introduction 53
10.2 Estimates of Crud Thicknesses 54
10.3 Estimates of Crud Quantities 55
10.3.1 Fuel, Pressure Vessel, Steam Generator, and Piping Surface Areas 56
10.3.2 Suspended and Dissolved Crud 57
10.3.3 Crud Generation Rates 57
10.3.4 Summation of Crud Quantities 58
10.4 Conclusions 60

11 TOPIC 9—RETROGRADE SOLUBILITY AND SOLIDS DEPOSITION 61
11.1 Introduction 61
11.2 Solution Compositions and Model Input 62
11.3 Simulation Results—Below the Boiling Point 64
11.4 Simulation Results—Above the Boiling Point 72
11.5 Conclusions 78

12 TOPIC 10—ORGANIC MATERIAL IMPACTS 81
12.1 Introduction—Coating Application and Failure Modes 81
12.2 Vapor-Phase Processes 82
12.3 Aqueous-Phase Processes 83
12.3.1 Epoxy Coatings 83

12.3.2 Alkyd Coatings 84
12.3.3 Vinyl Coatings 84
12.3.4 Inorganic Zinc Coatings 84
12.4 Coating Particle Transport 85
12.5 Leaching of Organics from Coatings 85
12.6 Estimation of Maximum Leachable Organic Concentration and Radiolysis Rates 87
12.7 Conclusions 89
12.8 Areas for Further Work 89
13 SUMMARY AND RECOMMENDED TOPICS FOR FURTHER EVALUATION 91
14 REFERENCES 95

FIGURES

Figure 1: Oconee Nuclear Station Unit 2 Reactor Building Emergency Sump During the Replacement Strainer Installation (Oconee 2007) 2
Figure 2: Dependence of G Value for ClO_3^- Formation by γ-Radiolysis of NaCl Solution in Water 12
Figure 3: Effects of Polar Organic Absorption Loading on Inorganic Particle Attraction 52
Figure 4: Solids Predicted to Form from ICET #1 Fluids Below Boiling 67
Figure 5: Solids Predicted to Form from ICET #2 Fluids below Boiling 68
Figure 6: Solids Predicted to Form from ICET #3 Fluids Below Boiling 69
Figure 7: Solids Predicted to Form from ICET #4 Fluids Below Boiling 70
Figure 8: Solids Predicted to Form from ICET #5 Fluids Below Boiling 71
Figure 9: Solids Predicted to Form from ICET #1 Fluids above Boiling 72
Figure 10: Solids Predicted to Form from ICET #2 Fluids above Boiling 73
Figure 11: Solids Predicted to Form from ICET #3 Fluids above Boiling 73
Figure 12: Solids Predicted to Form from ICET #4 Fluids above Boiling 74
Figure 13: Solids Predicted to Form from ICET #5 Fluids above Boiling 74
Figure 14: Minor Solids Predicted to Form from ICET #1 Fluids above Boiling 75
Figure 15: Minor Solids Predicted to Form from ICET #2 Fluids above Boiling 75
Figure 16: Minor Solids Predicted to Form from ICET #3 Fluids above Boiling 76

Figure 17: Minor Solids Predicted to Form from ICET #4 Fluids above Boiling 76

Figure 18: Minor Solids Predicted to Form from ICET #5 Fluids above Boiling 77

TABLES

Table S.1: Topic Areas and Objectives in this Study xii

Table S.2: Research Topics, Approach, Findings, and Importance and Recommended Scope of Further Studies xiv

Table 1: Experimental and Expected In-Containment Conditions 11

Table 2: Measured G Values for γ-Radiolysis of 5.3 M NaCl Solution in Water 11

Table 3: Changes in Cement Composition with the Progression of Carbonation 21

Table 4: Comparison of ICET Concrete and Aged Concrete Properties 25

Table 5: Percentage of Surface Areas below Containment Flood Level 28

Table 6: Experimental Conditions in the ICET Tests 29

Table 7: Composition of Precipitates from ICET #1 Results 29

Table 8: Mean Weight Gain/Loss Data for Submerged ICET Coupons 30

Table 9: Corrosion Product Generation Based on Bounding Areas 31

Table 10: PWR Crud Characteristics 54

Table 11: Compounds Added to ICET Cooling Solution 63

Table 12: Components Analyzed in ICET Cooling Solution 63

Table 13: Experimental Conditions in the ICET Tests 63

Table 14: ESP Output for ICET #1 at 140°F 66

Table 15: Water Activity and Activity Coefficients for Soluble Species in Post-LOCA Coolant 79

Table 16: Research Topics, Approach, Findings, and Importance and Recommended Scope of Further Studies 92

EXECUTIVE SUMMARY

During a loss-of-coolant accident (LOCA) in a pressurized water reactor (PWR), the integrity of the reactor coolant system (RCS) is abruptly lost through an opening in the system pressure boundary. Remedial actions initiated automatically to limit the damage from the accident include 1) actuation of the containment spray system (CSS) in most plants to maintain containment building pressure below pre-established set points to prevent building damage and to scrub radioiodine from the containment air (minimizing offsite doses) and 2) actuation of the emergency core cooling system (ECCS) to provide an emergency supply of borated water from the refueling water storage tank (RWST) to the core for cooling and to take the core below criticality. The reactor coolant, containment spray, and borated water injected by the ECCS drain to the floor of the containment building and are collected by the recirculation sump. Debris generated by the LOCA and latent debris washed from the wetted parts of the containment building also are present in the water collected on the floor. Ultimately, the collected water is recirculated from the sump, through a heat exchanger, into the reactor pressure vessel, and typically, just after the breach, through the containment spray nozzles.

The recirculation flow thus has the effect of transporting some of the containment pool debris towards the sump where it may accumulate on the sump strainer or be ingested into the pump suction line. Debris on the sump strainer potentially impedes coolant flow while ingested debris potentially diminishes the functionality of ECCS components downstream of the screen or decreases its capability to transfer heat from the fuel in the reactor core. Screen hole sizes of replacement sump strainers are typically $^{1}/_{12}$ inch (~2 mm) to limit the quantity of downstream solids.

The Nuclear Regulatory Commission (NRC) established Generic Safety Issue 191, "Assessment of Debris Accumulation on PWR Sump Performance", to evaluate the effects of post-LOCA debris on the performance of the ECCS and CSS in recirculation mode at PWRs. Among other actions, experimental testing studies of integrated chemical effects were sponsored by NRC to determine the impacts of cooling water composition, debris types, and materials corrosion on the nature of the debris. In these studies, the fuel itself was presumed to remain intact with no cladding failure.

A team of five independent reviewers then gave critical consideration to the integrated chemical effects and related testing results. The reviewers subsequently worked with NRC in performing a "phenomena-identification-and-ranking-table" (PIRT) exercise to holistically evaluate possible chemical-effect issues that could arise during the post-LOCA time period that may impact ECCS functionality. A particular interest was to identify issues deserving additional consideration to verify that post-LOCA chemical effects have been sufficiently addressed.

The PIRT exercise identified 10 topical areas, particularly as they apply to sump strainer blockage and downstream effects, as meriting further attention in light of findings that had been obtained in the integrated chemical effects or other relevant testing and analysis of chemical effects in post-LOCA conditions. The further evaluation of these topics is the subject of this study. The topic areas and the objectives pursued for this study are summarized in Table S.1.

Table S.1: Topic Areas and Objectives in this Study

Topic	Objectives
Radiation effects	Study the effect of the post-LOCA radiation environment in the reactor vessel, containment pool, and contaminated sump strainer on the containment pool chemical constituents.
Carbonation of concrete	Evaluate the effect of carbonation or other aging processes of concrete on the leaching rates and dissolved species from aged concrete and concrete dust and compare this with research programs that used relatively fresh concrete samples.
Alloy corrosion	Evaluate the effect of material alloy variability on the corrosion rate and dissolved species of important submerged containment pool metals.
Galvanic corrosion	Identify galvanic corrosion effects and specific galvanic configurations that could most significantly alter the amounts and types of chemical byproducts.
Biological fouling	Assess the potential for biological fouling of sump strainers due to bacteria, algal, or other biological growth during the 30-day post-LOCA mission time.
Co-precipitation and other synergistic solids formation	Identify conditions that could significantly promote co-precipitation of chemical species or enable synergistic production of more or different solids than had been considered.
Inorganic agglomeration	Identify conditions affecting inorganic agglomeration in the post-LOCA coolant.
Crud release effects	Evaluate the quantities and chemical/radiation effects related to metal corrosion oxides (crud) within the RCS released during the post-LOCA time period.
Retrograde solubility and solids deposition	Identify likely chemical species and estimate quantities that could precipitate at the reactor core because of retrograde solubility. Also indicate which, if any, preexisting solid chemical species could be deposited onto the reactor fuel.
Organic material impacts	Identify the organic materials that could exist in significant quantities in the post-LOCA containment environment that have the most significant (either beneficial or detrimental) impact on chemical effects within the post-LOCA coolant environment.

NRC engaged Pacific Northwest National Laboratory (PNNL) to evaluate these topics by first summarizing existing relevant information pertaining to these topics and then analyzing this information to address the topic objectives. For most topics, the additional analysis consists of analytical scoping calculations and performance of literature searches to provide sufficient technical rationale to evaluate the issues of significance in the formation of chemical products

and debris that could affect ECCS performance. NRC also tasked PNNL with identifying issues where existing knowledge is insufficient to appropriately address these objectives.

As discussed in the present report, sufficient data or prior related studies were found already to exist to sufficiently address some of the questions raised in the 10 topic areas. In other areas, however, further investigation would allow more confident prediction of their effects. The supplemental investigations may entail continued scrutiny of the abundant technical literature, bench- or engineering-scale laboratory testing, and/or additional modeling.

The areas that will most likely benefit from further evaluation and the scope of the evaluations are summarized in Table S.2. Also given in Table S.2 are qualitative rankings of the perceived importance of the open technical questions. The rankings are given as low, medium, and high in increasing order of their potential impact in adversely affecting ECCS performance. Topics for further study as described in this report have been selected with a conservative (inclusive) bias.

Table S.2: Research Topics, Approach, Findings, and Importance and Recommended Scope of Further Studies

Topic	Approach	Current Findings	Scope of Further Study & Importance Rank
1. Radiation effects	Evaluate coolant water radiolysis to form H_2O_2, ClO_3^-, ClO^-, HOCl, HNO_3, H^+, and H_2 and silica and insulation debris radiolysis for effects on pH and reduction/oxidation (redox) potential.	Radiation effects on pH were found to be minor in comparison with pH buffering. Knowledge of radiation influence on redox potential is limited and complicated by multiple reactions. Assessment of redox effects requires mixed potential modeling.	Mixed potential modeling, similar to that performed for Boiling Water Reactors (BWRs) and perhaps confirmed by experiment, could be used to assess radiolysis effects on redox potential in post-LOCA coolant. *Medium rank*.
2. Carbonation of concrete	Evaluate whether integrated chemical effects testing (ICET) findings would have been affected if aged (more fully carbonated) rather than new (3 to 11 months old) concrete had been used in testing.	The extent of carbonation in the tested concrete coupons are sufficient to have a negligible effect on ICET outcomes compared with outcomes expected had aged coupons been used.	No additional evaluation required.
3. Alloy corrosion	Evaluate whether use of different metal alloys would have affected ICET findings for post-LOCA system.	Aluminum dominated metal corrosion products found in ICET experiments. Variability of aluminum-alloy corrosion behaviors in two different studies and in general overview of aluminum corrosion suggests little change in outcome likely if other aluminum alloys are tested. Other metal alloys were sufficiently evaluated.	Further evaluations of aluminum alloy variation effects are not recommended.
4. Galvanic corrosion	Evaluate whether galvanic corrosion would affect the amounts and types of corrosion products in post-LOCA system.	Galvanic corrosion (between copper and low alloy steel) only affected limited metal surface area to yield negligible additional corrosion product quantities. Anodic reversal at elevated temperature may cause enhanced steel corrosion of limited quantities of galvanized parts.	Additional literature and laboratory evaluation of anodic reversal phenomenon for galvanized steel under post-LOCA conditions could be performed. *Low rank*.
5. Biological fouling	Evaluate whether growth of biota in post-LOCA coolant waters with low-light, low-nutrient, high-boron, high-temperature, and radiation-field stressors may occur, fouling sump strainers.	Many microbes can grow under one or more post-LOCA biological stressors, but growth and rates under stressor combinations are not known. Low light inhibits algal growth. Green flocculent solids found in Three Mile Island waters provide evidence for growth over long periods.	Inoculation tests of various microorganisms under post-LOCA coolant conditions (composition, lighting, temperature, nutrients, inorganic supports) are suggested. If microbes grow, later tests of their interactions with inorganic solids may be considered. *Medium rank*.
6. Co-precipitation and other synergistic solids formation	Determine how co-precipitation, organic complexation, and inorganic/organic agglomeration affect solids formation in the post-LOCA system.	No net effect of solids quantity is anticipated solely from inorganic constituents. Organic complexation is expected to have limited influence because of low complexation strength compared with hydrolysis and the chemical masking afforded by the calcium in post-LOCA waters. Physical interactions akin to organic-mineral-aggregates (e.g., tidal oil spills) are expected of inorganic solids with organic paint and lubricants to mobilize solids to sump strainers. Sump strainer heights	Could increase transportability of solids to sump strainers by interactions between floating organics (lubricants, paint, and plastic decomposition products) and inorganic solids. Consider effects in combination with Topics 7 and 10. *High rank*.

Table S.2: Research Topics, Approach, Findings, and Importance and Recommended Scope of Further Studies

Topic	Approach	Current Findings	Scope of Further Study & Importance Rank
		greater than the upper pool level may allow floating organics to pass through core to undergo radiolysis to CO_2.	
7. Inorganic agglomeration	Predict the roles of soluble organics and their decomposition products on inorganic agglomeration.	The contributions of organics and organic break-down products on inorganic agglomeration are not reliably predicted. The effects likely are small as most of the soluble/miscible organics will pass by water circulation to the core to be destroyed by radiolysis.	Consideration of inorganic agglomeration is best pursued in combination with higher priority issues under Topic 6 on synergistic (inorganic/organic) solids formation and in light of studies under Topic 10 on organic degradation. *Low rank*.
8. Crud release effects	Evaluate the quantities and availabilities of crud from RCS (steam generator tubes and piping), fuel, and core structures.	"Crud burst" conditions of increased oxygen concentration, physical shock, and abruptly altered pH and temperature will prevail in LOCA events, potentially mobilizing crud inventories. Crud solids, mostly from fuel, are projected to be ~1000 kg. Quantities are small compared with cal-sil insulation solids but could be significant for systems with limited particulate.	Crud solids contribute to fine solids loading from other sources [$Al(OH)_3$ from Al corrosion, Ca silicates and phosphates and silica from cal-sil reactions]. *Low rank*.
9. Retrograde solubility and solids deposition	Evaluate effects of retrograde solubility and solids deposition on hot core and fuel structures.	Thermodynamic modeling of ICET solution systems is performed at sub-boiling and above boiling to determine retrograde solubility and salt solids depositions on hot core and fuel structures. Retrograde solubility is observed for calcium-bearing solids, but the effect on solids loading is small because of already low calcium solubilities. Extensive borate salt depositions on fuel or component surfaces above boiling temperatures may be corrosive, based on use of borates as mineral fluxing agents in chemical analysis, will add to the solids load, and may impair heat transfer from the fuel.	High-temperature dried borate salts on pressure vessel and fuel cladding may be corrosive, and their deposition will impair heat transfer from the fuel, increasing cladding temperatures. Further literature or laboratory study (e.g., "evaporation and dry-out" in BWRs) would help determine magnitude of this effect. *Medium rank*.
10. Organic material impacts	Evaluate effects of physical and radiolytic degradation of organic materials from coatings (paints) and from lubricants.	Many paints undergo hydrolytic decomposition and loss of adherence under LOCA and post-LOCA conditions to contribute to load in coolant. Dissolved and suspended organics undergo radiolysis by passing through the core and fuel. Radiolysis is likely sufficient to fully decompose continually recirculating organics to CO_2 within days. Organics floating above sump strainers or retained behind strainers will survive radiolysis and can interact with solids as described in Topics 6 and 7.	Movement of floating organic past sump strainer and fuel/core for radiolytic destruction depends on strainer design. Effects of organics from paints and from lubricants to enhance sump screen loading should be considered in combination with Topics 6 and 7. *High rank*.

This page intentionally left blank.

ACKNOWLEDGMENTS

Input from the NRC and from three external peer reviewers was used to further define the issues and identify key studies in the technical literature. Robert Tregoning of NRC provided overall program guidance and technical information. Technical guidance and project management were provided by Ervin Geiger, Ching Ng, and Atta Istar of NRC. Paul Klein and John Lehning of NRC provided valuable critiques, technical information, and stylistic direction to the report. John Burke of NRC provided expert review of coatings (paints) issues and project management oversight.

The three peer reviewers, John Apps of Lawrence Berkeley National Laboratory (Berkeley, CA), Robert Litman of Radiochemistry Laboratory Basics (Epping, NH), and Digby D. Macdonald of Pennsylvania State University (State College, PA) provided critical review of the text with expertise and supporting information in thermodynamics, radiolysis, reactor operations and processes, and corrosion and materials performance.

This page intentionally left blank.

ABBREVIATIONS AND ACRONYMS

ACRS	Advisory Committee for Reactor Safeguards
AOA	axial offset anomaly
ASTM	American Society for Testing and Materials
BWR	boiling water reactor
BZ	Bromley-Zemaitis; thermodynamic model
cal-sil	calcium silicate
CFR	Code of Federal Regulations
CRDM	control rod drive mechanism
C-S-H	calcium silicate hydrate
CSS	containment spray system
DBA	design basis accident
DOE	U.S. Department of Energy
ECCS	emergency core cooling system
EPA	U.S. Environmental Protection Agency
EPRI	Electric Power Research Institute
ESP	Environmental Simulation Program
GSI	Generic Safety Issue; e.g., GSI-191, “Assessment of Debris Accumulation on PWR Sump Performance”
GWD/MTU	gigawatt-days per metric ton of uranium
HELB	high-energy line break
IAEA	International Atomic Energy Agency
ICET	integrated chemical effects testing
ICP	inductively coupled plasma (spectroscopy)
IOZ	Inorganic zinc
LOCA	loss-of-coolant accident
M	molar; moles/liter
MEK	methyl ethyl ketone
MIBK	methyl isobutyl ketone
MSE	Mixed Solvents Electrolyte; thermodynamic model
NPSH	net positive suction head
NRC	U.S. Nuclear Regulatory Commission
OMA	organic mineral aggregate
PIRT	phenomena identification and ranking table
PNNL	Pacific Northwest National Laboratory
ppb	parts per billion
ppm	parts per million
ppt	parts per trillion
PWR	pressurized water reactor
RCS	reactor coolant system
RMI	reflective metal insulation
RWST	refueling water storage tank
SG	steam generator
SRTC	Savannah River Technical Center
STP	standard temperature and pressure (0°C, 1 atmosphere)
TSP	trisodium phosphate

1 INTRODUCTION

During a loss-of-coolant accident (LOCA) in a pressurized water reactor (PWR), the integrity of the reactor coolant system (RCS) is abruptly lost through an opening in the system pressure boundary. The scenario begins with a high-energy line break (HELB) of the RCS inside the PWR containment. The reactor coolant is a solution of nominally 2,000 parts per million (ppm) boron as boric acid during power operation before the LOCA. The break damages and dislodges nearby materials (e.g., thermal insulation, coatings, and concrete), and some of this debris falls or is washed by the leaking coolant waters to the containment floor. The containment spray system (CSS) in most plants, is actuated to maintain the containment building atmospheric pressure below pre-established set points to prevent building damage and to scrub radioiodine from the air. As a result of this actuation, more of the debris generated by the LOCA is washed to the containment floor. Meanwhile, the emergency core cooling system (ECCS) begins to inject borated water from the refueling water storage tank (RWST) to the core for cooling and to reduce or maintain the neutron flux below core criticality. After passing through the core, this injected water from the RWST exits through the line break where it drains to the containment floor.

Besides the material dislodged in the HELB, the waters from these three sources encounter pre-existing (latent) debris in the containment building. The water drains to the bottom level of the containment building and passes through the sump strainer to reach the sump. After some time, which varies depending on the size of the break (e.g., 20 to 30 minutes for large breaks to hours for smaller breaks), the RWST becomes depleted, and the ECCS pumps switch over from drawing water from the RWST to drawing water from the sump and directing it through a heat exchanger into the reactor pressure vessel and through the reactor core. The ECCS is designed to be effective such that the fuel remains in a coolable geometry. The CSS pumps also may draw water from the containment sump to continue to cool the containment atmosphere and scrub airborne radioactive iodine from the air.

A continuous flow thus is established having the effect of transporting the water laden with the post-LOCA debris towards the sump where the debris encounters the sump strainer and where the debris may accumulate or be ingested into the pump suction line if it is capable of passing through the strainer. An example of one sump strainer design being installed is depicted in Figure 1. Other designs also exist. If debris accumulates on the sump strainer, the increasing head loss across the strainer may cause the net positive suction head (NPSH) to be insufficient for successful operation of the ECCS and CSS pumps.

The depth of the water on the containment floor likely will submerge the top of the sump strainer for a large-break LOCA. Therefore, floating materials for these breaks likely will not interact with the strainer. The debris or materials suspended within the water may either pass through the sump strainer or be retained, causing separate problems (Andreychek et al. 2007; NRC 2007). If the materials pass, they may cause damage to downstream components. For instance, the debris could plug or excessively wear close-tolerance components or deposit on surfaces within the ECCS or CSS systems. Plugging or wear may cause a component to either decrease its functionality or fail. Debris passing the strainer could deposit on the reactor fuel, reducing the efficiency of heat transfer. Dissolved or suspended material also could pass the fuel and undergo greatly increased radiolytic exposure. On the other hand, blockage of the sump strainer could impede or prevent coolant recirculation flow to the reactor core (e.g., through loss of adequate NPSH to ECCS pumps). This could exacerbate the accident condition by leading to fuel damage and increasing the uncontained radionuclide inventory.

Figure 1: Oconee Nuclear Station Unit 2 Reactor Building Emergency Sump During the Replacement Strainer Installation (Oconee 2007)

The ECCS must be capable of providing long-term cooling to bring the reactor to a safe shutdown condition and to initiate other post-LOCA recovery efforts. The present study only considers the initial 30-day post-LOCA time interval. Longer functioning times for the ECCS may be required, depending on the plant-specific design and operation procedures.

Incidents of degraded ECCS performance caused by debris clogging of pump suction strainers have been observed in the few (non-LOCA) incidents (e.g., Barsebäck-2, Sweden, and Perry-1, Ohio; both boiling water reactors [BWRs]) where most of the material found clogging strainers was fibrous insulation debris along with suppression pool sludge (Hart 2004, pp. 24–34). The sludge was primarily iron oxide particulate resulting from stirring the suppression pool water.

Chemical reactions initiated by the leaching or dissolution of debris materials or other effects in the coolant may diminish the flow through the sump strainer (ultimately causing loss of NPSH) or contribute to deleterious downstream effects during this 30-day window. Possible chemical effects include the formation of chemical by-products (e.g., precipitates, scales, coatings, and degradation products) because of interactions or degradations of wetted containment materials within the post-LOCA coolant. The wetted containment materials literally encompass all materials present in containment and notably include LOCA-generated debris, latent debris, structural materials for reactor system components (e.g., piping, reactor pressure vessel, steam generator, heat exchangers, and reactor internal structures), containment structural materials, ECCS pump, valve, and heat-exchanger internal components, intact insulation and electrical

materials, and fuel-clad material deposits. It is also possible that biological materials may grow in the post-LOCA environment, adding to the debris load.

If the ECCS and associated systems function as designed, then fuel damage and subsequent release of significant quantities of fission products, including irradiated fuel fragments, to the coolant system will not occur. For the purpose of the evaluations in the present document, fuel is presumed to remain intact.

The U.S. Nuclear Regulatory Commission (NRC) established Generic Safety Issue 191 (GSI-191) "Assessment of Debris Accumulation on PWR Sump Performance" to evaluate the effects of post-LOCA debris on the performance of the ECCS and CSS in recirculation mode at PWRs (NRC 2004a). The ECCS is required to meet the objectives of Section 50.46 of Title 10 of the Code of Federal Regulations (10 CFR 50.46), "Acceptance Criteria for Emergency Core Cooling Systems for Light-Water Nuclear Power Reactors." Section 50.46(b)(5) requires that licensees design their ECCS systems with capability for long-term cooling. After successful initiation, the ECCS must be capable of providing cooling to maintain the core temperature at an acceptably low value for a sufficient duration. Although the regulations require that long-term cooling be maintained indefinitely, 30 days is typically considered to be an appropriate time period to demonstrate ECCS functionality. Beyond this time, the decay heat loading is small, making alternative cooling possible should ECCS functionality be lost.

As part of the GSI resolution, the Advisory Committee for Reactor Safeguards (ACRS) recommended in 2003 that an adequate technical basis also be developed to resolve associated sump performance issues related to chemical reaction products in the post-LOCA sump pool. In September 2004, NRC issued a Generic Letter on the topic of potential debris blockage during design basis accidents (DBAs) at PWRs (NRC 2004a). Work on chemical effects began before this letter, and NRC and the nuclear industry sponsored continued research to assess chemical effects in post-LOCA PWR environments.

As part of these efforts, a program of integrated chemical effects testing (ICET) was performed to investigate, through engineering-scale studies, the influence of post-LOCA coolant composition and material corrosion on debris properties. To explore more completely the possible chemical effects that may affect ECCS performance after a postulated LOCA, the NRC convened a panel of five experts in 2005 to review the ICET program and other studies and, in 2006, conduct a phenomena-identification-and-ranking-table (PIRT) exercise on the research outcomes. A report was developed to summarize the PIRT findings and to identify significant remaining issues raised during the PIRT for consideration in the evaluation of chemical effects (Tregoning et al. 2007). Based on the findings of the NRC report, 10 topics with potential significance to sump strainer blockage or downstream effects were identified that had received insufficient attention in prior studies.

Further investigation of the 10 significant remaining issues was proposed as an outgrowth of the PIRT exercise. The scope of further investigation is summarized by the following two tasks:

1. Initiate analytical scoping calculations, conduct literature searches, and conduct limited small-scale or bench-top testing as appropriate to provide sufficient technical rationale to evaluate the significance of the issues identified by the PIRT panelists in the forming of chemical products and debris that can affect ECCS performance.

2. Summarize available relevant information pertaining to the post-LOCA environment for those PIRT items identified for further evaluation that are deemed by the reviewers as not conducive to evaluation using scoping calculations or limited testing.

The objectives of first task were pursued using only information from open publications and additional analysis as warranted; no laboratory testing was performed to evaluate the significance of these listed phenomena in the forming of chemical products and debris that can affect ECCS performance.

In accomplishing the first task, the objectives of the second task were achieved to guide possible further evaluation. The direction and extent of recommendations for additional evaluation, whether by calculation, literature survey, or laboratory testing, were addressed under the second task activities.

The activities under both tasks were performed by scientists and engineers of Pacific Northwest National Laboratory and by an engineer from Fluor Federal Services who have particular expertise on the 10 research topics and can inform directions of further studies, as required.

A brief overview of the 10 identified topics is presented in Section 2 of this report. Sections 3 through 12 focus, in order, on the 10 topics and provide, as necessary, the background of the topics, scope of knowledge, results of the evaluations, and guidance on the direction of further research. Areas of further research are summarized in Section 13. The technical references are provided in Section 14.

2 OVERVIEW OF THE 10 TOPICS OF STUDY IDENTIFIED IN THE PIRT

The objective of this work is to evaluate the validity and importance of chemical effects phenomena selected from a review of the conclusions drawn from the PIRT exercise (Tregoning et al. 2007). Based on the PIRT document, NRC identified 10 general areas of study as having received insufficient attention in the prior studies and experimentation. Many of the chemical effects derived from consideration of the ICET (Dallman et al. 2006) and related experimentation that has occurred over the past several years were studied to address issues raised under GSI-191.

To address the specific identified questions within each area, the task investigators were directed by NRC to use tools such as analytical scoping calculations, review and evaluation of the technical literature, and performance of limited small-scale or bench-top testing. Based on these calculations, reviews, and limited testing, the investigators then were directed to advance sufficient technical rationale to assess the significance of the cited phenomena in the forming of chemical products and debris that can affect ECCS performance.

If, despite the investigations, no conclusive assessment could be made because prior studies were inadequate or inconclusive or if the studies necessary to satisfy the objectives were beyond the scope of limited testing, the investigators were to identify these deficiencies and outline the broad approaches that could be used to evaluate the significance of these effects.

The 10 areas of study are:

1. <u>Radiation Effects</u>. Study the effect of the post-LOCA radiation environment in the reactor vessel, containment pool, and contaminated sump strainer on the containment pool chemical constituents. Specifically:

    a) The effect of radiolysis on the aqueous solution reduction/oxidation (redox) potential (and subsequent consequences of redox changes) and subsequent effects on corrosion/oxidation rates of submerged metals and chemical byproduct formation. These should include but not be limited to:

        1) The formation of hypochlorite and other catalytic effects that likely exist in the post-LOCA containment environments and their effects on corrosion rates of metals

        2) The generation of hydrogen through radiolysis.

    b) The effect of radiation on the nature and properties of inorganic and organic materials found or produced (e.g., through precipitation) in the containment building that could affect ECCS performance. These should include, but not be limited to, the de-polymerization of inorganic/organic coatings and insulating materials to produce gels and particles.

2. <u>Carbonation of Concrete</u>. Evaluate the effect of carbonation or other aging processes of concrete on the leaching rates and dissolved species from aged concrete and concrete dust

and compare with ICET and other NRC and industry-sponsored research programs that evaluated relatively fresh concrete samples.

3. Alloy Corrosion. Evaluate the effect of material alloy variability on the corrosion rate and dissolved species of important submerged containment pool metals (e.g., Al, Fe) that have been evaluated in ICET and other NRC and industry-sponsored research programs.

4. Galvanic Corrosion. Identify galvanic corrosion effects and specific galvanic configurations that could most significantly alter the amounts and types of chemical byproducts observed in NRC and nuclear-industry-sponsored single-effect and integrated research on chemical effects.

5. Biological Fouling. Assess the potential for biological fouling of sump strainers due to bacteria, algal, or other biological growth in post-LOCA containment environment during 30-day ECCS mission time.

6. Co-precipitation and Other Synergistic Solids Formation. Identify post-LOCA conditions that could significantly promote co-precipitation of chemical species or enable other synergistic effects to produce a greater volume or significantly different types/properties of water-borne solids than currently observed in separate effects or integrated testing performed by NRC and the nuclear industry.

7. Inorganic Agglomeration. Identify post-LOCA conditions where inorganic agglomeration may be most significantly (either adversely or beneficially) affected by post-LOCA containment pool conditions and variability compared to findings in NRC and industry-sponsored laboratory testing.

8. Crud Release Effects. Evaluate the quantities and chemical/radiation effects related to Fe and Ni corrosion oxides (crud) within the RCS released during the post-LOCA time-period. Investigate both initial crud release from post-LOCA thermal and chemical transients within the first hour and subsequent release due to ongoing chemical reactions of RCS materials.

9. Retrograde Solubility and Solids Deposition. Identify likely chemical species and estimate quantities that could precipitate at the reactor core due to retrograde solubility. Also indicate which, if any, preexisting solid chemical species could be deposited onto the reactor fuel.

10. Organic Material Impacts. Identify the organic materials that could exist in significant quantities in the post-LOCA containment environment that have the most significant (either beneficial or detrimental) impact on chemical effects within the post-LOCA coolant environment. Describe or quantify the impact, as appropriate, of these likely sources.

3 TOPIC 1—RADIATION EFFECTS

This section of the report is a response to issues regarding radiolysis-enhanced degradation that were raised in Section 5.2 of the PIRT evaluation of the chemical effects associated with GSI-191, "Assessment of Debris Accumulation on PWR Sump Performance" (Tregoning et al. 2007). Among the issues raised by the PIRT evaluation is the potential for activated debris to accumulate at the sump strainer and exacerbate degradation of the ECCS via radiolysis.

Radiolysis arises from the emitted radiation of radionuclides that are in fixed locations (mostly in fuel and core structures) or loose and transportable (either as solids or as dissolved species) within the circulating waters. Radiolysis occurs when the radiation impinges on the circulating water, on the solutes, on the solid material debris being transported by the water, and on the materials in contact with the flowing water.

Radiolysis of the coolant waters can produce many reactive species that can affect the pH and redox potential of the solids-bearing aqueous solution that arise from operation of the ECCS and CSS in the 30 days after a LOCA. Radiolysis of coolant water produces hydroxyl radicals (·OH), hydrogen radicals (·H), hydrogen ions (H^+), and other species. These species, in turn, react with themselves or with other dissolved species (e.g., chloride ion, Cl^-, and nitrogen, N_2) in secondary reactions to form hydrogen peroxide (H_2O_2), chlorate (ClO_3^-), hypochlorite (ClO^-), hypochlorous acid (HOCl), nitric acid (HNO_3), and hydrogen gas (H_2). Radiolysis of solid particles (e.g., silica, SiO_2) transported by the water, especially past the high dose rate regions in the core, also can occur.

Introducing these radiolysis products may significantly influence the corrosion rates of physical debris and containment materials by altering the pH or the redox potential of the containment pool. However, it is noted that plants typically have buffer systems in place that maintain the pH of the containment pool between 7 and 10, which may neutralize the pH effect of radiolysis products. In addition, the redox potential is dependent on the concentration of dissolved species in the containment pool.

During regular operation, 25 to 50 cm^3 (at standard temperature and pressure [STP] of 0°C and 1 atmosphere, respectively) of hydrogen per kg of water is intentionally added to the RCS to lower the redox potential and prevent RCS components from sensitization to stress corrosion cracking and minimize general corrosion. However, following a LOCA, species originating from the wide array of submerged containment materials may react and enter the containment pool without the presence of a radiation field. It would be difficult to discriminate between corrosion products formed as a result of the LOCA hydraulic shock and ensuing chemical phenomena from those corrosion products formed by radiolytic effects. The impact of radiolysis also is limited to the flooded portions of the containment, and thus, radiolysis impacts only a fraction of the containment surface areas. The fractions of metal and concrete surface areas subject to immersion have been estimated (Andreychek 2005; see also Table 5 under Topic 3, alloy corrosion). About 5% of the zinc and aluminum are immersed, about 25% of the copper and copper/nickel, and about 34% of the carbon steel.

The subject of this topic is to assess radiolysis-assisted corrosion issues raised by the PIRT evaluation and determine their significance in a post-LOCA environment. The ECCS prevents massive fuel failures by providing adequate cooling, and, as a result, fuel damage and distribution of fuel particles to the containment pool is not anticipated. Therefore, the radiolysis

is confined to that provided by the activation products released from the RCS and the irradiation of the coolant water, contained solutes, and transported particles that pass the intact fuel and activated core structural materials.

The results of a literature review and initial scoping calculations for this assessment are summarized in the following sections. The radiolysis phenomena arising from water and from dissolved species are described in Section 3.1. These include hydrogen peroxide (Section 3.2), chlorine species (Section 3.3), nitric acid (Section 3.4), and hydrogen ions and hydrogen gas (Section 3.5). The radiolysis of sodium metaborate ($NaBO_2$) solution is a new consideration and is discussed in Section 3.6. The effects of radiolysis on the solution redox potential are considered in Section 3.7. The radiolysis of solid silica and insulation debris is addressed in Section 3.8. Conclusions are presented in Section 3.9. The discussion of organic radiolysis is deferred to Topic 10, organic material impacts.

3.1 Solute Radiolysis Phenomena

Radiolysis is the breaking of one or more chemical bonds through exposure to an energetic flux of radiation. Although the sustained fission chain reaction has ceased in a post-LOCA environment, the gamma-radiation decay field surrounding the fuel in the reactor vessel is expected to be on the order of 10^6 rad/h. Other forms of radiation, such as alpha, beta, and neutron, are assumed to be negligible in the proposed scenario because it is assumed that fuel failures have been prevented and the fission rate has significantly declined because of control rod insertion. Thermal stresses resulting from decreasing temperatures are expected to result in spallation of corrosion products (i.e., crud; see Topic 8 on crud release effects) that are part of the crud layer on the fuel cladding and reactor internal structures. This effect may be particularly significant for fuel rods, as crud tends to plate on surfaces of high heat flux, and the rods will be subjected to large thermal gradients following a LOCA event and the activation of the ECCS. The spallation of corrosion products will introduce activated species such as ^{24}Na, ^{7}Be, ^{51}Cr, ^{58}Co, ^{60}Co, ^{54}Mn, ^{56}Mn, ^{95}Zr, ^{97}Zr, ^{55}Fe, ^{59}Fe, ^{59}Ni, ^{63}Ni, ^{95}Nb, ^{97}Nb, ^{125}Sb, and ^{65}Zn to the containment pool. The radiation field from the collection of these activated species at the sump strainer is unknown but is estimated to be on the order of 10^3 rad/h.

The volume of water circulating in the post-LOCA containment pool ranges from about 35,000 to 160,000 ft^3 (i.e., 990,000 to 4,500,000 liters) with an average of about 43,000 to 74,000 ft^3 or 1,200,000 to 2,100,000 liters (Table 7 of Andreychek 2005). The volume of coolant in the reactor pressure vessel is about 3,500 ft^3 or ~100,000 liters (Andreychek 2005). Because the dose rate in the pressure vessel is 1000-times higher than anywhere else in the post-LOCA recirculation flowpath, the dose experienced by the circulating coolant will be proportional to the time the coolant spends in the pressure vessel. That time, in turn, will be proportional to the volume fraction of the pressure vessel to the total coolant volume, which is ~0.05 to 0.08. Therefore, the radiation field experienced by the circulating coolant will be, on average, $(0.05 \text{ to } 0.08)\times10^6 \cong 8\times10^4$ rad/h. To a good first approximation, the radiolytic yield rates (G values, in terms of species formed or destroyed per 100 eV of absorbed dose) experienced at 10^6 rad/h dose rate are expected to be the same as experienced at 8% of that dose rate, i.e., 8×10^4 rad/h. Thus, the total radiolytic effect experienced by the receptor molecules at a continuous 8×10^4 rad/h exposure is the same as would be experienced by exposure to 10^6 rad/h for 8% of the time.

The subsequent impact of these radiation fields on coolant chemistry and physical debris within the containment pool is of significant interest. If radiolysis products, such as hydrogen peroxide

(H_2O_2), chlorate (ClO_3^-), hypochlorite (ClO^-), hypochlorous acid (HOCl), nitric acid (HNO_3), and hydrogen (both H^+ ions and H_2 molecules), are generated in quantities sufficient to alter the redox potential or overcome the pH buffering in a typical PWR ECCS, then the corrosion of physical debris and core containment components may be accelerated. If a sufficient amount of corrosion takes place in the 30 days following a LOCA, the increasing volume of solids may block the sump strainer and impair ECCS performance. The following subsections discuss the radiolysis products specifically addressed by the PIRT evaluation and present calculations of the anticipated radiolytic specie concentration and their subsequent impact on pH. Changes in pH were evaluated assuming the presence of borate/boric acid or sodium tetraborate buffer (~2,800 ppm as boron, ~0.26 moles of borate/boric acid per liter) and, for some reactors, an additional trisodium phosphate (TSP) buffer (4,000 ppm as $Na_3PO_4 \cdot 12H_2O$, ~0.01 moles of phosphate per liter) as described in the ICET experiments (Dallman et al. 2006). Despite the use of TSP or, in some cases sodium hydroxide, to adjust the pH, the coolant water buffering capacity (maintenance of pH) is dominated by the 26-fold higher concentrations of borate/boric acid compared with TSP. Therefore, the borate/boric acid system was selected for the present analysis because it is the most representative, occurring in all coolant systems, and dominates the pH buffering. The containment pool was assumed to have this buffer present while exposed to an average 8×10^4 rad/h gamma radiation field.

Radiolytic specie contributions to the redox potential in a post-LOCA PWR containment pool were not described in the open literature. The redox potential would be susceptible to temporal variations in radiation flux, temperature, oxygen saturation, and the ongoing evolution of chemical reactions. Consequently, the specific influence of radiolysis on redox potential is not presented in the following subsections as it would require the development of a mixed potential model. Development of such a model is outside the scope of this effort but might be considered for further investigations, as described in Section 3.7. However, the specie concentrations resulting from radiolytic speciation of chloride-containing water and the subsequent impact on pH are described in the subsequent sections. This evaluation is important because the redox potential is dependent on concentration, and pH is a primary determinant of corrosivity in an aqueous environment.

3.2 Formation of H_2O_2

Gamma irradiation of water causes hydrolysis and leads to the formation of many species of molecules and ions, including hydrogen peroxide (H_2O_2). The formation of H_2O_2 is of concern because of its potential to increase the pH and redox potential of the RCS.

Pastina and colleagues have studied the radiolysis of water under gamma (γ), beta (β), and alpha (α) irradiation (Pastina and LaVerne 2001). The radiolysis events occurring for γ-irradiated water are of primary concern for this application. The radiolytic yields typically are expressed by G values, which are the number of molecules or species produced or destroyed per 100 electron volts (eV) of absorbed dose. The expected rate (or G value) for H_2O_2 production under γ-irradiation of water is 0.70 molecules/100 eV. This production rate is equivalent to 1.0 ppm/h in the radiation field experienced by the sump water (80,000 rad/h) and could lead to a H_2O_2 concentration of 720 parts per million (ppm, by weight) after 30 days if the H_2O_2 is not diminished by other reactions.

However, in addition to being produced in water under γ-irradiation, H_2O_2 is also destroyed by radiolysis, by interaction with other radiolytically produced species, or by disproportionation to form H_2O and O_2. Thus, model calculations have shown that after 100 seconds of irradiation at

90,000 rad/h (~2,500 rad), the H_2O_2 concentration in neat water (i.e., water without other solutes) reaches an equilibrium concentration of ~0.3×10^{-6} moles/liter or ~10 parts per billion (ppb, by weight; Pastina and LaVerne 2001). This limiting value is found to be nearly independent of dose rate. This result agrees with the general assessment that there is no net water decomposition by gamma radiolysis (Pastina and LaVerne 2001). Pastina and LaVerne (2001) also measured the radiolytic decomposition of 5×10^{-5} M H_2O_2 in water by γ-irradiation at 90,000 rad/h. In the absence of dissolved H_2 and even in the presence of 8×10^{-6} M dissolved H_2, the H_2O_2 concentration decreased to ~10×10^{-6} M or ~0.34 parts per million (ppm) but was below 10^{-6} M at higher H_2 concentrations. The H_2 concentration established by radiolysis of neat water is about 10^{-6} M. Therefore, the H_2O_2 concentration in neat water gamma-irradiated at 90,000 rad/h will lie between (0.3 to 10)$\times10^{-6}$ M.

Pastina and LaVerne (2001) also demonstrated experimentally that the gamma radiolysis of water in the presence of dissolved H_2, the condition expected initially in the RCS, formed even less H_2O_2 (note that the H_2 overpressure used in reactor operations will be essentially dissipated in the first few moments of the LOCA).

The H_2O_2 concentrations measured at pH 6.4 and pH 11 are about 10^{-5} M (0.3 ppm) for water initially containing 2.9×10^{-4} M oxygen (i.e., the concentration in water in equilibrium with atmospheric oxygen) irradiated to 0.3×10^{6} rad/hour or 1.7×10^{6} rad/hour dose rates (Kabakchi et al. 1967).

The peroxide concentrations observed in spent fuel pools exposed to the atmosphere are relevant to forecasting the peroxide concentration that may arise in the post-LOCA coolant transiting the fuel core. Peroxide is a constituent of concern for spent fuel pools for its deleterious effects on the organic ion exchange resin used for pool-water maintenance. In an informal survey of seven PWRs, peroxide concentrations measured in spent fuel pools both during refueling outages and between outages range from 3 to 6 ppm, or about (1 to 2)$\times10^{-4}$ M H_2O_2 and thus are much higher than those observed in laboratory testing.[1]

Based on the calculation of Pastina and LaVerne (2001) and the observations of Kabakchi and colleagues (1967), the H_2O_2 production concentrations from the radiolysis of water range from about (0.3 to 10)$\times10^{-6}$ M. In contrast, the H_2O_2 concentrations observed in spent-fuel pools are about 10- to 100-times higher, ranging from (1 to 2)$\times10^{-4}$ M. The H_2O_2 concentrations at either set of levels can influence the RCS water chemistry by modifying the redox potential and the corrosion potential of any immersed metal or alloy. The influence on redox is considered later in this narrative.

3.3 Formation of ClO_3^-, ClO^-, and HOCl

It is anticipated that the water in the ECCS could contain up to 100 ppm chloride (Cl^-). Radiolysis of this solution has the potential to form chlorate (ClO_3^-), hypochlorite (ClO^-), and hypochlorous acid (HOCl), which could in turn alter the pH and redox potential of the ECCS.

Chloride is a constituent of post-LOCA coolant and arises from the radiolytic breakdown of electrical cable insulation. A radiolysis of water that contains sodium chloride (NaCl) at various concentrations and pH values was performed by Kelm and Bohnert (2004, p. 60). Experiments were performed using γ- and α-radiation. The gamma radiation is the more influential radiation

---

([1]) Data from Robert Litman, Radiochemistry Laboratory Basics, Epping, New Hampshire.

type present in the post-LOCA environment considered in the present evaluation. Sodium chloride concentrations and γ-radiation dose rates studied by Kelm and Bohnert (2004) exceed the expected Cl^- concentration and bound the dose rate expected in containment, respectively. Table 1 shows a comparison of the test conditions to the conditions expected in containment.

Table 1: Experimental and Expected In-Containment Conditions
(Kelm and Bohnert 2004)

Conditions	Experimental	Expected Containment
Gamma dose rate	20,000–120,000 rad/h	80,000 rad/h [(a)]
Cl^- concentration	1–5.3 moles/liter	0.0028 moles/liter (100 ppm)
(a) Time-weighted average, fluctuates between ~1×10^3 and 1×10^6 rad/h as water passes core.		

Experiments were performed for the 5.3 moles NaCl per liter solution at three pH values (2, 7, and 12), which bound the expected in-reactor pH (7 to 10). Radiolysis of chloride-bearing water formed ClO_3^-, ClO^-, and HOCl. Only ~10^{-5} moles of HOCl per liter were detected (this was near the experimental detection limit). Since HOCl is a weak acid (pK_a is 7.5), the ClO^- concentration is expected to range from ~3×10^{-6} to 10^{-5} moles per liter at pH of 7 to 10 in the coolant, and the acid dissociation at the projected HOCl concentration will be driven by the more concentrated buffering solution.

Chlorate, ClO_3^-, was observed in measurable quantities; the G values determined for ClO_3^-, presented in Table 2, show that maximum production occurs at pH 7.

Table 2: Measured G Values for γ-Radiolysis of 5.3 M NaCl Solution in Water
(Kelm and Bohnert 2004)

pH	G Value (ClO_3^- formed per 100 eV)
2	0.005
7	0.072
12	0.027

Based on these measurements and assuming no back reactions, after 30 days at pH 7, the concentration of ClO_3^- would be only about 77 ppm in a 5.3 moles/liter NaCl solution. However, these experiments also showed that the G value is highly dependant on the Cl^- concentration. Figure 2 presents a plot of G values as a function of concentration for various NaCl concentrations. Also shown on this plot is a logarithmic fit to these data to estimate the G value at the expected RCS Cl^- concentration of 100 ppm.

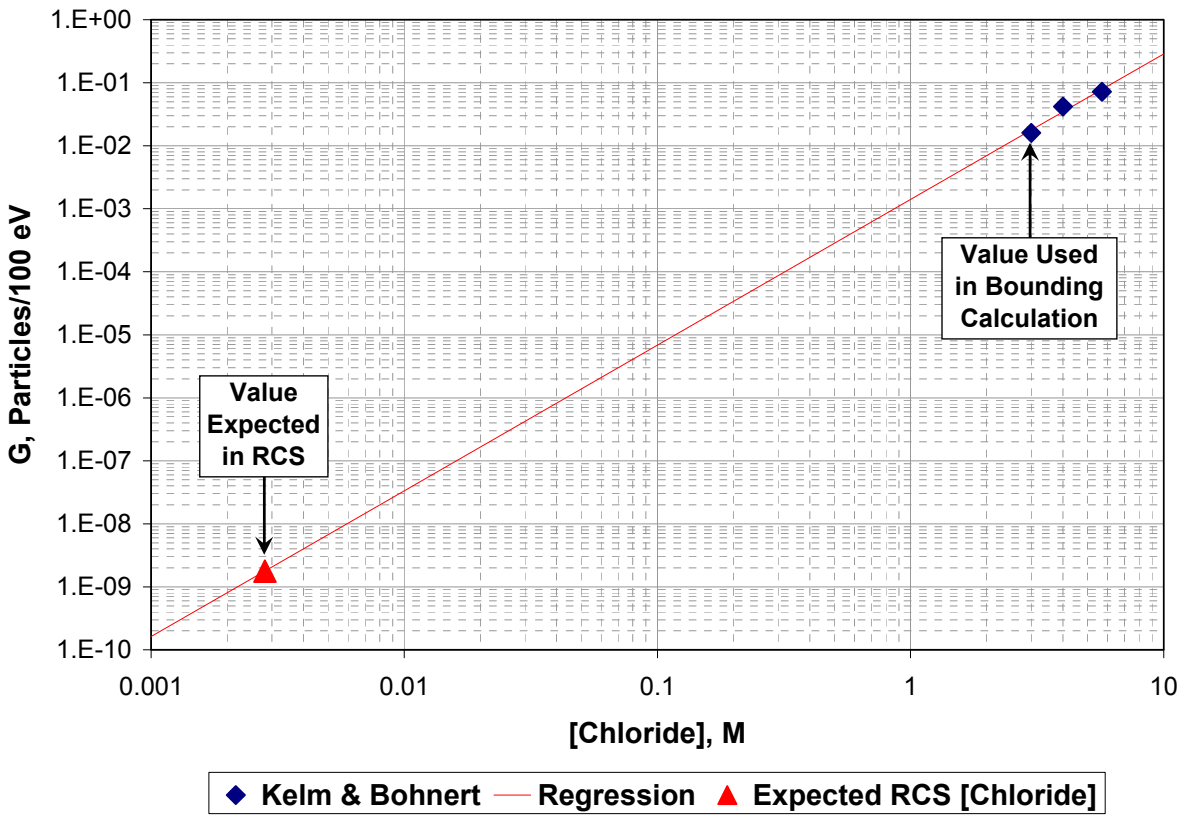

Figure 2: Dependence of G Value for ClO_3^- Formation by γ-Radiolysis of NaCl Solution in Water

Extrapolating from the data at high concentration in Figure 2, the G value at the expected NaCl concentration of 100 ppm will be 1.8×10^{-9} molecules/100 eV. Although an extrapolation over this range may be subject to error, Figure 2 offers some perspective between the relative chloride concentrations studied by Kelm and Bohnert (2004) and those expected in containment. Further calculations of the radiolytic yield of ClO_3^- were conducted using the yield value determined for the lowest concentration where G was measured (3 moles/liter), not the extrapolated value shown in Figure 2. The G value for ClO_3^- at this concentration is 0.016 molecules/100 eV, producing 1.3×10^{-6} moles/liter·h at the 80,000 rad/h expected dose rate. These conditions would yield ~10^{-3} M (~83 ppm) ClO_3^- after 30 days, which may be significant in altering the redox properties of the solution. However, it is important to remember that this calculation is highly conservative for the in-reactor conditions as it is based on a yield value determined from a solution with over 500-times the chloride concentration expected in containment.

Even at their maximum anticipated concentrations, HOCl and ClO^- (~10^{-5} moles/liter) and ClO_3^- (~10^{-3} moles/liter) are expected to have negligible impacts on pH in the RCS. Mixed potential calculations would be necessary (Section 3.7) to determine effects on solution redox properties.

3.4 Formation of HNO_3

The irradiation of water in the presence of dissolved nitrogen gas, N_2, can produce nitric acid (HNO_3). This is significant because the production of a strong acid like HNO_3 will lower the pH in the RCS and possibly overcome the buffer in the RCS to produce a corrosive environment.

The production rate for HNO_3 in neutral unbuffered water is given by Weber et al. (1992, pp. 33–36) as 0.0068 molecules/100 eV (determined at a dose rate of 600,000 rad/h, intermediate between the dose rate in the reactor, 1 Mrad/h, and the average dose rate) and by Beahm et al. (1992) as 0.007 molecules/100 eV. The G value is low because the solubility of N_2 in water is low. The generation rate is lower as pH increases. Thus, in 2.8×10^{-2} M KOH (pH ~12.4), nitrite (NO_2^-) rather than nitrate (NO_3^-) is formed (Linacre and Marsh 1981). A value of 0.007 molecules of HNO_3/100 eV will be used for the following calculations. This production rate is equivalent to 5.80×10^{-7} moles/liter·h in the anticipated average radiation field of the circulating coolant (80,000 rad/h) and could lead to a HNO_3 concentration of 4.18×10^{-4} moles/liter in 30 days. Although the pH for this concentration of HNO_3 in neutral water is 3.38, this concentration of HNO_3 is negligible compared with the borate buffer concentration of ~0.26 moles/liter. Because yields of HNO_3 from radiolysis of higher pH water will be lower yet, the concentration of HNO_3 in the buffered containment pool considered here will not have any measurable impact on the pH.

3.5 Formation of H^+ and H_2

The formation of hydrogen ions (H^+) and hydrogen molecules (H_2) during radiolysis of water is considered in this section. The expected G value for H^+ due to gamma irradiation of water is 0.66 molecules/100 eV. This production rate is equivalent to 0.98 ppm/h at the expected dose rate of 80,000 rad/h and could lead to an H^+ concentration of 706 ppm after 30 days if H^+ were not also consumed in other reactions. The expected G value for H_2 due to gamma irradiation of water is 0.46 molecules/100 eV. This yield is equivalent to 0.67 ppm/h at the expected dose rate of 80,000 rad/h and could lead to an H_2 concentration of 483 ppm after 30 days if H_2 were not also consumed in other reactions.

As discussed in Section 3.1.1, Pastina and LaVerne (2001) have found no net decomposition of water by gamma radiolysis. Model calculations have shown that after 2 milliseconds of irradiation at 90,000 rad/h, the H^+ concentration in water will reach an equilibrium concentration of about 10^{-10} moles per liter or 1.8 parts per trillion (ppt). This limiting value is trivial in comparison with the H^+ concentration in neutral water (10^{-7} moles per liter), and this equilibrium concentration has been found to be nearly independent of dose rate. These same model calculations showed that after 100 s of irradiation at 90,000 rad/h, the H_2 concentration in water will reach an equilibrium concentration of about 10^{-6} moles/liter and establish an equilibrium H_2 concentration in the vapor phase.

The expected water temperature for the majority of the 30 days assumed in these calculations is 165°F. At this temperature, the solubility of H_2 in water is 1.3×10^{-5} mole fraction or 7.2×10^{-4} moles per liter in equilibrium with one atmosphere of H_2 gas (Lide 2007). The partial pressure of H_2 in equilibrium with 10^{-6} moles H_2/liter therefore, is 0.0014 atmospheres within the containment vessel and is far below the ~0.04 atmosphere flammability limit, assuming that the hydrogen concentration due to radiolysis is maintained constant at 10^{-6} moles/liter.

Calculations of the H^+ and H_2 concentrations generated by the gamma radiolysis of water suggest that radiation will have a negligible contribution to the inventory of these species within the containment pool. The concentration of H^+ produced by radiolysis in the RCS will quickly (~2 milliseconds) approach the limiting value of 1.8 ppt. This concentration of H^+ is small compared with the buffer capacity of the coolant and is not expected to have any noticeable effect on RCS chemistry in the coolant. Similarly, the concentration of H_2 produced by radiolysis will approach the limiting value of 10^{-6} moles per liter in the first 100 seconds and will remain at this level or lower for the remaining 30 days as the hydrogen establishes equilibrium with its partial pressure in air. Other sources of hydrogen, such as the concentration injected during normal RCS operation, were not considered in the above calculation as these sources are essentially lost to the solution system in the blow-down period of the LOCA. However, the expected production of H_2 due to radiolysis will have a negligible incremental impact on the initial RCS concentration of H_2.

3.6 Radiolysis of Sodium Metaborate

Sodium metaborate ($NaBO_2$) has been proposed as a containment spray chemical that may be used instead of sodium hydroxide (NaOH) to provide enhanced pH control while minimizing other chemical effects (Reid et al. 2006). However, it has not yet been used in PWR CSS. Sodium metaborate also is the product of decomposition of sodium borohydride, $NaBH_4$, to release hydrogen gas, H_2 (Cloutier et al. 2007):

$$NaBH_{4\,(aq)} + 2\,H_2O_{\,(l)} \rightarrow NaBO_{2\,(aq)} + 3\,H_{2\,(g)}$$

where the subscripted aq, l, and g indicate, respectively, the materials in the aqueous (water-dissolved), liquid, and gaseous phases. The radiolytic re-generation of sodium metaborate to form sodium borohydride has been the subject of recent research (DOE 2004).

From these results, it appears that introducing sodium metaborate to irradiated conditions in the post-LOCA coolant, if kept sufficiently alkaline, may form sodium borohydride and perhaps lead to enhanced hydrogen-gas-generation rates. However, sodium metaborate, when added to lower pH systems (as would occur when the CSS discharge combines with the pH ~7-10 coolant in the containment sump), will convert to sodium tetraborate and other more acidic boron salt species (Nies and Hulbert 1967). The product solutions would be essentially no different that the systems using NaOH, boric acid, and sodium tetraborate whose radiolytic behaviors are presumably already well known. Therefore, the use of sodium metaborate is not anticipated to introduce any novel chemical or radiolytic effects to the post-LOCA coolant.

3.7 Mixed Potential Effects

It is important to note that various radiolysis products are able to modify the redox properties of the environment and that these changes in redox potential can influence metallic corrosion rates. Thus, redox properties potentially can be modified by even small amounts of radiolytically produced hydrogen and hydrogen peroxide (i.e., chemically reducing and oxidizing, respectively). Secondary effects, such as loss of radiolytically produced H_2 from the hot coolant to the atmosphere, or scavenging of oxidizing species such as hydroxyl radicals, OH, by organic species, can cause further alteration of solution redox properties.

Such behavior is evident from published studies of the impact of radiolysis on the redox properties of BWR primary (liquid water) coolant (Macdonald and Urquidi-Macdonald 2006), albeit at much higher dose rates than are relevant to a LOCA. The same Mixed Potential Model employed in those reactor studies might be used to establish how radiolytic products affect the redox potential of the post-LOCA coolant system. As seen in earlier sections, hydrogen and hydrogen peroxide are products of water radiolysis. Imposing hydrogen overpressures during PWR operation to control the corrosion of the reactor vessel, piping, steam generator, and fuel cladding wetted by the coolant and adding hydrogen peroxide to control crud release during shut-down operations indicate the importance that these two species exert when added intentionally to PWR systems.

For example, increasing the potential caused by the presence of radiolytic hydrogen peroxide in the post-LOCA coolant might be sufficient, with the prevailing chloride concentration, to cause massive passivity breakdown and pitting corrosion of aluminum. To assess the potential for massive pitting corrosion, the calculated (or measured) corrosion potential needs to be compared with critical pitting potential data for the aluminum alloys of interest. Of particular concern is the fact that the current, at potentials above the prevailing critical pitting potential, is a very strong function of the over-potential, indicating that any displacement of the corrosion potential in the positive direction, even by the small amounts of radiolysis products produced, could have a quite deleterious impact on the rate of aluminum hydroxide production.

It is noted that pitting corrosion will not contribute large quantities of corrosion products to the post-LOCA system because of the highly localized nature of the attack. Of more concern is the effect of radiolysis on general corrosion with the higher area of affected metal.[(2)]

A number of robust radiolysis models are now available. One or more of these models could be used to verify that the estimated H_2O_2 concentration obtained in the previous section is, indeed, realistic.

3.8 Radiolysis of Solid Species

Among the concerns regarding ECCS degradation via formation of a localized radiation field (~10^3 rad/h) at the sump strainer are the accelerated precipitation of solid species and the continued corrosion of solid debris that has collected on or near the sump strainer. Higher fields of ~10^6 rad/h are present in the vicinity of the core. The additional formation of corrosion products leads to an increase in the volume of solids gathered at the sump strainer, which may result in loss of NPSH. The purpose of this section is to discuss the effects of radiation on these materials.

(2) Note that the effects of 100-ppm levels of hydrogen peroxide, as well as 100-ppm levels of citrate, phosphate, chloride, nitrate, sulfate, bicarbonate, acetate, arsenate, silicate, dichromate, molybdate, and mixtures of these ions, on the corrosion of alloy 1245 aluminum have been studied (Troutner 1957). Also studied were the effects of pH change. Only pH, citrate, and phosphate had discernable effects. The most influential parameter was pH (minimum rate at pH ~6); 100-ppm citrate increased corrosion and 100-ppm phosphate decreased corrosion. Hydrogen peroxide at 100-ppm levels had no discernable effect on aluminum general corrosion. Borates also can indirectly affect aluminum (Tagirov et al. 2004).

3.8.1 Solid Silica Precipitates

Silica may be introduced to the containment pool from a number of different sources, including fiberglass insulation, concrete, latent solid mineral debris, and silicon-based greases. In water, silica dissolves to form $Si(OH)_{4\,(aq)}$, which ionizes to $SiO(OH)_3^-$ as the pH increases (the pK_a of $Si(OH)_{4\,(aq)}$ is 9.7 at 25°C and 10.8 at 90°C; pp. 47-48 of Iler 1979). Polymeric silica species also may form at higher dissolved silica concentrations, but are expected to be minor. Silica dissolves to about 200 to 500 ppm (silicon basis) at a pH from 7 to 10. Silica further dissolves in the presence of radiation, and glass is more reactive in acidic or basic solutions (Plodinec et al. 1982; Bates et al. 1988; Litman 2006). Dissolution rate enhancement also is expected due to the high specific surface areas of fiberglass. Because RCS buffers range in pH from 7 to 10, the silicate species, $SiO(OH)_3^-$, forms with increased pH within the containment pool even without the aid of a radiation field. In any event, silicate compounds that are rendered soluble by chemical reaction with or without the assistance of radiation are not anticipated to contribute directly to the clogging of the sump strainer or loss of NPSH, but may contribute by secondary reactions.

Subsequent reactions between the dissolved silicate species and the array of possible submerged containment materials and corrosion products underscores the complexity of the containment pool environment (the thermodynamic equilibria of silicates and other species are described under Topic 9 on retrograde solubility and solids deposition). As a result, attempting to quantify the additional solids volume that results from the soluble silicate species contributed by radiation alone in a post-LOCA environment is difficult. Fortunately, previous studies in other research areas have been directed toward separating chemical and radiation effects in systems containing silicate species.

Results of studies of the radiolytic stability of vitrified radioactive waste are useful to understand radiological corrosion of silicates in the post-LOCA containment environment. The influence of gamma radiation on the pH of groundwater and the subsequent solubility of contained waste glass has been studied. Although radiolysis resulted in HNO_3 production, the pH (8.1) was not lowered beyond the pH of the natural carbonate buffering (pH 6.4) within the groundwater when exposed to a radiation field of 2×10^5 rad/h for 278 days (Bates et al. 1988). Because buffering likewise should occur in the post-LOCA system, little effect of radiolysis on pH is expected as noted previously in considering the dissolved solutes.

Mixtures of waste glass and groundwater were irradiated at ~2×10^5, 9×10^2, and 0 rad/h to determine the influence of radiation on pH and glass solubility. Radiolysis briefly lowered the pH when a radiation field of 2×10^5 rad/h was applied, but the system eventually became controlled by the glass reaction as was observed for the 9×10^2 and 0 rad/h systems. As the glass reacted, the pH increased, and the solution became basic. Final pH levels ranged between 7 and 8 for samples irradiated at 2×10^5 rad/h for 60 days and samples irradiated at 9×10^2 rad/h for 300 days. Although the pH was found to be a balance between radiolysis products, secondary phase precipitation, and buffering capacity of the solution, radiolysis effects were only significant under a field of 2×10^5 rad/h and were short lived relative to the glass reaction and limited by the buffer capacity of the solution (Bates et al. 1988). Based on these findings, the assumed maximum dose rate of 1 Mrad/h in the core (just a factor of 5 higher than the 2×10^5 rad/h dose rate studied), and the fact that most of the silica will not experience the high fields in the core but rather fields on the order of 1,000 rad/h only, it is expected that any supplementary effect of radiolysis on fiberglass degradation and precipitation of silicate corrosion products in the post-LOCA buffer system will be negligible.

3.8.2 Degradation of Insulation Debris

In the post-LOCA environment, pieces and particles of thermal insulation are expected to be significant sources of debris that may gather at the sump strainer. Three types of insulation include reflective metal insulation (RMI), fiberglass, and cal-sil (calcium silicate). The corrosion rates of these materials are influenced by the containment pool pH. Although radiolysis can influence the pH, the calculations presented in Section 3.1 indicate that the concentration of radiolysis products is too small to change the pH within the containment pool. Even the production of a strong acid like HNO_3 by radiolysis results in concentrations that are too small to overcome plant buffer systems. As a result, radiolysis is expected to have negligible influence over the corrosion of insulation debris collected in the containment pool. The degradation of large insulation debris will be primarily influenced by the solution chemistry of the containment pool, which will have an initially neutral to high pH resulting from the buffer solution.

In a previous analysis, El-Alaily and Ahmed (2002) studied the degradation of fiberglass insulation in varying concentrations of sodium hydroxide (NaOH) under various irradiation doses. Results indicated that weight loss due to dissolution of fiberglass in a solution of 1 M NaOH (pH 14) increased from 18 to 20 wt% as the irradiation dose increased from 0 to 7×10^6 rad over a period of 250 hours (~10.5 days). Since the total dose expected at the sump strainer after 720 hours (30 days) is 0.72×10^6 rad and the RCS buffer is much less basic (pH 7 to 10 vs. pH 14), the degradation of fiberglass in the post-LOCA environment due to radiation is not expected to be significant compared to the degradation due to chemical reaction. Furthermore, dissolution of the fiberglass by radiolysis would not contribute to sump strainer clogging. Subsequent reactions between the dissolved species and the array of possible materials within the containment pool that may form solid phases and contribute to sump strainer clogging are separate, secondary chemical reactions that are not dependent upon the presence of a radiation field.

Organic radiolysis is discussed in Section 12.

3.9 Conclusions and Issues for Further Research

Results of the literature review and initial scoping calculations presented in this section indicate that quantities of acidic products resulting from radiolysis of dissolved chloride are insufficient to overwhelm the buffered containment environment and thus are unlikely to accelerate corrosion and thus impair the ECCS in the 30-day time frame of interest. The post-LOCA borate buffer system likewise is adequate to neutralize radiolytically produced HNO_3. As a result, the pH, which is one of the principle measures of a corrosive environment, remains unchanged.

Although the literature review and initial scoping calculations indicate that radiolytic speciation will have a negligible effect on pH, less information was found in the open literature to specifically address the influence of radiolytic species on the redox potential (caused, for example, by H_2O_2 generation) and the subsequent changes in corrosion mechanisms available in a post-LOCA environment.

Previous research efforts to permit the manipulation of water chemistry to control the reduction potential and hence prevent primary system components (e.g., Type 304 stainless steel) in weld-sensitized BWRs from suffering stress corrosion cracking have used a mixed potential model (Macdonald and Urquidi-Macdonald 2006).

A similar mixed potential model approach might be applicable to the post-LOCA environment described here, but there are significant differences between the previously studied functioning BWR primary system and a post-LOCA PWR in pump recirculation mode. Among the differences is the presence of high borate/boric acid buffer concentrations in the post-LOCA PWR and its less-intense gamma radiation field compared with the BWR RCS during normal power operations. Consequently, the post-LOCA environment will contain lower radiolytic dose to contribute to a radiation effect and a greater number of species from submerged, plant-specific containment materials to influence the containment-pool reduction potential with or without radiation. Since the contribution of chemical species to the reduction potential is proportional to concentration (and may be influenced by the high ionic strength and number of solutes in the coolant), reasonable estimates are needed of the different specie concentrations and their generation rates in the post-LOCA PWR containment pool if such projections are to be made.

A comprehensive radiolysis/mixed potential modeling study would address the differences between control operational experience with coolant chemistry and the present surveyed literature data. However, it will be difficult to differentiate between the effects of radiolysis on the reduction potential of the containment pool from the contributions made by containment materials and debris subjected to elevated temperatures in a buffered aqueous environment.

Alternatively, the corrosion behavior of the containment materials may be studied experimentally in a simulated post-LOCA environment (e.g., temperature, pH, presence of a buffer, and other chemical and physical factors). Radiation effects may be studied by applying the appropriate gamma radiation field or by introducing the anticipated species arising by radiolysis based on model calculations or technical literature resources. Either approach would elucidate the corrosion behavior of individual containment materials and may be extended to include any secondary reactions of interest between the dissolved species or corrosion products from different containment materials.

The kinetics of the corrosion mechanisms also should be considered for either mixed potential modeling or experimentation with the objective to determine if the amount formed in the 30-day post-LOCA period is sufficient to impair ECCS performance. Although an experimental simulation would provide more conclusive evidence of radiation effects in the post-LOCA environment, the initial data and estimates of radiolytic concentrations and pH indicate that radiolysis does not significantly influence the corrosiveness with respect to the pH of the containment pool.

4 TOPIC 2—CARBONATION OF CONCRETE

Questions were raised in the PIRT report in Sections 5.3.3.2.1 and 5.3.5 (Tregoning et al. 2007) about the differences that might arise in test behavior had aged concrete been used in testing instead of the relatively fresh concrete coupons that were used.

As shown in Section 2, the concern with concrete carbonation states:

> Evaluate the effect of carbonation or other aging processes of concrete on the leaching rates and dissolved species from aged concrete and concrete dust and compare with ICET and other NRC and industry-sponsored research programs which evaluated relatively fresh concrete samples.

In the ICET experiments (Dallman et al. 2006), concrete and concrete dust samples were used that had been prepared before the commencement of the month-long testing at 60°C. The concrete test materials' aging times were not stated in the reference reports. However, the concrete specimens were cast in August 2004.[(3)] The ICET #1 experiment commenced on November 21, 2004, and ended 30 days later on December 21, 2004. The ICET #5 experiment began July 26, 2005, and ended August 25, 2005. Therefore, the concrete test coupons had aged in air between 3 months (for ICET #1) and 11 months (for ICET #5). To understand the concrete carbonation issue mentioned in the PIRT, it is necessary to understand the reactions involved in the curing and aging of concrete. The time of exposure to carbon dioxide present in the air is important in this aging.

A discussion of concrete chemistry in its curing reactions and aging is provided in Section 4.1. Carbon dioxide uptake in the concrete (i.e., carbonation) is discussed in Section 4.2 followed by a description of a means to measure carbonation in Section 4.3. The projected differences arising from use of fresh concrete versus aged concrete in the ICET experiments are described in Section 4.4. Section 4.5 outlines the conclusions from these evaluations.

4.1 Concrete Curing and Aging Chemistry

Concrete consists of a mixture of Portland cement and aggregate in which the aggregate provides strength but, aside from adhering to the cement in surface reactions, does not chemically alter with age. The dry Portland cement powder consists of alite (Ca_3SiO_5, or tricalcium silicate), belite (Ca_2SiO_4, or dicalcium silicate), tricalcium aluminate ($Ca_3Al_2O_6$) and other calcium aluminates, tetracalcium ferrite aluminate ($Ca_4Al_2Fe_2O_{10}$), lime (CaO), minor alkali sulfate, and other compounds of variable composition. The cement alteration begins upon mixing the dry cement powder (and combined aggregate) with water (MacLaren and White 2003). A sequence of reactions following mixing is called cement hydration and primarily occurs with tricalcium silicate, Ca_3SiO_5, called C_3S, a leading phase in the dry cement mixture. The C_3S hydration reaction has the following approximate stoichiometry:

(3) Based on the message, "Email; Concrete Coupons," 2:16 PM, October 15, 2007, from John Gisclon, EPRI Consultant, to Rob Tregoning. Gisclon states, "I consulted my log book for 2004, and it appears that the concrete sample coupon composition question was raised in early August. It looks like new coupons were cast with the correct structural Portland cement shortly after that time and delivered to the University of New Mexico in Mid-September."

$$2\ Ca_3SiO_{5\ (s)} + 6\ H_2O_{\ (l)} \rightarrow 3\ CaO{\cdot}2SiO_2{\cdot}3H_2O_{\ (s)} + 3\ Ca(OH)_{2\ (aq)}$$

where the subscripted s indicates solid phase, l liquid phase, and aq aqueous phase. With hydration time, the $Ca(OH)_2$ solution concentration increases, ultimately, to precipitate and form crystalline $Ca(OH)_{2\ (s)}$; the solid phase is called portlandite. The $CaO{\cdot}2SiO_2{\cdot}3H_2O$ product is an approximation of the nanocrystalline X-ray indifferent solid phase that forms in combination with the portlandite. This solid phase is commonly called calcium silicate hydrate (C-S-H) gel and serves as the glue to bind various solid phases in the cured concrete. Another source of C-S-H, dicalcium silicate (Ca_2SiO_4 or C_2S), reacts with water in an analogous way as C_3S to form C-S-H gel according to the following approximate stoichiometry with a lesser relative contribution from $Ca(OH)_2$:

$$2\ Ca_2SiO_{4\ (s)} + 4\ H_2O_{\ (l)} \rightarrow 3CaO{\cdot}2SiO_2{\cdot}3H_2O_{\ (s)} + Ca(OH)_{2\ (aq)}$$

The C-S-H gel holds together the aggregate and the unreacted solid phases in the source dry cement powder while the gypsum ($CaSO_4{\cdot}2H_2O$) added to the cement as a set retarder reacts hydrothermally to form $Ca_3(Al,Fe)_2O_6{\cdot}CaSO_4{\cdot}12H_2O$ (AFm, for Al-Fe-monosulfate) and $Ca_3(Al,Fe)_2O_6{\cdot}3CaSO_4{\cdot}32H_2O$ (Aft, for Al-Fe-trisulfate; ettringite) during curing of the cement. Though much of the reaction occurs within about the first 15 hours, completion of the hydration reactions takes extended times (on the order of hundreds of days), continuing to release $Ca(OH)_2$ from the tri- and dicalcium silicate, Ca_3SiO_5 and Ca_2SiO_4, and form more C-S-H gel while the cement pore waters remain saturated with respect to portlandite, $Ca(OH)_2$.

4.2 Concrete Carbonation Reactions

The carbonation process of concern raised in the PIRT analysis is the reaction of the dissolved $Ca(OH)_2$ within the concrete with carbon dioxide gas (subscript g) from the air to form solid calcium carbonate, $CaCO_3$, phases:

$$Ca(OH)_{2\ (aq)} + CO_{2\ (g)} \rightarrow CaCO_{3\ (s)} + H_2O_{\ (l)}$$

The $CaCO_3$ phase being formed is either aragonite or vaterite (polymorphs of $CaCO_3$; Slegers and Rouxhet 1976) or calcite, another $CaCO_3$ polymorph, and vaterite, which slowly transforms to calcite (Lagerblad 2006).

The decomposition of concrete with carbonation involves the conversion not only of the $Ca(OH)_2$ to $CaCO_3$ but also the decomposition of the C-S-H gel and the AFm and AFt phases. The diagenesis of cement with the progression of carbonation is shown in Table 3 (Lagerblad 2006). It is seen that the various phases in the cement disappear and are replaced by other phases as the carbonation reactions progress. Ordinarily, the first phase to disappear is $Ca(OH)_2$, and it is replaced by $CaCO_3$. The $Ca(OH)_2$ acts as a pH buffer and supplier of calcium ions in solution. The existence of the finely grained C-S-H gel is jeopardized by the ingress of CO_2, and the gel begins to break down, yielding its calcium ions to react with CO_2 to form $CaCO_3$ and amorphous silica, $SiO_{2\ (am)}$ (Slegers and Rouxhet 1976). The C-S-H itself remains physically intact until the $CaO\text{-}SiO_2$ ratio falls below about 1.0 at about pH 12.5 (Lagerblad 2001). The AFm [$Ca_3(Al,Fe)_2O_6{\cdot}CaSO_4{\cdot}12H_2O$ or monosulfate] phase then is attacked as the pH falls below about 11.6 and forms AFt [$Ca_3(Al,Fe)_2O_6{\cdot}3CaSO_4{\cdot}32H_2O$ or ettringite] plus $CaCO_3$ and $[Al,Fe(III)](OH)_3$. The AFt is lost between pH 11.6 and 10.5 to form more $CaCO_3$ and $[Al,Fe(III)](OH)_3$.

Table 3: Changes in Cement Composition with the Progression of Carbonation

Phases and Conditions Present in the Progression of Carbonation				
Intact Concrete	**First Stage**	**Second Stage**	**Third Stage**	**Fully Carbonated**
$Ca(OH)_2$	–	–	–	–
C-S-H	C-S-H (1)	C-S-H (2)	C-S-H (3)	$SiO_{2\,(am)}$ (with some CaO)
–	$CaCO_3$	$CaCO_3$	$CaCO_3$	$CaCO_3$
AFm	AFm	AFt/$(Al,Fe)(OH)_3$	$(Al,Fe)(OH)_3$	$(Al,Fe)(OH)_3$
AFt	AFt	AFt	$(Al,Fe)(OH)_3$	$(Al,Fe)(OH)_3$
pH ≥12.5 [(a)]	pH <12.5	pH <11.6	pH <10.5	pH <10
(a) The pH of saturated $Ca(OH)_2$ solution is 12.5; other alkalis (e.g., NaOH) will raise the pH.				

4.3 Measuring the Extent and Rate of Carbonation

Because the portlandite is more alkaline than the product $CaCO_3$, the progression of carbonation of cement can be followed by measuring the pH of the pore water in the cement. This is conveniently monitored in the field by using the pH indicating dye, phenolphthalein. The dye color is magenta above pH 9 and colorless below this pH. Because of the higher alkalinity and solubility of $Ca(OH)_2$ compared to $CaCO_3$, no color indicates complete carbonation or conversion of $Ca(OH)_2$ to $CaCO_3$ while the magenta color indicates the presence of at least some $Ca(OH)_2$.

Phenolphthalein and thermal analysis studies of carbonation depth in 36-year-old concrete in the United Kingdom were made from both exterior and interior surfaces (Parrott and Killoh 1989). The complete carbonation of the interior surface, relevant to the containment structures exposed during a LOCA, was found by the phenolphthalein test to occur to a depth of 25 mm while thermal analyses showed partial carbonation continuing from a 20- to 65-mm depth. The zone of partial carbonation indicates the onset of decomposition of the C-S-H gel, which is unstable in the absence of accompanying $Ca(OH)_2$.

The concrete exposure conditions of temperature, moisture, contact (e.g., to gas, soil, water), atmosphere (including CO_2 partial pressure), surface coating, and the strength class of the concrete all affect the rates and degrees of carbonation. These effects were surveyed and the results applied to a diffusion-controlled carbonation rate law having a parabolic form, i.e., rate proportional to the square root of the exposure time (Lagerblad 2006). The depth of carbonation, d_c, thus follows a rate law of the form:

$$d_c = k\sqrt{t}$$

where k is the rate constant, and t is the time in years. According to the surveyed experience, for high-compressive-strength (>35 MPa) industrial concrete with indoor exposure to normal humidity air, the rate constant, k, has a nominal value of 3.5 mm/year$^{0.5}$ (Lagerblad 2006) with the rate constant decreasing with increasing strength (Figure 1, Table 11, and related references in Pade and Guimaraes 2007).

Painting may affect the rate of concrete carbonation, but the effects can either retard the carbonation rate slightly or enhance the rate. Thus, a correction factor of 0.7 on the rate expression is suggested for indoor house concrete (where k = 6 mm/year$^{0.5}$) and 0.9 for outdoor house concrete (where k = 4 mm/year$^{0.5}$ if sheltered, 1.5 mm/year$^{0.5}$ if exposed to the weather), both retarding the carbonation rate compared with bare concrete for these house concretes that have lower strength than the high-strength infrastructure concretes used in reactor containment. No distinction among paint types (e.g., alkyd, latex, epoxy) is made (Lagerblad 2006; Sections 5.1.2 to 5.1.3).

The effect of painting high-strength infrastructure concrete, such as that used in the reactor containment, is a balance between CO_2 diffusion inhibition caused by some coatings and the diffusion enhancement provided by other coatings (e.g., silane and siloxane) by dehydrating and opening the concrete pores. The overall correction factor is judged (Lagerblad 2006) to be a factor of 1.0 for infrastructure concrete, i.e., no acceleration or retardation is accorded the coating compared with bare concrete. Based on these assessments of the effects of concrete coatings, and for conservatism in the present analysis, a factor of 1.0 is used for the present evaluation.

The carbonation depth equation may be checked against the analyses reported in the prior testing of 36-year-old concrete by Parrott and Killoh (1989). The full carbonation depth as determined by calculation is $d_c = k\sqrt{t} = (3.5\,\text{mm/year}^{0.5})\sqrt{36\text{ years}} = 21\text{mm}$ and compares well with the 25-mm fully carbonated depth found by measuring field-aged material.

The approximate depth of carbonation expected for concretes in the containment buildings of PWRs, whose times since construction are on the order of 35 years, therefore, would be about 21 to 25 mm according to the parabolic rate equation (Lagerblad 2006) and the measured value of a 36-year-old field specimen (Parrott and Killoh 1989). It is noted that the rate equation-predicted depth of carbonation increases only from 19 mm to 22 mm following 30 to 40 years of air exposure, respectively, the range of the age of most PWRs.

Carbonation also occurs underwater. The rate constant, k, for the depth of carbonation for wet or submerged high-strength concrete surfaces at ~10°C is 0.5 mm/year$^{0.5}$ (Lagerblad 2006). The carbonated depth for the immersed concrete at 30-days' exposure to 10°C water thus would be ~0.14 mm. Under the 60°C ICET conditions, the rate of carbonation would tend to be lower because of the lower intrinsic solubility of CO_2 in water at 60°C (about ⅓ of that at room temperature) and higher because of the increased reaction rates usually observed for increased temperatures. The net effect on the carbonation rate likely is negligible based on the lack of temperature effect in the water-mediated carbonation rate of $Ca(OH)_2$ in humid nitrogen (Shin-Min et al. 1999). Furthermore, as would be true in the containment building during a LOCA, active air exchange does not occur, and the LOCA begins with an alkaline spray that would scrub the CO_2 from the air space. The amount of atmospheric CO_2 available in the ~2000-liter vapor space of the ICET vessel (compared with ~950 liter water volume) would be about 0.027 moles and would be scrubbed to much lower levels by the initial alkaline spray. This amount is negligible compared with the ~3.7 moles of $Ca(OH)_2$ present in fresh concrete in each coupon (see the following section).

Therefore, for the purposes of this evaluation, it is assumed that the amount of concrete coupon carbonation occurring during a 30-day period of 60°C water immersion is insignificant based on the carbonation rate and CO_2 availability. As a result, the additional carbonation of the coupons caused by absorption of dissolved CO_2 during immersion in the ICET experiments would be

appreciably lower than the carbonation that already occurred from the prior 3 to 11 months of air exposure.

4.4 Carbonation and the ICET Experiments

The depth of carbonation of the concrete coupons prepared for the ICET experiments and left exposed to air before testing can be predicted because the exposure time is known to range from 3 months (for ICET #1) to 11 months (for ICET #5). The depth of carbonation for the ICET #1 coupon thus is about 1.75 mm. The ICET #5 coupon carbonation depth is predicted to be 3.35 mm. As discussed in Section 4.3, the contribution from underwater carbonation is negligible.

Overall, the total carbonation occurring in the relatively fresh concrete coupons during the ICET experiments is expected to be small (from ~1.8 to 3.4 mm) in comparison with the depth of carbonation of concrete in PWRs (~20 to 25 mm). However, the carbonation of the concrete dust (21.2 grams; Dallman et al. 2006) used in the ICET testing is assumed to be complete as the particles are relatively small compared with the ~1.8- to 3.4-mm penetration of the carbonate front predicted by air exposure.

These rate data and information on the dimensions and properties of the concrete coupons are combined to determine if significant bias was introduced in the ICET experiments by using relatively fresh concrete coupons instead of aged coupons.

According to the ICET operations, the dimensions of each concrete coupon were 12×12×2 in. (30.48×30.48×5.08 cm) to give 384 in.^{2} or 2,480 cm^2 surface area. The immersed area of the concrete coupon was 100% of the total or 2,480 cm^2 (Dallman et al. 2006).[(4)] The volume of carbonated concrete subject to immersion ranges from 430 cm^3 (and a mass of ~1,030 grams at a density of 2.4 g/cm^3) for ICET #1 to 800 cm^3 (~1,920 grams) for ICET #5. If the concrete had been aged and carbonated to a depth of 21 mm, the carbonated volume and mass would be ~5,210 cm^3 and 12,500 g, respectively.

The concrete composition used in the ICET experiments is ~17.4 wt% Portland cement, and the Portland cement is 62.7 wt% CaO or 44.8 wt% calcium (Appendix B of the Consolidated Data Report; Dallman et al. 2006). Therefore, the weight fraction of calcium, from cement, in the concrete coupons used in the ICET experiments is 0.078 (7.8 wt%). Based on studies of fully carbonated concrete, the fraction of calcium that remains not carbonated in the cement is 0.24 (page 10 of Lagerblad 2006); i.e., 0.76 of the calcium in fully carbonated cement is transformed to $CaCO_3$. The weight fraction of calcium that is present in fully carbonated concrete thus is 0.059 to yield 14.8 wt% $CaCO_3$ in fully carbonated concrete. This is equivalent to 3.55 moles $CaCO_3$ per liter of fully carbonated concrete. The $CaCO_3$ solubility in the saturated pore water is ~0.00014 M (Lide 2007).

The concentration of $Ca(OH)_2$ in non-carbonated cement paste is 4.35 M (Table 6 of Bary and Sellier 2004). Assuming that the density of cement paste is 2.3 g/cm^3 (slightly lower than that of cured concrete; i.e., aggregate sinks slowly in curing concrete) and with the cement being 17.4 wt% of the concrete coupons prepared for the ICET experiments (equivalent to 18.1 volume %), the cured non-carbonated concrete in the ICET coupons contains 0.79 moles

(4) Tables within the report describing the ICET experiments show 34% immersion (Dallman et al. 2006). In practice, however, the concrete coupons were 100% immersed in all tests.

$Ca(OH)_2$ per liter of concrete or 3.7 moles of $Ca(OH)_2$ in each concrete coupon. The solubility of $Ca(OH)_2$ in the saturated pore water is ~0.020 M (Lide 2007).

An initial appreciation of the net difference between the conditions of the concrete used in the ICET experimentation and the concrete in the PWR suffering a LOCA is seen by comparing the first and last columns, respectively, in Table 3 and from the calculations of the concrete properties.

The attributes of 3- and 11-month-old concrete coupons used in the ICET #1 and #5 experiments are compared in Table 4 with the attributes of similarly dimensioned ~30- to 40-year aged concrete. Based on the carbonation rate law, $d_c = (3.5\ mm/y^{0.5})t^{0.5}$, the ICET #1 and #5 concrete coupons would be carbonated to a depth of about 1.75 and 3.35 mm, respectively, and thus have undergone about 8% and 17% total carbonation. Had 30- to 40–year-old concrete coupons been used, the depth of carbonation would have been about seven-times deeper and the coupon carbonation would have been about 87% complete.

The outer carbonated layer of concrete, and its contained $CaCO_3$, armors the inner non-carbonated concrete against leaching attack. This is because the $CaCO_3$ as calcite occupies 11% more volume than the source $Ca(OH)_2$ and serves to seal the concrete pores to water intrusion. As shown in Table 4, the $CaCO_3$ also has ~100-fold lower water solubility than does $Ca(OH)_2$. The net effect is that carbonation very quickly drives the concrete surface chemistry to be controlled by $CaCO_3$. The question then becomes one of diffusion of $Ca(OH)_2$ through the $CaCO_3$ rind and into the solution or diffusion of bicarbonate, HCO_3^-, through the rind and into the coupon. It is not clear which dominates.

Evidently, the armoring effect of $CaCO_3$ was sufficient during the ICET #1 experiment to prevent large-scale leaching of $Ca(OH)_2$. In this experiment, fiberglass insulation was the only added solid phase besides the test coupons, and the pH was controlled to a goal value of 10 (actual pH was ~9.4) in a sodium borate solution.[(5)] The calcium concentrations were found to vary between about 8 and 16 mg/liter and reached a steady concentration of about 12 mg/liter or 0.0003 M (moles per liter). As shown in Table 4, the calcium concentration observed in ICET #1 is closer to that limited by solubility of the calcite, $CaCO_3$, phase (0.00014 M at pH 9.4, a difference of a factor of ~2) than to the concentration had all of the $Ca(OH)_2$ in the submersed portion of the concrete coupon dissolved (0.0036 M, a difference of a factor of 12). If, instead, a 30- to 40-year-old concrete coupon had been used in the ICET #1 experiment, the calcium from dissolving all of the available $Ca(OH)_2$ (0.00051 M; see Table 4) approaches the $CaCO_3$ solubility limitation, and there would be no apparent impact.

The slightly higher calcium concentration observed in ICET #1 than that expected solely from calcite dissolution may be due to limited $Ca(OH)_2$ dissolution from within the coupon. Using aged concrete coupons might have decreased the calcium concentration slightly. It is noted that the calcium contributed from the fiberglass insulation and other sources evaluated during ICET #1 is expected to be negligible compared with that from the more abundant and leachable concrete.

---

(5) Calcium leaches from fiberglass as shown in separate 5-day Nukon glass testing (Jain et al. 2005). However, the straight line increase in total calcium projected to be leached for both fiberglass and concrete by Jain and colleagues (2005) was not observed for fiberglass and concrete together in ICET experiments #1 and #5, which each reached steady state in ~5 days (Dallman et al. 2006).

However, the impact of using aged coupons probably would have been minimal. This is shown by considering the 0.0006-M calcium concentration found for ICET #5, the only other ICET experiment having no other calcium-impacting perturbation (such as TSP addition in ICET #2 and #3, which would decrease calcium concentration, or inclusion of cal-sil solids in ICET #3 and #4, which would increase calcium concentration) beyond that of the concrete coupon. The ICET #5 calcium concentration is higher than observed in ICET #1, but the pH is lower (8.2 in ICET #5 versus 9.4 in ICET #1), enhancing $CaCO_3$ solubility. As shown in Table 4, the expected calcium concentration in equilibrium with $CaCO_3$ at pH 8.2 is 0.0022 M where the observed calcium concentration is 0.0006 M, a difference of a factor of 3.5. If $Ca(OH)_2$ leaching were controlling calcium concentration, the concentration would have been about 0.0033 M, a difference from what was observed by a factor of 5.5.

Table 4: Comparison of ICET Concrete and Aged Concrete Properties

Property	Comparison of Concrete Sources	
	ICET Concrete	Aged Concrete
Dominant simple calcium phase	$Ca(OH)_2$	$CaCO_3$ (calcite)
Equilibrium water pH with dominant Ca phase	12.5	9.4 (under ICET #1) 8.2 (under ICET #5)
Equilibrium [Ca] in pore water, M, for dominant calcium phase	0.020	0.00014 (pH 9.4, ICET #1) 0.0022 (pH 8.2, ICET #5)
Dominant source Ca phase concentration within concrete	0.79 moles $Ca(OH)_2$/liter (non-carbonated concrete)	3.55 moles $CaCO_3$/liter (fully carbonated concrete)
Carbonated depth, cm	0.18 (ICET #1), 0.34 (ICET #5)	2.1
Coupon dimensions, cm	5.08×30.48×30.48	5.08×30.48×30.48
Coupon volume, liters	4.72	4.72
Non-carbonated dimensions, cm	4.73×30.13×30.13, 4.41×29.81×29.81	0.88×26.28×26.28
Carbonated concrete coupon volume, liters	0.43, 0.80	4.11
Non-carbonated concrete coupon volume, liters	4.29, 3.92	0.61
Fraction coupon immersed	1.00	1.00
Water volume, liters	946	946
Limiting [Ca], M, if all available $Ca(OH)_2$ dissolved	(0.79×4.29×1.00/946=) 0.0036 (ICET #1) (0.79×3.92×1.00/946=) 0.0033 (ICET #5)	(0.79×0.61×100/946=) 0.00051
Observed [Ca], M, ICET #1 (pH ~9.4; Volume 2 of Dallman et al. 2006)	0.0003	
Observed [Ca], M, ICET #5 (pH ~8.2; Volume 6 of Dallman et al. 2006)	0.0006	

4.5 Conclusions

The technical and engineering literature was reviewed to investigate the effects of the reaction of CO_2 with concrete and its contained Portland cement (carbonation). The literature show that the $Ca(OH)_2$ present in Portland cement converts to $CaCO_3$ to force ensuing decomposition of calcium silicate hydrate (C-S-H) gel and calcium aluminate/ferrate sulfate (AFt and AFm)

phases also present in Portland cement. The carbonation reaction was shown to change the cement pH and proceed according to parabolic rates.

Based on the carbonation rates found in the technical literature, the predicted effects of use of 30- to 40-year-old concrete coupons in the ICET experiments were determined and compared with the results observed for the 3- to 11-month-old coupons actually used in the ICET experiments with the goal to determine if using aged concrete coupons would have changed the tests' outcomes. The ICET #1 and #5 experiments, which used 3-month and 11-month-old coupons, respectively, were most readily evaluated because they did not have the calcium-perturbing influences of added cal-sil or TSP. The observed calcium concentrations were a factor of ~10 lower than the calcium concentrations expected in the unlikely event that all of the available $Ca(OH)_2$ dissolved from the concrete coupons. Instead, the concentrations observed in both ICET #1 and ICET #5 were within a factor of ~2 to 4 of the concentrations expected for equilibrium with $CaCO_3$ as would be observed for aged coupons. Therefore, the anticipated net impact of using the relatively fresh coupons in the ICET experiments instead of using 30- to 40-year aged (more carbonated) coupons is minimal on both calcium availability and concentration and on solution pH, especially within the 30-day post-LOCA window.

5 TOPIC 3—ALLOY CORROSION

The containment buildings of nuclear power plants are designed to prevent releases of radioactive materials and to remove decay heat from the reactor core in the event of a LOCA. This is in part accomplished through a CSS and ECCS. Continuing to operate these systems depends on recirculating the water collected in a sump, which is protected from the effects of debris by a strainer (Johns et al. 2005; Shaffer et al. 2005; Ghosh et al. 2007). In the few (non-LOCA BWR) incidents of strainer blockage, the primary material found clogging the strainers was fibrous insulation debris along with suppression pool sludge. The sludge was mostly iron oxide particulate resulting from agitation of the suppression pool water. For the 30-day core cooling needed after a LOCA event, an additional contribution to debris plugging may be the formation of corrosion products from exposed metal surfaces that are submerged in coolant solutions. The post-LOCA water constituents intended, for example, to retain the iodine in alkaline CSS spray may favor metal corrosion and generation of precipitates.

The issue of the effect of different alloys on the quantity of metal corrosion products generated in the post-LOCA period was raised in Sections 5.3.3.2.3 and 5.3.5 of the PIRT document (Tregoning et al. 2007). The effective generation rate for additional corrosion products is governed by 1) the coolant chemistry, 2) coolant flow and temperature conditions, and 3) the exposed metal surface areas. Studies have been done to measure or model corrosion rates and speciate corrosion product for materials present in containment (Griess and Bacarella 1971; Jain et al. 2004; Dallman et al. 2006). This section reviews the main results of recent work (Dallman et al. 2006), reviews the influence of varying alloy compositions on corrosion rate, and indicates possible areas for further study on the generation of corrosion products in post-LOCA conditions.

The materials and exposed surfaces in containment are described in Section 5.1, and the properties of the coolant solution are provided in Section 5.2. The conclusions arising from consideration of alloy effects are given in Section 5.3.

5.1 Materials and Exposed Surfaces in Containment

The primary source of corrosion materials is likely to be pre-existing sources, such as RCS crud and corrosion products dislodged from the exterior surfaces of carbon steel piping (e.g., reactor vessel, steam generators, and pressurizer) that are wetted from the CSS. The interaction of the exposed containment materials with the coolant solutions could cause additional corrosion products to form. Table 5, excerpted from the ICET test plan (Andreychek 2005), summarizes the types of materials and percentages of surface areas potentially exposed to ECCS water during a post-LOCA event and serves as guidance for materials considered in recent corrosion testing. Previous work by Griess and Bacarella (1971) considered the corrosion of the Table 5 materials in reactor ECCS solutions. The more recent work (Dallman et al. 2006) considers solutions thought to be more representative of the post-LOCA conditions.

Table 5: Percentage of Surface Areas below Containment Flood Level
(Andreychek 2005)

Material	Submerged, %	Comment
Zinc galvanizing	5	The submerged value accounts for grating and duct work that might be submerged.
Zinc coatings	4	Addresses both non-topcoated zinc primer applied as a non-topcoated system as well as zinc primer exposed as a result of delamination of topcoat.
Aluminum	5	Aluminum is generally not located at elevations inside containment where it may be submerged.
Copper	25	Majority of surface from control rod drive mechanism, CRDM, coolers and instrument air lines. [(a)]
90-10 Cu/Ni	25	Majority of surface present in containment fan coolers.
Concrete	34 [(b)]	The submerged value accounts for limited damage to floor and wall surface areas that will be submerged due to RCS piping being elevated above the containment floor.
Carbon steel	34	Structural components and piping.
Fiberglass	75	The submerged value accounts for most of the insulation material fiberglass to remain in areas where it will wash down into the sump pool.
Calcium silicate	75	The submerged value accounts for most of cal-sil to remain in the areas where it will wash down into the sump pool.

(a) The magneto windings in the CRDM have copper; the CRDMs themselves do not have copper or copper alloys. Copper grounding straps are also significant and considered in more detail in Section 6 on galvanic corrosion.
(b) Note that the concrete coupons in the ICET experiments actually were completely (100%) immersed.

5.2 Conditions of Coolant Solution

During a LOCA event, the chemical corrosion environment is generated by the interaction of containment materials with coolant solutions that contain dissolved boron to maintain sub-criticality and that are chemically buffered above pH 7 to retain iodine fission product gas. The impact of coolant solution chemistry on containment material surfaces has been studied as part of the ICET experiments. The principal coolant conditions associated with ICET experiments #1 to 5 are summarized in Table 6.

The inductively coupled plasma spectroscopy (ICP) analyses for the elements found in the precipitates generated during ICET experiment #1, with the carbonate value obtained by separate titration, are shown in Table 7. The analytes accounted for 55%, 84%, and 78% of the total sample composition with the balance attributed to oxygen [hydroxide also might account for some of the balance, such as for $Al(OH)_3$].[(6)] The main components of the precipitate are carbonate, aluminum, boron, sodium, and some calcium. Various sodium borates were observed by X-ray diffractometry. The ICP results indicate that the most significant interaction is that of the coolant solution with concrete or with aluminum surfaces. The presence of other

(6) The digestion method used to prepare the ICP samples was not described (Dallman et al. 2006), but it is almost certain that only acid digestion was used. If so, silicate dissolution is limited to its solubility in acid (~10^{-3} moles/liter), and silicon results most likely are understated.

corrosion products containing iron, copper, nickel, and zinc seems to be very small (<1%), at least for the composition of precipitates from ICET #1.

Table 6: Experimental Conditions in the ICET Tests

Test #	Total Boron, mg/L	NaOH Added, mg/L	TSP [(a)] Added, mg/L	Borax [(b)] Added, mg/L	Test pH Range	Insulation Material	
						Fiberglass	Cal-sil
1	2,800	7,677	–	–	9.3–9.5	100%	–
2	2,800	–	4,000	–	7.1–7.4	100%	–
3	2,800	–	4,000	–	7.3–8.1	20%	80%
4	2,800	9,600	–	–	9.5–9.9	20%	80%
5	2,400	–	–	1,060	8.2–8.5	100%	–

(a) As $Na_3PO_4 \cdot 12H_2O$.
(b) As $Na_2B_4O_7 \cdot 10H_2O$.
From Dallman and colleagues (2006) and Klasky and colleagues (2006). Further details on solution composition are given in Table 11 and Table 12 of the present report.

Table 7: Composition of Precipitates from ICET #1 Results

Analyte	Concentration, ppm by Weight		
	11/27 Precipitate (Day 6)	12/08 Precipitate (Day 17)	12/17 Precipitate (Day 26)
CO_3^{2-}	208,000	169,000	217,000
Al	38,600	99,600	89,200
B	125,000	202,000	139,000
Ca	3,980	3,800	3,660
Cu	145	126	118
Fe	ND	5	ND
Pb	ND	ND	ND
Li	9	9	ND
Mg	63	34	28
Ni	1	1	2
K	310	354	359
Si	733	754	422
Zn	76	6	ND
Na	17,000	363,000	334,000
Total, wt%	55	84	78

ND = not detected.
From Dallman and colleagues (2006) and Klasky and colleagues (2006).

A summary of ICET general corrosion results for all tests is given in Table 8. Aluminum was the only material with significant weight loss. For Test #1, about 25% of the aluminum coupon was lost compared with only about 2% for the uncoated steel, which had the second greatest weight loss. This result has prompted further study to focus on the properties and behaviors of aluminum surfaces in post-LOCA environments (Zhang et al. 2005; Klasky et al. 2006). The weight gain for concrete is likely due to absorbed water. Although by convention, metallic corrosion is defined in terms of the loss of metal, the metal coupons were not cleaned in the ICET experiments. As a result, the weight gain for most metallic surfaces likely is due to the accumulated corrosion products and/or non-corrosion mineral deposits after exposure.

Since the mineral deposits are not associated with metal loss on the sample, weight-gain data should not be used unless the goal is to measure the propensity toward deposition.

Table 8: Mean Weight Gain/Loss Data for Submerged ICET Coupons

Coupon Type	Initial Weight, g	Weight Changes, g, for ICET Experiments				
		#1	#2	#3	#4	#5
Copper	1,317.3	0.1	<0.1	0.3	0.2	-0.2
Inorganic Zinc	1,625.2	3.1	3.8	1.8	2.3	1.6
Galvanized Steel	1,054.83	0.0	28.6	15.0	0.3	0.1
Aluminum	392.0	-98.6	-0.9	0.6	0.0	-11.2
Uncoated Steel	1,025.2	-23.3	1.4	-1.1	0.2	0.0
Concrete	8,586	233.0	240.7	180.5	239.6	225.9
From Dallman and colleagues (2006) and Klasky and colleagues (2006).						

As noted by Klasky et al. (2006):

> Corrosion in alkaline solutions is an electrochemical process. In a stationary solution, the corrosion rate decreases with exposure time. In a flowing solution, the corrosion rates increase with increasing flow velocity. The corrosion rate is influenced by adding organic and inorganic inhibitors to the alkaline solution and by the addition of some metal elements into the aluminum alloy. Sodium silicates have been found to be an effective inhibitor, with inhibition efficiency almost 100%. Thus, in ICET Test 4, the corrosion of aluminum was inhibited by the dissolution of calcium silicate. All corrosion processes on all metals and alloys in aqueous environments at temperatures below 374°C are electrochemical processes.

The ICET experiments identified the primary sources of corrosion products as well as the conditions that inhibited their generation during the test series (Dallman et al. 2006).

General corrosion rates observed in the ICET experiments were greatest for aluminum (Table 9). Table 9 also shows a bounding calculation of the corrosion product quantities generated based on the submerged containment surface areas as reported by Andreychek (2005). Aluminum clearly dominates the projected quantities of metal corrosion products formed.

It has been postulated that other aluminum alloys may have different corrosion rates than the aluminum alloy used in the ICET experiments. Thus, the type of aluminum alloy might affect the quantity of aluminum solids contributing to strainer plugging under different post-LOCA temperature and chemistry conditions. Although alloying can improve the corrosion resistance of many metals, alloying does not generally improve the corrosion resistance of aluminum. Instead, alloying is used to improve aluminum's strength or workability.

Table 9: Corrosion Product Generation Based on Bounding Areas
(Table 5.1 of Andreychek 2005)

Material	Rate 140ºF, mils/yr [(a)]	Corrosion Product /Metal Volume Ratio [(b)]	Bounding (30-day) Corrosion Product Generation in Containment, m^3
Zinc galvanizing	2	1.27	0.006
Zinc coatings	2	1.27	0.01
Aluminum	126	1.69	1.43
Copper; 90/10 Cu/Ni	0.2	3.39	0.002

(a) Jain and colleagues (2005).
(b) Ratio of corrosion product to source metal volumes based on material densities (Lide 2007).

In general, it has been observed that pure aluminum, 99.0% or purer (the 1000 alloys, commonly designated 1xxx), is more corrosion resistant than any of the aluminum alloys (Davis 1999, pp. 33–35). Wrought alloying elements include copper (the 2xxx alloys), manganese or magnesium-manganese (the 3xxx alloys), silicon (the 4xxx alloys), magnesium-chromium or magnesium-manganese-chromium (the 5xxx alloys), magnesium-silicon (6xxx), or zinc-magnesium or zinc-magnesium-copper (the 7xxx alloys). The composition of the alloy used in the ICET experiments [given in note (4) of Table B-5 of Dallman et al. 2006] is consistent with the 3003 alloy (ASTM 2007).

Reportedly, of these, only the 5xxx alloys approach, or may possibly slightly exceed, the general corrosion resistance of the 1xxx (pure aluminum) alloys. Magnesium increases the resistance of aluminum to general corrosion in high pH solutions to a small extent, although it may increase susceptibility to stress corrosion cracking and corrosion along grain boundaries (Craig and Anderson 1995, pp. 16–18).

However, specific studies of aluminum-alloy corrosion under conditions similar to those expected under certain post-LOCA environments, ~0.15 M sodium hydroxide (NaOH) containing ~0.28 M boric acid (H_3BO_3; equivalent to 3000 ppm boron), have been performed (Griess and Bacarella 1971). The corrosion resistance was tested in spray and immersion at 55°C (131°F) and 100°C (212°F). The 1100, 3003, 5052, and 6061 alloys were tested at 100°C, and these alloys plus alloys 5154 and 5454 were tested at 55°C. Under 55°C spray conditions, alloys 5052, 3003, and 5454 were the most corrosion resistant followed by, in order, 6061, 1100, and 5154. The differences in corrosion rates were relatively low, however, with the highest rate only about 40% greater than the lowest rate. The corrosion resistance in 55°C immersion tests decreased in the order 5154 ~5454 > 5052 > 6061~3003 > 1100, but again, the difference was small with the highest rate about 70% greater than the lowest rate. For 100°C in spray and immersion tests, the order of decreasing corrosion resistance was 5052 >> 3003~6061 > 1100 (Griess and Bacarella 1971). The performance of the 5052 alloy, particularly at 100°C, was exceptionally good compared with the other alloys tested, such that this alloy was tested at 140°C as well. However, its performance is not representative of most aluminum alloys, including that of the 3003 alloy apparently used in the ICET experiments. Generally, lower corrosion rates were observed in immersion than in spray conditions.

More recent testing compared the corrosion resistance of 3003, 5005, and 6061 aluminum alloys to that of grade 1100 (commercially pure) coupons in 200°F pH 8.0, 2500 ppm boron (as boric acid), for 12 and 24 hours (Reid et al. 2007). The corrosion rates for the 3003, 5005, and 6061 alloys were ~79 to 92% of the rates observed for the commercially pure aluminum, a result

qualitatively similar to that observed by Griess and Bacarella (1971) under comparable conditions. The authors concluded that the impact of alloy composition, with respect to the amount of aluminum corrosion product, is not significant.

The corrosion quantity for the 3003 alloy, based on the ICET findings and on typical conditions within containment, thus is a first-order and likely a realistic estimate of the contribution of aluminum alloy corrosion to the post-LOCA pool solids volume. In the opinion of Reid and colleagues (2007), better identification of the aluminum alloys present in containment and the use of data from those alloys will not significantly alter the amount of aluminum metal corrosion precipitates projected based on commercially pure aluminum corrosion rates.

5.3 Conclusions

With the exception of aluminum, there was little metallic corrosion exhibited during the ICET series. Therefore, for the other metals, it is judged that the potential differences in corrosion rates, mechanisms, and surface areas occurring in the 30-day post-LOCA window would have little relative impact on the total solids loading of the sump strainers compared with the amount of loose solids that already exist in the containment structure (latent debris) or that will be generated as a result of the LOCA (e.g., shredded insulation). Additionally, alloy variation is expected to have little impact on sump strainer loading.

The various aluminum alloys (with the possible exception of alloy 5052) generally have corrosion rates similar to that of the 3003 alloy used in the ICET experiments. Therefore, more detailed consideration of the types and quantities of specific aluminum alloys present in the containment and the use of alloy-specific corrosion rates are not likely to materially influence the aluminum corrosion results already obtained in ICET and other test programs.

6 TOPIC 4—GALVANIC CORROSION

The fourth sub-task requests that further work should:

> Identify galvanic corrosion effects and specific galvanic configurations that could most significantly alter the amounts and types of chemical byproducts observed in NRC and nuclear industry-sponsored single-effect and integrated research on chemical effects.

This question arises from Sections 5.3.3.2.2 and 5.3.5 of the PIRT report (Tregoning et al. 2007).

Conventional galvanic effects occur by the electrical linkage of two dissimilar metals with the corrosion mediated by an aqueous phase to close the circuit. An electrochemical couple arises between the metals with the effect of giving higher corrosion rates to the less-noble component of the couple. Galvanic corrosion results in enhanced attack on the less-noble component of the couple, driven by the large area of the coupled, more-noble component upon which oxygen reduction occurs. The distance from the fusion line (or contact region) between the two components over which corrosion of the less noble component occurs is determined by the throwing power of the ionic current flowing from the anode (the less-noble component) to the cathode (the more-noble component). The magnitude of this current is a function of the conductivity of the environment and the thickness of the thin solution layer on the metal surface for those cases where intermittent wetting occurs. A decrease in both properties leads to a decrease in the throwing power of the current and to a decrease in the current magnitude and of the galvanic corrosion. Furthermore, theory shows that the current density or rate of metal loss on the anode decreases roughly exponentially with distance from the fusion line, so that the damage is concentrated on the anode close to the junction between the two metals.

For PWR containment systems, the outcomes of galvanic corrosion are considered for two cases. In Section 6.1, galvanic corrosion is considered for copper with carbon steel. Section 6.2 considers anodic reversal. Conclusions on these topics are presented in Section 6.3.

6.1 Galvanic Corrosion for the Copper–Carbon Steel Couple

The most likely galvanic couple is that between the copper grounding straps used for large equipment within containment and the connected carbon steel structures that would become submerged in coolant waters under post-LOCA conditions. Because the grounding straps are cathodic with respect to the steel, the carbon steel will form corrosion products in a region locally around the strap connection points. Assuming an affected region of 1 m^2 on each carbon steel surface surrounding the anchoring point of the grounding strap and a total of 100 grounding straps, an affected area of 100 m^2 is estimated. The 1-m^2 affected area is based on the expectation of well distributed corrosion over the carbon steel surface because of the borate coolant solution's high conductivity (Uhlig 1948, pp. 491-492). The 100 grounding straps is a conservative estimate of the number of grounded pieces of equipment within containment. The galvanic couple existing between stainless steel and copper would have copper as the anode, with proportionately much lower surface area, and its contribution to the corrosion product inventory compared to that of the carbon steel is considered to be negligible.

The exchange current density of 0.3 milliamperes/cm^2, considered bounding for iron with galvanic coupling in a salt solution (Uhlig 1948, p. 490), would result in a 100 mils/year corrosion rate or a corrosion depth of ~0.021 cm in the 30-day post-LOCA window. The volume of corroded steel then would be ~21 liters producing ~55 liters (0.055 m^3) of $Fe_2O_3 \cdot xH_2O$ (rust) assuming a particle density of rust of 3.0 g/cm^3. At a bulk density of 2 g/cm^3 (based on the sloughed rust deposit being ~50 volume% liquid water when dispersed in water), 55 liters (0.055 m^3) of rust corresponds to 110 kg of wet solids. Therefore, even taken as an order-of-magnitude estimate, it is likely that only a small amount of corrosion product will be produced from galvanic couplings as compared with aluminum alloy corrosion (1.43 m^3; see Table 9). More importantly, the 110 kg is only a fraction of the ~1,400 kg of crud conservatively estimated to be released during a LOCA (see Topic 8 – Crud Release Effects). Overall, surface areas affected by galvanic effects are limited leading to limited corrosion product contribution from this process to sump strainer clogging.

6.2 Anodic Reversal

A prospective uncertainty in the area of galvanic corrosion is a phenomenon described as "Anodic Reversal." In anodic reversal, the normally protective anodic coating, such as zinc, can become cathodic relative to steel. This issue has only recently been identified, and little relevant information has been located. The anodic reversal phenomenon is discussed in books pertaining to zinc corrosion (Porter 1991; Zhang 1996) and is manifest even at temperatures as low as 55°C. The anodic reversal phenomenon occurs because zinc corrosion products are less adhesive to the underlying parent zinc metal at elevated temperatures. Given this behavior, pits in the zinc coating can occur. If the pit penetrates to the steel at elevated temperature, steel will corrode preferentially to the zinc because the steel is anodic to the zinc at the hot water temperature whereas the zinc is anodic at lower temperature. Alternatively, the zinc coating may be discontinuous and leave an exposed steel surface that is anodic to zinc at elevated temperature.

Although no evidence of anodic reversal was observed in the 60°C ICET experiment temperatures, anodic reversal might occur in initial post-LOCA conditions which can exceed 60°C over the first several days following the LOCA. The influence of insulation covering zinc-coated steel may be low because most containment structure pipe work is stainless or carbon steel with only small amounts of zinc-coated material. However, no literature with respect to GSI-191 containment conditions has been identified. The absence of study of this likely small impact phenomenon under post-LOCA conditions commends it with only low priority for further consideration.

6.3 Conclusions

The impact of galvanic corrosion, expected to be most manifest in the coupling of copper grounding straps to carbon steel in the immersed post-LOCA coolant, on the quantity of metal corrosion products is estimated to be <60 liters. This estimated quantity is judged to be conservative (high) but is insignificant in comparison with the contributions from general corrosion of aluminum described in Topic 3, alloy corrosion or with respect to contributions from latent debris and crud release (Topic 8). The co-precipitation of iron with aluminum hydroxide is not expected to occur and has no net effect on total solids quantity (see Topic 6 on co-precipitation and other synergistic solids formation).

Anodic reversal under higher temperature post-LOCA conditions is an area of some uncertainty with respect to galvanized steel surfaces. However, because of the limited time that the post-LOCA containment pool is at elevated temperatures, this contribution is expected to be less significant than the other, previously described, source terms. The direction and scope of any studies undertaken to reduce this uncertainty remain to be determined.

This page intentionally left blank.

7 TOPIC 5—BIOLOGICAL FOULING

A key unanswered question, that was raised in Sections 5.3.4 and 5.3.5 of the PIRT report (Tregoning et al. 2007) is: *Can microbes grow in the presence of the unique set of multiple stressors found in a post-LOCA environment?* Various extremophilic microorganisms defined herein as bacteria, archaea, fungi, or algae, are capable of growth under one or more of the harsh conditions present in a post-LOCA situation (Pikuta et al. 2007).

The observation of a greenish flocculent material in samples taken from Three Mile Island (Shults 1979) suggests that microbial growth is possible in a post-LOCA environment, although this observation may have been due to the introduction of organic material and microbes from river water. A news article in *Science* (Booth 1987) reported that, following the Three Mile Island accident, defueling was difficult due to low visibility "caused by fine sediment and by the hardy organisms that thrived in the reactor vessel." These reports are anecdotal and vague with regard to the types of microbes present and would not by themselves suggest growth of various microbes is indeed possible in a post-LOCA situation. However, additional information outlined in this section suggests that biological growth can occur in post-LOCA conditions. If such growth of biological organisms occurs in the post-LOCA waters, additional materials can be generated that could contribute to sump strainer blockage.

The topic of biological growth in the post-LOCA system is addressed in this portion of the report. Section 7.1 lists stressors to biological growth while Section 7.2 lists microorganisms that may survive in post-LOCA conditions. The implications and outcomes of these considerations are presented in the conclusions, Section 7.3. The paths of further research are suggested in Section 7.4.

7.1 Biological Stressors

From a microbiological perspective, the stresses in a post-LOCA situation are:

- High radiation environment (1 rad/h and locally higher)
- Very high initial temperature (~130°C)
- Moderately high sustained temperatures (55 to 60°C)
- High concentrations of boron (2,400 to 2,800 ppm)
- Neutral to alkaline conditions, pH 7-12
- Low or no light
- Oligotrophic conditions (i.e., low available fixed carbon and nitrogen)
- Presence of ~10^{-5} M hypochlorite from radiolysis (Topic 1, Section 3.3).

Microorganisms that can survive under one or several of these stressors are known. However, the ability of any microorganism to survive and, further, pose a risk to passage of coolant waters through the sump strainers remains to be considered. Examples of microorganisms that may survive in post-LOCA conditions are considered in the following section.

7.2 Microorganisms That May Survive in Post-LOCA Conditions

The reactor is not a sterile environment. Potential sources of viable microbes (and small amounts of fixed carbon and nitrogen) within the reactor building are dust introduced on a daily basis. In addition, dust, fungal spores, pollen and other airborne organic materials are introduced when the refueling hatch is open. The growth of "slime molds and algae" was observed on "external system metallic surfaces" at Seabrook during several fuel cycles.[7] Thus, the microbes necessary to seed growth in a post-LOCA situation are likely to be present as a result of normal operations and it is impractical to prevent their introduction to the reactor environment.

Many bacteria and fungi capable of growth in high radiation environments have been described. The best studied bacterium is *Deinococcus radiodurans* (Brooks and Murray 1981). Various bacteria have been isolated from the oligotrophic, high radiation conditions found in spent nuclear fuel storage pools, although the growth of these bacteria was very slow under these conditions (Sarro et al. 2005). Radio-tolerant bacteria (Romanovskaya et al. 2002) and fungi (Moore 2001) have been isolated in the soils surrounding Chernobyl and even within the containment structure (Zhdanova et al. 2000). It is likely that radiation-resistant microbes or their spores would be present in virtually any reactor.

Thermophilic and thermo-tolerant microbes are widely distributed in the environment, though most hyperthermophilic organisms reside in unusual locations, like deep sea hydrothermal vents. Prokaryotes (bacteria and archaea) that can grow at temperatures up to 121°C are known with many species that grow in the 80 to 100°C range (Kashefi and Lovley 2003). Eukaryotic microbes, such as fungi, can grow at temperatures up to ~60°C and can survive brief periods at much higher temperatures. Certain bacteria and almost all fungi produce spores that are easily transported by air into any environment and thus they could be introduced pre- or post-LOCA. Spores are hardier than vegetative (actively growing) material. Thus, some spores would likely survive the harsh temperature and pH conditions in the early post-LOCA environment, especially in the surfaces above water. These spores could serve as an inoculum after the harshest conditions had passed.

Boric acid and borate salts are used as preservatives and microbial growth retardants. Nevertheless, bacteria, cyanobacteria, algae, and fungi that can grow in the presence of high borate concentrations are known. The bacterium *A. metalliredigens* was isolated from a leachate pond adjacent to a borax plant where boron concentrations ranged from 2,000 to 3,000 ppm (Ye et al. 2004). Blooms of algae and cyanobacteria were observed on this pond at the time of sampling indicating that both eukaryotic and prokaryotic algae are also capable of tolerating high boron concentrations. Fungi that can grow on wood treated with borax as a preservative have been described in the scientific literature (Cookson and Pham 1995). The fungus, *Paecilomyces variotii*, can grow well in borax solutions at boron concentrations of 1,100 ppm and is still capable of slow growth at 1,700 ppm (Parker et al. 1999). A remarkable strain of the fungus *Penicillium notatum* grew well in media containing 50,000 ppm of boric acid (Roberts and Siegel 1967). Penicillium is a fungal genus represented by various species throughout the world, although this particular strain of *P. notatum* is probably not as widely distributed.

There are prokaryotic and eukaryotic microbes classified as alkaliphilic or alkali tolerant that can grow at a pH as high as 12. One example of an alkaliphilic bacterium is *Alkaliphilus*

([7]) Litman, R. 2007. Personal email communication to Cal Delegard dated December 6, 2007.

metalliredigens (Ye et al. 2004). This bacterium can grow at pH 7.5-11. It is also salt-tolerant and has a metal-reducing metabolism capable of growth with Fe(III), Cr(VI), or Co(III) as electron acceptors. Two examples of alkaliphilic or alkali tolerant fungi are *Acremonium alkalophilum* and *Chrysosporium lucknowense*.

Certain species of microbes can tolerate very low fixed carbon and nitrogen (oligotrophic) conditions and some species thrive only under such conditions. There is no quantitative definition of an oligotrophic condition but it can be loosely defined as carbon source concentrations less than a few hundred parts per million. Oligotrophic bacteria and fungi have been observed to grow on bare concrete walls or stone and other natural or artificial environments where the source of fixed carbon and nitrogen was not apparent (Wainwright et al. 1993). However, some carbon and nitrogen must have been present on the surfaces or captured from volatiles in the atmosphere in order to support growth and the production of biomass. Thus, an inability to identify the sources of fixed carbon and nitrogen in test systems or in the actual reactors does not preclude the growth of microbes in an actual post-LOCA situation. With regard to other nutrients, the amount of phosphorous available in the TSP plants would be highly favorable to microbial growth. Sulfur concentrations could potentially be limiting, although traces of sulfate in the water or leached from the concrete (which contains gypsum, or calcium sulfate dihydrate, admixtures) would likely be sufficient to support growth of microbes. Essential trace metals, such as iron, are unlikely to be limiting in the reactor environment. While it is clear that microbial growth can occur under very low nutrient conditions, extensive growth within the 30-day window considered most relevant to a post-LOCA event seems unlikely, though data regarding this supposition are lacking.

Photosynthetic microbes such as algae and cyanobacteria could also grow under low fixed carbon and nitrogen situations at rates that would certainly be relevant within the 30-day post-LOCA window. Photosynthetic microbes fix CO_2 obtained from the atmosphere. In the case of cyanobacteria (blue-green algae), many species are able to reduce N_2 through the action of the enzyme nitrogenase, such that they can grow in the absence of fixed carbon or nitrogen if sufficient light is available. The presence and level of light in the post-LOCA containment must be taken into account if photosynthetic microbes are to be considered. However, the observation of greenish flocculent material in samples taken from Three Mile Island (Shults 1979) suggests that algal growth may be possible although algae were not specifically observed, and the presence of light where growth was found was not mentioned.

Potential sources of carbon include breakdown products from alkyd (Alion 2007) or other paints (see Topic 10 on organic material impacts) and petroleum-based oils and grease that leak from pumps or are washed from cranes or other mechanical apparatus during a LOCA. If the lubricant reservoirs of one or more of the RCS pumps were penetrated during the LOCA, a potentially large source of fixed carbon, 200 gallons per pump, could be introduced into the reactor environment. This would provide ample fixed carbon for growth of bacteria and fungi. The ability of heterotrophic microorganisms (fungi, bacteria, and archaea) to utilize alkyd paints is largely unknown. There is one reference to fungi capable of growth on surfaces painted with alkyd paints (Upsher 1984). It is reasonable to expect that heterotrophic microbes could grow on alkyd paints since lipases and other esterase type enzymes are common in most microbes. A wide variety of bacteria and fungi are known to be capable of metabolizing hydrocarbons.

As discussed under Topic 1, Radiation Effects, coolant water contains approximately 100 ppm (0.0028M) of chloride. Depending on pH, hypochlorite or hypochlorous acid (OCl^-/HOCl) can form by radiolysis of this coolant water. Radiolysis is expected to yield about 10^{-5} M OCl^-/HOCl from this contained chloride. Although some disinfection of less resistant microbes might occur

at this level of OCl^-/HOCl (see, for example, Tsai and Lin 1999), it would not inhibit all microorganism species. Because the main concern with respect to pump fouling is with potential biofilm growth, the microbes inside the biofilm would be well protected from the hypochlorite once the biofilm was established by organisms resistant to the hypochlorite and other adverse environmental conditions.

The structures of microbial biofilms often impart a protective effect with regard to stress on the microbial biofilm community as a whole. The growth of microbes by attachment to the high surface area insulation materials, fiberglass and calcium silicate, could lead to the formation of biofilms and add to the fouling problem on strainers in the sumps. The fact that these insulation materials are likely to be suspended in the water (75% of this material was considered to be in the submerged fraction in the test cases) suggests that microbial growth on these materials is an issue that should be considered. The formation of biofilms on metal coupons suspended in spent nuclear fuel pools testifies to the ability of bacterial communities to grow under these high radiation and oligotrophic conditions (Sarro et al. 2005).

7.3 Conclusions

There are many microbes that are capable of growth under one or more of the biological stresses discussed above. However, the growth of microbes under the unique combination of stresses in a post-LOCA environment has not been researched. The literature with regard to radiation-resistant, hyperthermophilic and alkali-tolerant microbes is abundant. The literature on microbial boron tolerance is relatively sparse, but it clearly indicates bacteria, fungi, and likely algae exist that can grow in the high boron concentrations expected in a post-LOCA reactor containment. While the available data shows that microbial growth is possible under post-LOCA concentrations of boron, it does not address the probability of microbial growth or the rate of growth for different organisms. The interaction of microbes with inorganic solids also is not known. In other words, it is not known whether the growth rate would be sufficient to foul pump strainers or the pumps themselves within the relevant 30-day time frame.

It is expected that oligotrophic conditions would be the most likely condition in a post-LOCA environment, unless there was a leak of hydrocarbons from pump lubricant oil reservoirs. In the presence of significant hydrocarbon or other fixed carbon sources, microbial growth could occur since boron-resistant, thermophilic, and alkaliphilic microbes exist. Under severely oligotrophic conditions, it is unlikely that heterotrophic microbial growth would be significant within the bulk recirculating water in the 30-day time frame, since biomass accumulation is proportional to the amount of carbon present. However, if oligotrophic microbes formed a biofilm on the pump strainers, they could utilize the low carbon concentrations in the bulk fluid that continuously passes over them to accumulate a locally significant amount of biomass. Finally, keeping natural or broad spectrum artificial light at low levels might be necessary to prevent significant algal growth even under oligotrophic conditions since photosynthetic organisms are not dependent on fixed carbon sources.

Review of the technical literature thus indicates that biological paths may exist to produce accumulations of biological material that could potentially contribute to sump strainer blockage or hinder coolant flows. For these reasons, biological fouling merits further consideration.

7.4 Issues for Further Research

Further studies of bacteria, fungi, and algae could be used to determine how widespread borate resistance is within different taxonomic groups of microbes in the natural world and if the boron concentrations tolerated by these organisms are relevant to a post-LOCA situation. One approach would be to use an enrichment culture. This technique would use soils, compost, or sewage sludge that are rich sources of different types of microorganisms to inoculate water containing 300 to 3,000 ppm boron at neutral or alkaline pH. Multiple sources might be tested to verify coverage of the wide range of microbes available in nature. Potential liquid, solid, or airborne carbon sources in a reactor building (including coatings and lubricants) would be used to provide the carbon source. The isolated borate-tolerant organisms could be tested for temperature, alkaline pH, and radiation resistance.

There appear to be no studies of biological growth under the unique combination of stressful conditions expected in a post-LOCA nuclear reactor containment environment, i.e., high borate, initial thermal shock, high initial temperature, high radiation flux, transiently high pH, low or no light and low nutrient availability. This is a gap in knowledge that may profit from further study. Such a study ultimately would require a laboratory where growth and study of microorganisms in the presence of radionuclides is permitted but could begin by using radiation-generating devices to provide the radiation dose. Further studies then might be considered to determine the potential interactions of the microbial growths, if any, with inorganic solids.

This page intentionally left blank.

8 TOPIC 6—CO-PRECIPITATION OR OTHER SYNERGISTIC SOLIDS FORMATION

Concerns were raised in the PIRT document in Sections 5.4.1, 5.4.2.1, 5.4.2.2, and 5.4.3 that phenomena occurring under post-LOCA conditions might lead to situations affecting coolant flow through the sump strainers or to downstream effects in the coolant pumps by co-precipitation and other synergistic interactions to form solids of greater volume or of significantly different types or properties than were considered under conditions in prior testing (Tregoning et al. 2007). This section addresses phenomena associated with co-precipitation and the synergistic interaction of organic liquids and solids – many arising from coatings (see Topic 10, organic material impacts) – with inorganic solids. Section 8.1 discusses co-precipitation phenomena. The effects of complexation by organic materials on co-precipitation also are addressed in this section. Synergistic solids formation, primarily by physical interaction of water-insoluble organics with inorganic solids, is discussed in Section 8.2 (chemical interactions of organic materials with inorganic materials to cause inorganic agglomeration are discussed in Topic 7). The conclusions drawn from considerations raised in these topics are summarized in Section 8.3.

8.1 Co-Precipitation

Co-precipitation is the incorporation of substances that ordinarily are soluble into solids that do precipitate. By this mechanism, low chemical concentrations of radionuclides which would ordinarily be soluble in solution can be carried by inclusion into larger quantities of precipitating solid phases.

Because of the highly diverse and complex mixture of solid and solution phases present under post-LOCA conditions, co-precipitation of chemical species is certain to occur. In the five ICET experiments, reactions with dissolved species (e.g., calcium, aluminum, silicate, phosphate, borate, carbonate) occurred to form borate, phosphate, and silicate coatings (or evidence of such coatings) on aluminum metal, aluminate coatings on fiberglass, and precipitates of calcium silicate, calcium carbonate, and calcium phosphate. These latter compounds are agents frequently used in coprecipitation reactions. Their impact in the post-LOCA system would be primarily as scavengers of the chemically trace but radiologically important multivalent steel (e.g., ^{51}Cr, ^{58}Co, ^{60}Co, ^{54}Mn, ^{56}Mn, ^{55}Fe, ^{59}Fe, ^{59}Ni, ^{63}Ni, and ^{65}Zn), cladding (^{95}Zr, ^{97}Zr, ^{95}Nb, ^{97}Nb), and other activation products freed from the reactor coolant loop of the PWR and multivalent fission products (^{89,90}Sr, cerium isotopes, ^{125}Sb) from incidental fuel leakage. The effect of scavenging could add to the sump strainer radiolytic load if the scavenged crud products do not settle within containment.

The co-precipitation likely would be lower for the monovalent ^{24}Na activation product and the cesium (Cs) and iodine (I) fission product isotopes which would largely remain dissolved and circulate with the coolant waters. Some inclusion ("imbibing") of dissolved radiosodium and radiocesium could occur in formation of sodium aluminosilicate minerals such as borate sodalite, $Na_6[Al_6Si_6O_{24}]\cdot x(Na,Cs)BO_2\cdot yH_2O$:

$$6\ NaOH + x\ (Na,Cs)BO_2 + 6\ Al(OH)_3 + 6\ SiO_2 + (y\text{-}2)\ H_2O \rightarrow$$

$$Na_6[Al_6Si_6O_{24}]\cdot x(Na,Cs)BO_2\cdot yH_2O$$

or phosphate sodalite:

$$6\ NaOH + x\ (Na,Cs)_3PO_4 + 6\ Al(OH)_3 + 6\ SiO_2 + (y\text{-}2)\ H_2O \rightarrow$$

$$Na_6[Al_6Si_6O_{24}]\cdot x(Na,Cs)_3PO_4\cdot yH_2O$$

depending on the coolant buffer system. Iodide (I^-) or iodate (IO_3^-) also could be imbibed in the aluminosilicates as the corresponding sodium salts. However, the conditions required to form the borate sodalite or phosphate sodalite are strongly alkaline (molar concentrations of NaOH; Barrer 1982) and thus in regimes not attained by the post-LOCA solutions. Cesium is not sufficiently abundant in the coolant to form pollucite, $(Cs,Na)_2[Al_2Si_4O_{12}]\cdot 2H_2O$, another alkali aluminosilicate mineral.

Most likely, some surface adsorption (e.g., ion exchange) or inclusion of the ^{24}Na, ^{137}Cs, or radioiodine in solids will occur (e.g., on soil contamination; concrete surfaces), but the overall uptake of the monovalent cations ($^{24}Na^+$ and $^{137}Cs^+$) is expected to be small. The low uptake is caused by the normally low affinity of monocharged ions for solid surfaces and especially by the highly competitive concentrations of sodium in the coolant (e.g., PWRs using sodium tetraborate or TSP in the ECCS and those PWRs using cal-sil which has high concentrations of contained sodium). Cesium would have higher uptake than sodium because large concentrations of non-radioactive cesium are not present in the solution but the cesium still would have to compete with sodium.

The affinities of cesium for cement and soil have been studied and found to be moderate. The distribution coefficient of cesium onto calcium silicate hydrate [C-S-H; a principal phase in Portland cement, $(CaO)_x\cdot SiO_2\cdot yH_2O$ with a Ca:Si mole ratio, x, of 1.5 for fresh cement] is about 12 ml/g and increases to ~200 ml/g as x decreases to 1 (Viallis-Terrisse et al. 2002; Noshita et al. 2001, pp. 115–122) as would happen for aged concrete (see Topic 2, concrete carbonation). Assuming that the depth of influence of concrete is 2.5 mm and given that the concrete surface / water ratio in the post-LOCA pool is 0.045 ft^2/ft^3 (Andreychek 2005), less than 0.5% of the cesium would sorb onto the concrete at the 12 ml/g distribution coefficient but about 8% sorbs at a distribution coefficient of 200 ml/g. Distribution coefficients for cesium uptake on four different soils at pH 5 to 10, with 0.02 M background calcium, are similar (ranging from 11 to 210 ml/g) to the uptakes found for cement (Giannakopoulou et al. 2007). Highest uptakes are found at pH 8 and for clay soils. Overall, given the high competitive sodium concentrations, much less than 1% cesium uptake from the post-LOCA coolant onto solids is anticipated.

Uptake of radioiodine as I^- or IO_3^- on mineral solids is expected to be negligible, as is borne out by studies of radioiodine mobility in soils, while uptake on organic soil constituents occurs (e.g., Xiangke et al. 2001; Hakem et al. 1996) meaning that some iodine might partition to painted surfaces. Uptake of iodine onto copper metal by surface precipitation as CuI (cuprous iodide) also might occur (Haq et al. 1980).

Complexation by organics arising from the decomposition of paints, plastics, and lubricants in the post-LOCA system also might alter the distribution of the polyvalent activation products to the solid phases. The organic complexants, as will be seen in the following section, are alcohols, simple organic acids, and perhaps aldehydes. None of these, however, are highly potent complexing agents, particularly at the neutral to alkaline pH of the post-LOCA coolant where hydrolysis would be important. The organic complexant effects on co-precipitation of

multivalent radionuclides also would be chemically masked by the abundant calcium present in the systems containing cal-sil and even from the lesser amounts of calcium from concrete. The chemical masking by calcium ions (Ca^{2+}) occurs not only because Ca^{2+} is present in relatively high concentration in the coolant but also because Ca^{2+} possesses high propensity for organic complexation. Therefore, Ca^{2+} is a formidable competitor for any organic complexants and would serve to decrease their impact on redistribution of the polyvalent radioactive activation and limited fission products. The Ca^{2+} also would occupy the organic complexants and prevent their surface complexation with fixed or less mobile inorganic solids.

The painted surfaces slowly release their water-soluble or miscible organics which then will pass with the water through the reactor core and undergo radiolysis. The irradiation dose rates near the fuel core are sufficient to quickly break down the organics to form carbon dioxide (see Topic 10 on organic material impacts). Thus, water-soluble organic species are not expected to have marked effects on the co-precipitation reactions between the trace radionuclides and the bulk solids.

The co-precipitation of aluminum (e.g., from aluminum metal corrosion) with iron (from iron corrosion or from oxidation of Fe^{2+} released from the RCS coolant; see Topic 8 on crud release) also might occur where the Fe^{2+} is readily air-oxidized to Fe^{3+}. Titration experiments show that Al^{3+} and Fe^{3+} do not interact during neutralization or form a mixed solid phase. These experiments also show that Al^{3+} and Fe^{2+} interact and it is likely that the Fe^{2+} is absorbed onto the precipitating Al hydroxide surfaces where it remains susceptible to air oxidation (Bertsch et al. 1989). In any event, the quantity of dissolved Fe^{2+} available in the RCS coolant at the time of a LOCA is very small (on the order of grams; see Topic 8 on crud release). In addition, both aluminum(III) and iron(III) have abysmally low solubilities as their respective hydroxides in pH-neutral solutions (~10^{-7} moles/liter, Wefers and Misra 1987, and ~10^{-9} moles/liter, Liu and Millero 1999, respectively, at pH 7). Thus, no appreciable enhancement of their combined solids quantities would transpire even if co-precipitation did occur.

8.2 Synergistic Interactions of Organic Materials with Inorganic Solids

The greatest previously unconsidered contribution to the nature and mobility of solids that can reach the sump strainers would be that provided by the combination of water-immiscible organics arising from paint and plastic decomposition (Topic 10, organic material impacts) with the inorganic solids contributors such as the fiberglass and cal-sil insulation, the concrete and other dust particles, the corrosion solids, and the inorganic precipitates. Contributions of organic lubricants (leakage of lubricant from one back-up RCS coolant pump; estimated 200 gallons from rupture of one such tank) and other mechanical equipment lubricants also would add to the organic loading. If the post-LOCA pool level is higher than the top level of the strainers, the floating organics would not be pumped past the core fuel and suffer complete radiolytic destruction to form carbon dioxide. If the pool level is lower than the strainers, the floating organic liquids, unless filtered and retained on the debris bed, could pass the strainers, and, with sufficient turbulence, be carried by the water to encounter the high radiation fields around the fuel and be converted to carbon dioxide.

The interaction of immiscible organics from paint or plastic decomposition and lubricants with inorganic solids could cause enhanced dispersion of the inorganics within the water column in analogy with the observation of organic-mineral-aggregates (OMAs) in studies of crude oil spill interactions with natural minerals (Li et al. 2007). In these studies, fine mineral solids interact

with crude oil to form OMAs, increasing the concentration of suspended solids in the water column under the highly mixing wave action conditions occurring in near-shore marine areas.

For most tests, 0.6-μm particle-size kaolin was used as the prototypical mineral and mixed with light crude oil in filtered natural seawater. The resulting OMA particle sizes were about 50 μm. With the addition of a marine oil spill chemical dispersant[(8)] to the mixture of oil, seawater, and kaolin, the particle size decreased to about 10 μm but the solids loading in the water column further increased.

As stated by Li and colleagues (2007):

> The effect of mineral fines increases the suspended particle concentration in the water column and droplet stability; once formed, OMAs neither readily breakup further nor recoalesce after dispersion. The synergistic effect of dispersants and mineral fines enhances the transfer of oil from the surface downward into the water column; and a large number of small particles is produced as a result of interaction of dispersants and mineral fines with crude oil. The small particles tend to be suspended in the water column rather than settle down to the bottom because of the hydrodynamic mixing.

The interactions of oil with minerals other than kaolin have been observed in both natural marine and fresh water conditions. It has been found that the formation of OMAs is seemingly little affected by the mineral type (ranging from various calcareous minerals such as calcite and aragonite, to quartz and smectite clays) or the water salinity (Owens and Lee 2003).

It is highly plausible, therefore, to expect that significant interaction of the dispersed organic coatings and lubricants will occur with the significant inorganic solids burden present into the coolant in the post-LOCA period. Like the case with OMAs observed in oil spills in nature and in laboratory conditions, similar interactions could be expected under post-LOCA conditions to increase the particle size and cause the paint, other coating, and lubricant organics to buoy the concrete, dust, insulation (cal-sil and fiberglass) mineral solids, and their alteration products.

The buoyancy interaction would serve to decrease the density of the solid inorganic particles that otherwise would cause the solids to settle in quiescent areas of coolant flow within the reactor containment building and thus increase their transport to the sump strainer. At the same time, the organics, which to a large extent would float on the surface of the post-LOCA coolant and perhaps collect at the upper wetted regions of the sump strainer, would be weighed down by their denser inorganic load and be carried at various depths in the flowing coolant. This mixing of organic and inorganic materials is analogous to the formation of the OMA suspensions in marine and fresh waters, which act to “float” the inorganic minerals and “sink” the crude oil, delivering more of both to the intermediate water column.

The net effect in the post-LOCA coolant thus would be to increase the quantity of solids behaving at near-neutral buoyancy, increasing their flow to the sump strainers while increasing the size of the particles being delivered to the sump strainers. Both effects work to the detriment of flow through the sump strainers by increasing the quantity and particle size of the solids. The smaller organic/inorganic accretions passing the sump strainer would then pass the fuel and be irradiated, resulting in radiolytic decomposition of the organics assuming negligible attenuation or acceleration caused by the physical association of the organic/inorganic particles.

---

(8) Corexit 9500® oil spill dispersant, Nalco Energy Services, PO Box 87, Sugar Land, TX.

The post-LOCA coolant, containing organics (from paints, plastics, materials associated with fiberglass insulation, and lubricants) and inorganic solids from thermal insulation (fiberglass and cal-sil), concrete, and latent debris dust thus shares many similarities with the observed formation of OMAs from oil spills under widely varying natural conditions of temperature, salinity, oil type, and mineral type. The organics serve to buoy the inorganics to make them more transportable to the sump strainer and also create deformable particles in a mixture in sizes that, once transported, potentially offer greater obstruction to the flow.

The combined effect of organics acting as solids collection agents and as aids to flotation leads to significantly different types and properties of water-borne solids than have been observed to-date in separate effects or integrated testing performed under NRC sponsorship or by the nuclear industry. Because the extent of the interaction would not be known from first principles, experiments targeted to the effects of organic coatings to act synergistically with inorganic solids could be used to evaluate this effect. The organics to be considered in such tests include peeled paint, water-immiscible or insoluble species arising from paints, RCS pump lubricant, other lubricants, and their primary hydrolytic and radiolytic products.[9]

Solvents from the paints and their hydrolytic and radiolytic decomposition products likely also will report to the coolant in the post-LOCA period (see Topic 10 on organic material impacts for details on organic hydrolysis and radiolysis). Solvents will include toluene ($C_6H_5CH_3$) and xylene [$C_6H_4(CH_3)_2$] and their phenolic radiolytic decomposition products. Phenolics are phenyl alcohols, the prototype being phenol itself, C_6H_5OH. Thus, cresol [$C_6H_4(OH)CH_3$] and xylenol [$(CH_3)_2C_6H_3OH$] would form, respectively, from radiolysis of toluene and xylene. Other paint vehicles that could report to the post-LOCA coolant include perchloroethylene (Cl_2CCCl_2), methyl ethyl ketone (MEK, $CH_3COCH_2CH_3$), methyl isobutyl ketone [MIBK, $CH_3COCH_2CH(CH_3)_2$], methyl amyl ketone [$CH_3CO(CH_2)_4CH_3$], organic esters [e.g., *n*-butyl acetate, $CH_3(CH_2)_3O_2CCH_3$], simple alcohols [methanol, CH_3OH; ethanol, CH_3CH_2OH; and isopropanol, $HOCH(CH_3)_2$], and numerous others. The ketones and particularly the alcohols and esters may hydrolyze under the hydrothermal and radiolytic conditions to form the corresponding organic acids. Organic binders from fiberglass insulation also were postulated to be present in ICET experiments based on a persistent non-precipitating yellow color in the test solutions but the speciation and concentrations of the organics were not determined (Dallman et al. 2006). The water-soluble intermediate organic acids would be short-lived, however, and undergo continued radiolysis in passing the core to form, ultimately, carbon dioxide.

The phenolics are known constituents of crude oil and thus might be expected to interact with the inorganic solids load in the post-LOCA coolant based on observations in simulations of oil spill interactions.

The interactions of the other lower molecular weight solvents or paint vehicles or their breakdown products with the inorganic constituents are not known. It seems plausible, however, that if they are not immediately dissolved or dispersed in the water (where they would continue past the core and undergo destructive radiolysis) they would at least act in ways that cause them to be included in paint formulations and soften the more polymerized organics and make them more amenable to incorporating inorganic solids. The smaller organic molecules, which may have acted to stabilize dispersions of the insoluble organics into the aqueous phase,

(9) The authors are aware that 30-day integrated head-loss testing, including simulated RCP lubricant oil reservoir failure and including grease samples, has been performed and showed no significant head loss early in the test. However, the full test conditions and results have not yet been published.

again would more likely be carried in dissolved or dispersed form with the water and past the core where they would undergo radiolysis to form carbon dioxide.

8.3 Conclusions

Changes in solids formation and quantities between ICET experimental conditions and actual post-LOCA conditions wrought by co-precipitation or other synergistic effects were considered. The principal agents of change were expected from organics introduced by paints, plastics, and lubricants and their primary hydrolytic and radiolytic products.

The organics arising from these sources, including their hydrolytic and radiolytic breakdown products, were judged to be generally poor complexants that would not compete effectively with hydrolysis (discussion of organic breakdown is provided in more detail under Topic 10 on organic material impacts). If complexants did form, they would be chemically masked from interacting with radioactive activation or fission products or undergoing surface complexation on fixed inorganic solids by the much more abundant dissolved calcium ions. This masking is expected to occupy and consume any complexants that do form. Therefore, it is much more likely that the water-soluble organic complexants would proceed with the water past the fuel core to undergo complete radiolysis to form carbon dioxide.

Most of the radionuclides would be captured by the many varied solid phases by co-precipitation and other mechanisms. Lesser distribution to solid phases of monovalent radionuclides such as those of sodium, cesium, and iodine would occur. The radionuclide deposition to solid phases already was considered in dose source distribution.

In contrast, synergistic interactions of the water-immiscible organics with the inorganic solid phases have not been adequately considered in prior experimental studies. The water-immiscible organics include peeled paint and longer-chain oils from paint as well as RCS and other lubricants. The impact of the water-immiscible (and floating) organics would be greatly affected by the level of the sump strainers with respect to the surface level of the post-LOCA coolant. If the sump strainers are higher than the coolant-air surface, and with sufficient turbulence, the floating organic liquids and the smaller organic particles will be carried by the water to pass through the strainer, proceed to the core, and undergo complete radiolytic degradation to form carbon dioxide. If the strainers are lower than the coolant-air surface, the floating organics survive and are free to interact with inorganic solids.

The interactions of the organics with the inorganic solids have analogues in oil spills in marine and freshwater environments, and the technical literature on this subject offers meaningful parallels to the post-LOCA situation where the organics will act as inorganic solid particle collection agents and as aids to solids flotation or increased buoyancy. Both of these effects can have detrimental impacts on sump strainer performance. For these reasons, further experimental studies are suggested to determine the extent of interaction between the water-immiscible organics and the inorganic solids under post-LOCA conditions.

9 TOPIC 7—INORGANIC AGGLOMERATION

Inorganic agglomeration refers to physico-chemical interactions between established solid particles within the suspending fluid. Issues in inorganic agglomeration phenomena as contributors to chemical effects in the post-LOCA coolant were raised in Sections 5.3.2, 5.5.1, and 5.5.3 of the PIRT document (Tregoning et al. 2007).

In the case of the post-LOCA coolant system, inorganic agglomeration refers to the clumping of individual inorganic solid particles [e.g., of SiO_2, $Al(OH)_3$, FeOOH, and others from latent debris, insulation such as cal-sil, concrete, corrosion products, or crud as described under Topic 8, crud release effects] with themselves and with other inorganic solids. Factors affecting inorganic agglomeration in aqueous solutions such as the post-LOCA coolant water fluid include ionic strength, the types and concentrations of the dissolved inorganic ions, the surface charge of the solids and their pH with respect to the point of zero charge, PZC, of the constituent solid phases, organic surfactants, surface complexation, mechanical effects (e.g., shear), and temperature (Lagaly 2005).

Laboratory testing of the influence of post-LOCA coolant water composition and solids loading have been conducted under joint NRC and industrial sponsorship with the largest program being the five ICET experiments. Differences between the conditions used in the NRC and industry-sponsored laboratory testing and the actual post-LOCA containment pool conditions may be manifest in increased or decreased inorganic solid agglomeration whose subsequent effects may be difficult or impossible to predict. For example, higher coolant flow could produce larger particles by inorganic agglomeration that either may be beneficial by causing enhanced settling or not beneficial by making particles large enough to plug the sump strainer. Decreased agglomeration would keep the solids as small particles that are more likely to be carried by the coolant flow.

The ICET experiments were sufficiently broad to include pertinent ranges in inorganic solids, solution pH, inorganic ions and ionic strength, and shear. The ICET experiments also included variations in the pH buffering system (borate or combined borate and phosphate) and electrolyte concentration with some contributions for inorganic coatings. However, contributions from organic coatings and other organic constituents, including their hydrolytic and radiolytic breakdown products, were not included. The ICET and other experiments also did not investigate temperature variability. Temperatures will cycle in the coolant as it is heated passing the fuel and then cooled passing the heat exchangers. Note, however, that organics passing the fuel will be irradiated to levels sufficient to cause their total decomposition to carbon dioxide (see Topic 10, organic material impacts).

The behaviors of inorganic solids with respect to inorganic agglomeration phenomena are discussed in Section 9.1 and the further implications of organics in inorganic agglomeration are discussed in Section 9.2. Conclusions from these considerations are presented in Section 9.3.

9.1 Behavior of Inorganic Solids

The inorganic particles in the post-LOCA coolant have positive surface charge if they are in solution with pH below their PZC and have a negative surface charge if in a solution with pH above the PZC. The pH of the PZC for SiO_2 is around 3.0, that for FeOOH (from corrosion of

iron metal) is around 8.4, $Al(OH)_3$ is ~6.7, and ZrO_2 is ~6.5 (Iler 1979; Blesa et al. 2000). It is seen that many of the PZCs are near the operational pH of the five ICET experiments (ranging from ~7.1 to 9.9). The surface charges cause like-charged particles to repel each other and remain dispersed (or peptized). Oppositely charged particles are attracted to each other and may coagulate (equivalently, agglomerate or flocculate) to form larger aggregates. For example, at pH 7.5, FeOOH (which would have a positive surface charge) would be attracted to $Al(OH)_3$ (which would have a negative surface change). This is called heterocoagulation. However, the PZC values for particular solids also are affected by the presence of electrolytes (such as the sodium borate and sodium phosphate buffers) and thus may differ from their PZCs as measured in pure water.

At higher electrolyte concentrations (i.e., high ionic strength), overall neutralization of the surface charge can occur and cause coagulation. The ionic strength of the post-LOCA coolant is dominated by the dissolved boric acid (~0.2 moles per liter) and, for some PWRs, sodium phosphate (~0.01 moles/liter), which also contributes to the ionic strength. These electrolyte concentrations may have been the cause of the decreasing turbidity occurring as the ICET experiments evolved over 1- to 5-day time periods (Dallman et al. 2006). However, the effect on decreasing turbidity was not pronounced. Because the ICET experiments conservatively encompassed the expected range of inorganic particle loadings and the electrolyte composition, further investigation of the effect of ionic strength on inorganic agglomeration is not warranted.

9.2 Organic Effects on Agglomeration

As shown in Topic 10, organic material impacts, organic coating (paint) decomposition is expected under the radiation and hydrothermal conditions of the post-LOCA environment as well as with ordinary aging. The radiolytic decomposition products include water-soluble or dispersible species such as phenolic derivatives of the widespread toluene and xylene vehicles. The phenolics arising from the toluene and xylene are cresol and xylenol, respectively. Other organics present from paints are methyl isobutyl-, methyl ethyl-, and methyl amyl ketones, simple alcohols (methanol, ethanol, and isopropanol), organic esters, perchloroethylene, and others. The various organic compounds contribute their own decomposition products (e.g., hydroxylation of organic chlorides to form alcohols, radiolysis products) to the post-LOCA coolant. As discussed under Topic 10 (organic material impacts), solvents in paints also can remain for years within the air-exposed coating and be released upon water contact during the post-LOCA interval. It is not clear if any cleaning or decontamination (e.g., pressure washing) performed during refueling outages will release any solvent.

The organic vehicles used in many paints, and their decomposition products, may act to either clump solids together (as coagulants or flocculating agents) or cause the particles to disperse (i.e., act as dispersants). Most of these organics are electrically polar, having a negatively charged end (such as the carboxylate group, $-CO_2^-$, or an alcohol, -OH, or other oxygen-rich group) and an electrically neutral and carbon-rich organic end. The water-soluble or -miscible organics, if they do not interact with low mobility (e.g., large particle or fixed) solids to remain in the containment pool, will be carried by the coolant water past the reactor fuel, become strongly irradiated, and decompose to carbon dioxide.

Other organics present in the containment building and potentially wetted by the circulating post-LOCA coolant include wire insulations, lubricants on mechanical equipment, and as much as 200 gallons of lubricants per RCS pump. As is the case for paints and coatings, thermal degradation and radiolysis can break down these organic materials to form simpler compounds

that are electrically polar. If these organics are carried past the fuel in the core, irradiation (10^6 rad/h at the core, averaging 80,000 rad/h in the full circuit – see Topic 1 on radiation effects) will decompose them to carbon dioxide as shown in the discussion under Topic 10, organic material impacts. In contrast, if the organics are collected at the sump strainer (estimated 1,000 rad/h due to collection of activation product solids), little radiolytic decomposition is expected and even less would be expected in lower-dose regions of the containment.

Like the absorption of inorganic ions onto the inorganic particles, the negative ends of the organic species are electrostatically attracted to positively charged surfaces of the inorganic particles. The lipophilic ("fat-liking") ends of the organic species are not attracted to water (i.e., they are hydrophobic) but are attracted to each other. The addition of the polar organic compounds thus affects the agglomeration of the smaller inorganic particles (Figure 3).

At least three regimes of inorganic solid interaction are shown in Figure 3. In the absence of organic sorption (defined by part A in Figure 3), the like-charged inorganic solids repel each other. With the addition of a monolayer of the polar organic molecule to the surface of the inorganic solid, the fatty organic ends of the molecule project into the solvent (water) where they are attracted to similarly coated inorganic solids. The small monolayer-coated inorganic solids agglomerate to form larger clumps. This situation is shown in Figure 3, part B. However, with the provision of additional polar organic, a double layer of organic molecules forms to coat the inorganic solid. The negative ends of the organic molecules then project from the surface, effectively reversing the charge of the original inorganic solid particle. Two such negatively-coated particles now repel each other (as shown in Figure 3, part C), but become attractive to other particles having positive surface charge.

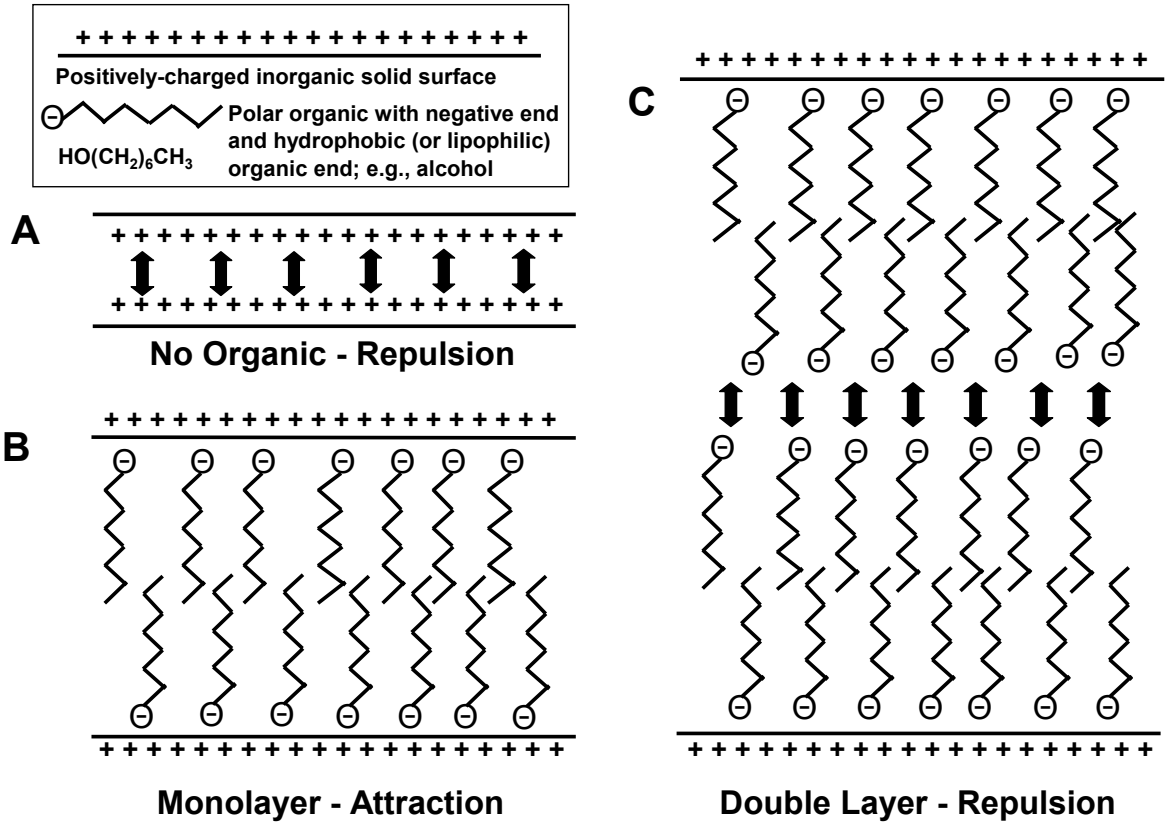

Figure 3: Effects of Polar Organic Absorption Loading on Inorganic Particle Attraction

A. No organic loading; particle-particle electrostatic repulsion
B. Monolayer organic loading; particle-particle lipophilic attraction
C. Double layer organic loading; particle-particle electrostatic repulsion.

None of the ICET experiments added organics of any kind (except as polyvinyl chloride pipe and the organics potentially associated with the Nukon fiberglass insulation) to any of the test formulations. The ICET experiments also did not investigate the effects of temperature cycling. Both of these factors, but especially the presence of organics, can affect inorganic particle solid agglomeration.

9.3 Conclusions

The unknown number and qualities of these organic constituents, the manifold interactions of the various inorganic solid particle types and electrolytes, and the complexity of the various post-LOCA systems prevent prediction, *a priori*, of the combined effects on inorganic constituent agglomeration or dispersion, and particle transport. Because of this complexity, a program of laboratory studies to determine the effects of the presence of organic compounds and their breakdown products on agglomeration of the inorganic solids may be useful. The studies would include the effects of PZC, solution composition, shear, and temperature on the constituent solid phases. Such a set of studies would be best pursued in combination with studies of the effects of synergistic solids formation as discussed in under Topic 6 and with the studies of organic stability suggested in under Topic 10.

10 TOPIC 8—CRUD RELEASE EFFECTS

The eighth subtask evaluates the quantities and chemical/radiation effects related to Fe, Cr, and Ni corrosion oxides (crud)[10] within the RCS released during the post-LOCA time-period. All non-LOCA sump-strainer plugging events resulted from the transport of pre-existing materials in the containment flow paths. However, in a LOCA, it is likely that pre-existing crud materials within the reactor core and on pressure vessel surfaces can become mobilized to flow paths and also reach containment sumps.

Questions on crud release were raised in the PIRT document in considering both pre-existing particulate crud (Sections 5.3.2 and 5.3.5) and post-precipitating crud (Sections 5.4.1 and 5.4.3) that arises, for example, when reduced dissolved iron, Fe(II), encounters oxidizing conditions and forms oxidized Fe(III) hydroxides (Tregoning et al. 2007). An introduction to crud characteristics is given in Section 10.1. Discussions on crud thicknesses as determined by various studies are provided in Section 10.2. Based on this background information and on further data, estimates of crud quantities available in a LOCA are provided in Section 10.3. Conclusions about crud release effects are provided in Section 10.4.

10.1 Introduction

As defined by Hazelton (1987):

> The word "crud" is used in the nuclear industry to designate the corrosion products (principally oxides of iron, nickel, chromium, copper, and cobalt) that form outside the core in PWR RCS heat exchangers, piping, pumps, etc.; that dissolve or are eroded away; or that circulate in the water coolant, and are deposited on fuel rods and non-heat-generating surfaces in the core and the reactor vessel. Crud does not refer to the dense, strongly adherent films formed by oxidation of fuel cladding, such as zirconium oxide.

Given the relatively slow rate of corrosion product generation, little corrosion and subsequent crud formation within the RCS (containing stainless steel-clad pressure vessel, zirconium-clad fuel, stainless and Inconel piping, and Inconel steam generators) is expected in the 30-day post-LOCA interval. However, additional work is valuable to examine pre-LOCA formation of corrosion products that may contribute to degraded ECCS performance.

Crud is finely divided and poorly soluble oxide particles that can become suspended in the reactor coolant or loosely adhere to metal surfaces where it can be transported through the RCS to accumulate and foul heat-transfer surfaces or clog flow passages. Crud species include various metal corrosion ferrite spinels. The prototypical ferrite is magnetite, Fe_3O_4 (density ~5.2 g/cm^3), but PWR crud generally is rich in nickel and appears as nickel ferrite and chromite phases such as $Ni_xCr_yFe_{3-x-y}O_4$ and $Ni_xFe_yCr_{3-x-y}O_4$ (density ~5.2 g/cm^2) as well as elemental nickel (density ~8.9 g/cm^3) and nickel oxide (NiO; density ~6.7 g/cm^3). Recently, another phase, bonaccordite (Ni_2FeBO_5 density ~5.2 g/cm^3) has been found deposited on fuel surfaces

(10) According to the NRC Glossary (http://www.nrc.gov/reading-rm/basic-ref/glossary/crud.html), crud is: *A colloquial term for corrosion and wear products (rust particles, etc.) that become radioactive (i.e., activated) when exposed to radiation. Because the activated deposits were first discovered at Chalk River, a Canadian nuclear plant, "crud" has been used as shorthand for Chalk River Unidentified Deposits.*

and monoclinic ZrO_2 (baddeleyite; density ~5.8 g/cm^3) is found on wick-boiling areas near the fuel cladding (Bergmann et al. 1983; Frattini et al. 2001; Guzonas and Webb 2002; Sawicki 2002).

According to the DOE (1993), crud can be mobilized abruptly as a "crud burst" by:

- increased oxygen (O_2) concentration,
- reduced (or significantly changed) pH,
- large temperature changes, or
- physical shock (for example, starting and stopping pumps, changing speeds of pumps, reactor scram, or relief valve lift).

All four of these crud burst initiating mechanisms are present in a LOCA.

Some characteristics of PWR crud, evaluated from steam generator (SG) tube and fuel rod or core deposits, are shown in Table 10. Characterization testing showed that the crud films formed on the steam generator are enriched in iron, chromium, and cobalt and depleted in nickel compared with the composition of the oxidized steam generator tubing itself. The films on the fuel are only enriched with iron and depleted in chromium and nickel. These elemental distributions are considered in more detail later in this section.

10.2 Estimates of Crud Thicknesses

Bojinov and colleagues (2002) placed coupons of type 316L stainless steel and a similar alloy (08X18H10T) in flow-through cells at a PWR (Loviisa-1 in Finland). Corrosion thicknesses as metal oxide of ~0.25-0.5 μm were established within 6 months but thicknesses increased little with exposure up to 18 months implying an expected diffusion-controlled corrosion rate. Corrosion product crystal size was ~1 μm. These coupons were not heat-transfer surfaces and thus may fairly represent the corrosion properties of well-insulated stainless steel pressure vessel and piping surfaces during the reactor operating period.

As shown in Table 10, steam generator tubing crud film thicknesses of 0.85-1.20 μm are reported for reactor tubes at power for 6 to 7 years. The rate of crud deposition on steam generator tubes was estimated to be 0.083 mg/cm^2-y over growth times from about 1.6 to 7 years and steam generator metal corrosion rates (0.06 to 0.24 mg/cm^2-y, based on metal, or 0.083 to 0.33 mg/cm^2-y based on oxide) are consistent with the oxide deposition rate. At a crud density of 5.2 g/cm^3 (typical of ferrites), the crud thickness develops at a rate of 0.16 μm/y. As a conservative extrapolation, a plant with 30-year-old steam generator tubing would have ~5 μm thick crud deposits.

Table 10: PWR Crud Characteristics

Crud Property	Value	Ref.[(a)]
Composition, wt% [(b)]	SG tube: Fe (14-22), Ni (20-39), Cr (20-38), Co (0.12-0.36)	1
	SG tube crud: Fe (14-22), Ni (20-30), Cr (20-38), Co (0.24) Core crud: Fe (39-47), Ni (19-24), Cr (0.8-2.5), Co (0.11) Oxidized SG tubing: Fe (6), Ni (52), Cr (13), Co (0.035)	2
Phase compositions	Mixed nickel ferrite, $Ni_xCr_yFe_{3-x-y}O_4$, and chromite, $Ni_xFe_yCr_{3-x-y}O_4$	1
	SG tube: Ni-Cr-Fe spinel, Ni, $NiFe_2O_4$;	2

	Fuel: $Ni_xFe_{3-x}O_4$, $0.4 \le x \le 0.9$ Stainless steel: Cr-rich oxide	
SG tube surface crud growth rate, mg/(cm^2-y)	0.083	1
SG tube corrosion rate, mg/(cm^2-y)	0.06 – 0.24	2
Tube crud thickness, μm	0.85-1.2 (for reactors at power for 6-7 years)	1
Tube crud density, g/cm^3	3.81-6.43 [(c)]	1

(a) Reference 1 is Bergmann et al. (1983); reference 2 is EPRI (1999). Additional insight from Guzonas and Webb (2002) and Sawicki (2002). Further details on fuel crud characteristics are provided by Hazelton (1987) and Sandler (1979).

(b) The steam generator tubes and control rod drive mechanism tubes historically are Inconel Alloy 600 – 8 wt% Fe, 72 wt% Ni, and 15.5 wt% Cr. More recent SG tubes and associated hardware use Inconel Alloy 690 (9 wt% Fe, 61.5 wt% Ni, and 29 wt% Cr) because of its improved resistance to stress corrosion cracking. The general corrosion resistance of Alloy 690 and its propensity to and extent of crud formation are expected to be similar to those of Alloy 600. The pressure vessel cladding and some piping is 304 or 316 stainless steel. For nominal 304 SS – 70 wt% Fe, 9 wt% Ni, and 19 wt% Cr; for nominal 316 SS – 67 wt% Fe, 12 wt% Ni, and 17 wt% Cr. Fuel cladding commonly is Zircaloy-4 – 1.3-1.6 wt% Sn, 0.2 wt% Fe, and 0.1 wt% Cr with the balance being Zr.

(c) The ferrite phase has a particle density of ~5.2 g/cm^3; water has a density of 1.0 g/cm^3. However, a crud density value of 1.2 g/cm^3 is reported by Hazelton (1987). If the 1.2 g/cm^3 value is correct, the volume fraction occupied by the ferrite phase in the crud is ~0.048 and the water volume fraction is 0.952, indicating a very dispersible material. Typical settled metal oxide sludges are approximately 0.75 volume fraction water which would give a crud bulk density of 2.05 g/cm^3.

Crud deposits as thick as 80 μm have been observed on PWR fuel cladding with thicknesses that increase with height on the assembly (Wilson and Comstock 1999, pp. 205–202). Average thicknesses near the middle of the assembly are ~3 μm but are ~15 μm ¾ of the way up the assembly.

More recently, significant axial power offsets have been observed in PWRs. The axial offset is defined as the integrated power output in the top half of the core minus the integrated power over the bottom half divided by the total power. In these axial offset anomalies (AOA), lower specific power production is observed at the upper half of the reactor. This lower power is attributed to the formation of thick crud layers on the cladding surfaces in high-duty plants, including deposition of the boron-bearing phase bonaccordite (Ni_2FeBO_5), which serves to poison the nuclear reaction and sometimes cause downrating of the reactor power. The AOA phenomenon is observed to commence with deposits at ~20-30 μm and deposits >80 μm have been observed (Henshaw et al. 2006a and b).

Crud flakes up to 140-μm thickness with insoluble needle-like bonaccordite particles (hardness like quartz; Roberts et al. 1990) and baddeleyite (ZrO_2; density ~5.8 g/cm^3) have been observed in the Callaway cycle 9 fuel assemblies (Sawicki 2002). Crud deposits of ~125-μm depth on the reactor cooling system piping were postulated (without attribution) in the PIRT document (Tregoning et al. 2007).

10.3 Estimates of Crud Quantities

A chemical milling of the internal parts of the reactor pressure vessel of units 2 and 3 of the Fukushima Power Station was undertaken. These BWR units had ~20 years of operation. The chemical milling removed 60-70 kg (as metal) of iron/nickel/chromium crud (Sato et al. 2000). This would be equivalent to ~90 kg of $(Fe,Ni,Cr)_3O_4$ from the pressure vessel materials. Though not from a PWR, this work is the only study known to directly inventory the quantity of metal removed as crud from the entire fuel-contacting coolant system in a light water reactor.

The quantities of crud that might be released in a LOCA can vary according to the time in the power cycle (later times lead to more crud) and the efficiencies of prior crud control operations. According to Fellers and colleagues (2002), "The shutdown evolution is managed from a process control perspective to achieve conditions most favorable to crud decomposition and to avoiding re-precipitation of metals." Modern crud removal techniques conducted upon shutdown are effective for the $Ni_xFe_{3-x}O_4$ phases, for NiO, and for Ni but not for the lesser amounts of chromium-rich phases present out-of-core (i.e., the protective layers on steam generators and piping) or for bonaccordite and monoclinic ZrO_2 which are found on the fuel and which have poor solubilities under the crud removal conditions.

Some information on crud quantities can be gathered by examination of the technical literature on crud formation and release during normal operations, particularly as observed during a controlled shutdown (Dacquait et al. 2002) or in specialized studies (Bojinov et al. 2002). Dacquait and colleagues (2002) found ~5.7 kg of nickel released during shutdown, mostly during the controlled oxidation step when hydrogen peroxide is added to the shutdown system, which they attribute to dissolution of metallic nickel or nickel oxide. Other experiences in crud release during PWR shutdown have been published (Section 2.2.2 of Volume 2; EPRI 1999). Thus, after cycle 5 at Seabrook, 7.05 kg of nickel were removed by the purification system. During shutdown for refueling #9 at Wolf Creek, 4.37 kg of filterable nickel and 0.94 kg of unfilterable nickel were captured by the purification system. The VC Summer plant collected 4.50 kg of nickel during refueling #10. The North Anna Unit 2 collected 4.41 kg of nickel in the purification system, apparently during refueling #12. These shutdown conditions, of course, are not characteristic of a LOCA, but serve to provide comparative background data.

Rather than use data obtained during controlled shutdown operations, knowledge or assumptions about the depth and uniformity of the crud deposits and estimates of the RCS surface area can be combined to estimate the quantity of crud deposited in PWRs. As will be seen, much smaller quantities of crud also can be present as solids or as precursor solutions circulating in the coolant. Information about RCS surface areas and crud circulating in coolant as well as crud generation rates and projected crud quantities is discussed in the following sections.

10.3.1 Fuel, Pressure Vessel, Steam Generator, and Piping Surface Areas

The surface areas available for crud collection within the PWR coolant circuit are estimated for the fuel, pressure vessel, the steam generator(s), and the connecting piping.

The surface area of the fuel is estimated based on nominal fuel structure and loading in a PWR. The number of pins in a fuel bundle is nominally 220 (range from ~179 to 264), and the number of bundles in a core is nominally 150 (range from ~121 to 193). Each fuel pin, about 1 cm diameter and ~4 meters long, has about 3100 cm^2 surface area. The total surface area of the fuel in a PWR core thus is $\sim 220 \times 150 \times 3100 \cong 10^8$ cm^2 = 10,000 m^2. This estimate is consistent with the calculated fuel surface area of the Cruas-1 PWR in France, 7,047 m^2, and the Isar-1 PWR in Germany, 8,215 m^2 (Macdonald and Urquidi-Macdonald 2006), 11,600 m^2 for a model plant (Henshaw et al. 2006b), and 7,000 m^3 for a Westinghouse PWR (Polley and Pick 1986).

Other wetted parts of the reactor coolant circuit include the pressure vessel, steam generator, and the hot and cold leg piping. Values for these PWR parts' surface areas were found for the Cruas-1 plant (900 MWe), France, and the Isar-2 plant (1,300 MWe), Germany (Macdonald and Urquidi-Macdonald 2006) as well as for the steam generators of the Doel-4 and Tihange-3

PWRs (both 985 MWe) in Belgium (Cummins et al. 2003). The wetted area of the Cruas-1 core structures is 2,418 m^2 (1674 m^2 stainless steel; 744 m^2 Inconel). No estimate for the Isar-2 plant core structures was provided. The three Cruas-1 steam generators have 13,362 m^2 surface area, and the four Isar-2 steam generators have 21,600 m^2 surface area. The three steam generators for Doel-4 (or Tihange-3) have 18,960 m^2 surface area. The Cruas-1 hot and cold piping has 240 m^2 area, and the Isar-2 hot and cold piping has 980 m^2 area. Henshaw and colleagues (2006b) provided model plant surface areas of 36,000 m^2 for steam generators, 380 m^2 for hot-leg piping, and 190 m^2 for cold-leg piping (no estimate given for the pressure vessel and associated core structure surface areas). Polley and Pick (1986) estimated 18,000 m^3 of Inconel 600 surface area and 2,700 m^3 stainless steel for a typical 4-loop Westinghouse PWR.

Combined, the total wetted surface area, excluding the fuel cladding, is 16,020 m^2 for the Cruas-1 PWR (compared with 7,047 m^2 fuel surface area) while the total wetted surface area of the Isar-2 PWR is ~25,000 m^2, estimating 3,000 m^2 surface area for the core structures (compared with 8,215 m^2 surface area for the fuel). For the model plant (Henshaw et al. 2006b), the total wetted surface area is ~51,000 m^2 (3,000 m^2 being estimated for core structures) of which 11,600 m^2 is fuel. For the 4-loop Westinghouse PWR, the total wetted surface area is ~27,700 m^3 (7,000 m^3 being fuel). Thus, the fuel surface area represents about ¼ to ⅓ of the total wetted surface of the reactor coolant circuit. The total wetted surface of a PWR varies from about 23,000 m^2 (Cruas-1) to 33,000 m^2 (Isar-2) to 51,000 m^2 (nominal plant) with potentially higher or lower surface areas in other plants.

10.3.2 Suspended and Dissolved Crud

Crud or crud precursors may be available in the form of undissolved and dissolved metals (iron, chromium, manganese, nickel) and their oxides circulating in the coolant. Collections of solution and solid samples in the recirculating coolant from a number of operating PWRs and analyses of these samples have been done at the Sizewell B plant in the UK (Barton et al. 2001). The dissolved and undissolved concentrations of these metals (chromium was not reported) were multiplied by the coolant volumes (Nuclear Engineering International 2006) to determine the inventory of circulating metals. The highest values were found for iron, and the highest total dissolved and undissolved iron value was 7544 ng/kg of water. However, this level of iron and the 235-metric ton coolant weight for this plant only correspond to 1.77 grams of iron. Therefore, the dissolved and suspended inventory is trivial compared with the crud quantities observed deposited on fuel surfaces.

10.3.3 Crud Generation Rates

The corrosion rate of the steam generator tubing is estimated to be 0.69 mg/dm^2 per month (Bergmann et al. 1983) and reported to range from 0.5 to 2 mg/dm^2 per month (page 2-2 of Volume 2 of EPRI 1999). For a 24-month cycle and a steam generator surface area of 24,000 m^2, the quantity of metal corroding per cycle thus corresponds to ~29 to 115 kg. For a 30-year-old plant, conservatively assuming continuing linear corrosion, the quantity of metal corroded from steam generator tubing is ~430 to 1,700 kg. This amount of metal is equivalent to ~590 to 2,300 kg of the expected metal oxide ferrite phase, M_3O_4 (M being Fe, Cr, and Ni with ~72 wt% as the metal M) or ~1,200 kg as the geometric mean of 590 and 2,300 kg.

If, instead, a more realistic parabolic rate is assumed (i.e., the corrosion layer is adherent and protective with the amount of corrosion proportional to $time^{½}$), the amount of metal corroded from steam generator tubing after 30 years (360 months) would be $360^{½}$-times (~19-times) the

monthly rate or ~23 to 90 kg. This is equivalent to ~32 to 124 kg of metal oxide, again for a 30-year-old plant. The amount of metal oxide from Inconel in a 4-loop PWR is estimated to be 15 kg after just the initial operating cycle (Polley and Pick 1986) and modeled to be 21.5 kg under similar conditions (Henshaw et al. 2006b).

As described earlier, Bojinov and colleagues (2002) studied the corrosion of type 316 SS and a similar alloy (08X18H10T) in flow-through cells at a PWR and found an ~0.25- to 0.5-μm corrosion thickness established within 6 months but increasing little with exposure up to 18 months. For a 24-month cycle, an ~2,000 m^2 stainless steel surface area based on Cruas-1 core structure and hot and cold piping values, and a 0.5-μm corrosion oxide thickness, the volume of oxide product is 1 liter. For the expected ferrite product with 5.2 g/cm^3 particle density, the metal corroded in a 2-year cycle is ~3.8 kg. If it is very conservatively estimated that stainless steel corrosion is linear with the number of cycles, the ~3.8 kg/cycle rate releases ~56 kg of metal over a 30-year plant time span.

Using the more realistic parabolic rate law, a 0.5-μm corrosion layer thickness established in 24 months would be about 1.9 μm when extrapolated to 30 years. This is equivalent to about 4 liters of oxide product or 15 kg of ferrite over a ~2,000 m^2 stainless steel surface area. The amount of oxide from stainless steel corrosion in just the first operating cycle of a 4-loop Westinghouse PWR was estimated to be 33 kg (Polley and Pick 1986) and modeled to be 0.6 kg (Henshaw et al. 2006b).

Zirconium contributions to crud by corrosion of fuel cladding are expected to be low compared with that lost by the iron, chromium, and nickel components of the RCS as suggested by the iron/chromium/nickel-rich crud compositions shown in Table 10. However, a ~100-μm oxide thickness is observed for Zircaloy-4 at near complete burn-ups greater than 50 to 55 GWd/MTU. The spallation of product zirconium oxide (ZrO_2) from cladding is occasionally observed. Based on ⅓ of the fuel loading present in an operating reactor being in its first cycle, ⅓ in its second cycle, and ⅓ in its final cycle, the average fuel burn-up is ~25 GWd/MTU. Therefore, the average ZrO_2 thickness on a fuel load clad with Zircaloy-4 is ~50 μm. Cladding being used in most modern reactors alloys, M5 and ZIRLO™, shows corrosion rates that are only 0.4- to 0.5-times the Zircaloy-4 rate, respectively (Lanning 2005). Based on the above values, the volume of ZrO_2 on 10,000 m^2 of Zircaloy-4 cladding is 500 liters, equivalent to 2,900 kg of ZrO_2. However, more realistically, the quantities are 250 liters (~1,400 kg) for ZIRLO™ and 200 liters (~1,200 kg) for M5.

Based on realistic parabolic corrosion rates for Inconel and stainless steel components and observed ZrO_2 thicknesses on modern cladding alloys (M5 and ZIRLO™), the metal oxide present in the RCS from metal corrosion in a mature (30-year-old) reactor thus is ~100 kg of ferrite from steam generator corrosion, ~15 kg of stainless steel ferrite from the piping and pressure vessel, and ~1,300 kg of ZrO_2 from the cladding or about 1,400 kg of total crud.

10.3.4 Summation of Crud Quantities

As a simplification of the discussion in Section 10.3.3, a uniform crud deposit that is 20 μm deep and has a density of 2.05 g/cm^3 (crud particle density of about 5.2 g/cm^3 but containing 75 volume% entrained water) could be assumed. The nominal 33,000 m^2 wetted surface area of a PWR would hold 1,300 kg of wet crud or ~800 kg of dry crud. These estimated quantities are seen to be much larger than the ~5 kg (as metal) released during controlled shutdown operations or the gram-quantities of metal present in dissolved or finely dispersed solid form

circulating in the coolant. The 800-kg estimate, however, is of the same order as the ~1,400 kg of metal oxide present as RCS surface corrosion products in a mature reactor detailed in Section 10.3.3.

The 800-kg estimate is based almost entirely on observations of crud thickness on fuel and is extrapolated to the steam generator tubing (where heat exchange occurs) and the process piping (where little heat exchange occurs). The stainless steel coupons tested under conditions without heat exchange showed minimal corrosion (Bojinov et al. 2002), indicating that the crud estimate for the largely stainless steel process piping is conservative (i.e., likely overestimates crud deposition). Because the stainless steel area (piping and core structures) of the Cruas-1 plant, ~2,700 m^2, represents only about 12% of the total RCS surface area, the conservatism from this source is not high. The relative areas of the RCS covered by stainless steel in low heat-transfer locations at other PWRs are expected to be similarly low.

Because observations show about 1-μm crud thickness on steam generator tubing after about 7 years of service (Table 10), meaning perhaps 2 μm of crud thickness after 30 years of service (based on parabolic kinetics), the 20-μm crud depth estimate for steam generator tubing likely is conservative (high). This conservatism is supported by the observation that nickel cobalt ferrite has retrograde solubility with temperature (Figure 2-6 of Volume 2 of EPRI 1999), and the surface temperature of the steam generator tubing is lower than that of the coolant while the fuel is hotter. Therefore, crud deposition should be lower on steam generator tubing than on the fuel.

During a LOCA, the increased O_2 concentrations from atmospheric exposure, physical shock, and changes in pH and temperature will occur with a degree of violence perhaps sufficient to dislodge the entire crud (metal oxide) inventory. Therefore, from these separate estimates based on crud thicknesses observed on fuel and extrapolated to other RCS surfaces, the entire ~1,400 kg dry crud inventory plausibly is available to release. The quantities of crud released also can vary, depending on the operating age of the reactor, its cleanliness (e.g., time since, and thoroughness of, prior cleaning operations), and the adherence of the corrosion products to the underlying source metal. These considerations may imply that perhaps only about half of the metal oxide (~700 kg) would be dislodged during a LOCA.

The conservative estimate of crud quantity available for displacement by a LOCA thus is ~1,000 kg, mostly as ZrO_2. At a nominal crud particle density of 5 g/cm^3, this corresponds to ~200 liters of solids volume. Particles with this density would not likely transport to the sump strainer under the expected containment pool flow velocities. However, the crud could transport to the strainers if buoyed by combining with lubricant oil to form an OMA as discussed in Topic 6, co-precipitation and other synergistic effects. If the crud had the nominal 1.2 g/cm^3 wet density advanced by Hazelton (1987), it would be transportable by itself and comprise ~800 liters of solids.

These quantities compare with ~1.4×10^6 liters (~50,000 ft^3) of nominal emergency coolant volume in a PWR (ranging from about 35,000 to 160,000 ft^3) and the 0.137 volume fraction of insulation materials (compared with water volume) added during the ICET experiments (Andreychek 2005), corresponding to ~1.9×10^5 liters of released solids in a nominal PWR. The insulation solids are fiberglass (e.g., Nukon) and cal-sil, i.e., the solids are fibrous and particulate, respectively. For ICET #3 and #4, cal-sil represents 20% of the insulation solids, or about 3.8×10^4 liters, and fiberglass the balance. The ~800-liter volume of wet crud released thus is ~0.4 vol% of the conservatively projected volume of total insulation materials used in the ICET experiments and about 2 vol% of the particulate (cal-sil) solids in tests with cal-sil.

However, the crud can constitute a large fraction of the particulate solids for systems without cal-sil insulation (exemplified by ICET #1, #2, and #5) and thus provide sufficient suspendible solids that can be caught on fiberglass-matted sump strainers and block flow.

10.4 Conclusions

The principal observed crud phase is nickel ferrite of variable composition, but significant amounts of ZrO_2 are present on the fuel cladding and may be released in a LOCA. Further study of crud release effects on sump strainer blockage are of lesser importance for reactor systems having significant sources of fine particulate such as those with cal-sil insulation or having high aluminum corrosion. However, the crud release may be a significant addition to the particulate load in post-LOCA coolants not already burdened with cal-sil. The crud solids, if flocculent and having the low reported ~1.2 g/cm^3 density, adds to the other readily suspended solids that may migrate to the sump strainer and collect onto fiberbeds or other filtering media and contribute to coolant flow impedance.

Two estimates of crud quantity were made based on uniform thickness and on limited measurements of crud thickness in various wetted parts of the RCS. The simplest crud quantity assessment, about 800 kg, is based on the assumption that crud loadings in other (largely unobserved) parts of the RCS, particularly the steam generators, are the same as are observed on fuel. The assumption of uniform crud loading extrapolated from loadings observed on fuel is taken to be conservative because 1) active efforts are made by PWR operators to limit crud and activity loading within the RCS, 2) the corrosion on stainless steel (process piping) is low, and its corrosion film is not easily displaced, and 3) nickel ferrite has retrograde solubility (i.e., its solubility is greater at lower temperature and thus crud deposition onto the steam generator tubing should be lower than onto fuel). Measurements or better estimates of crud deposition in the RCS may alter these conclusions, but likely in the direction to lower the estimated 800-kg quantity. Estimates of about 1,400 kg of total crud are made based on specific metal corrosion rates and their combined surface areas.

11 TOPIC 9—RETROGRADE SOLUBILITY AND SOLIDS DEPOSITION

The objectives of this portion of the investigation are twofold:

- Identify likely chemical species and estimate quantities that could precipitate at the reactor core and their incremental increase due to retrograde solubility
- Identify solid chemical species that could be deposited onto the reactor fuel.

These objectives arose in discussions from Sections 5.3.3.2.2, 5.3.5, 5.4.2.2, 5.4.3, 5.7.3.1, and 5.7.4 of the PIRT report (Tregoning et al. 2007). These objectives were investigated with thermodynamic modeling of the five ICET experimental conditions over a range of temperatures from 140°F (60°C) to 250°F (121°C).

An introduction to the thermodynamic modeling is given in Section 11.1 with the solution input parameters shown in Section 11.2. The results of the modeling below the boiling point of water are described in Section 11.3, and the results above boiling and up to 250°F (121°C) are shown in Section 11.4. The overall conclusions from this work are summarized in Section 11.5.

11.1 Introduction

To accomplish these objectives, the chemical speciation of the emergency cooling water was modeled for a hypothetical PWR accident in which the ECCS is activated. The OLI System's StreamAnalyzer (version 2.0) and Environmental Simulation Program (ESP, version 7.0) programs were used to evaluate equilibrium conditions in the ECCS based on the measured compositions for the ICET solutions after 30 days. Both OLI programs are supplied with several databanks based on either the Bromley-Zemaitis (BZ) aqueous ion activity coefficient model or the newly developed Mixed Solvents Electrolyte (MSE) model. The BZ model has been used for OLI System products since the inception of the company. It is a form of the Bromley activity coefficient model that has been extended to include neutral and common ion interactions and is based on concentrations in molality (moles per kg of water).

The MSE model was recently developed by OLI to allow modeling of species interactions in solutions of more than one solvent, up to the limit of a solvent fraction of 1.0 for any solvent. It can also model the composition when all of the solvents' fractions go to 0 and for the resulting solid-phase mixture up to the temperature of melting. The MSE model is based on concentrations in mole fraction rather than molality as in the BZ and other traditional aqueous activity coefficient models. This allows modeling and predictions outside the normal range of aqueous solutions into the region of solid phases up to melting temperatures.

There are two databanks supplied that are compatible with the MSE model. The first, MSEPUB (MSE Public), contains most species of interest for general modeling, and the second, CRMSE (MSE Corrosion), contains products from corrosion reactions as well as species of geological interest. In addition, the MSEPUB databank has thermodynamic data for an extensive collection of calcium and sodium borate species not available in the BZ databanks. For these reasons, and because the MSE databanks are the most current, it was chosen for the LOCA

simulations. Comparisons between the models were made initially to verify that there were no significant differences in prediction of the basic water chemistry, such as pH values and solubilities of common species.

Applying OLI StreamAnalyzer, version 2.0, to model the results of the ICET experiments themselves was described in work by the Center for Nuclear Waste Regulatory Analyses (CNWRA) at the Southwest Research Institute (McMurry et al. 2006). In the modeling performed by the CNWRA, the evolutions of the 30-day ICET experiments, including the interactions of the coolant waters, the insulation solids (Nukon and cal-sil), the concrete, and the metal corrosion at 60°C, were modeled to project the types and quantities of solids, including corrosion products, that form and the compositions of the equilibrium waters. In contrast, the modeling performed in the present case was undertaken to determine the behaviors of the salt- and particulate-laden ICET liquors upon encountering containment air with its associated carbon dioxide and by heating beyond 60°C when the liquors encounter the reactor pressure vessel and core fuel. The precipitation and alteration solid phases generated by solubility limits and when water is lost by evaporation were postulated based on the modeling.

The StreamAnalyzer model minimizes the system free energy to predict solid and solution phase compositions and is based on all reactions being reversible so that thermodynamic equilibrium can be attained. Although the model can accommodate kinetic data (e.g., reaction rates), the rate data must be supplied and are not part of the model package. Impediments and influences on attaining equilibrium include reaction activation energies and slow solid-solid reactions (particularly observed for low-solubility solids). The rate influences are further complicated by the brief times that the fluids are in contact with the hot pressure vessel and fuel surfaces. Therefore, notations or explanations are made based either on experience or the technical literature to describe why differences are observed between model-predicted and literature-reported behaviors. As in all thermodynamic models, careful examination of the input phases and model outputs are necessary to help verify consonance between the real and modeled systems. Based on the present model output, solid phases are identified that potentially form because of retrograde solubility and localized evaporation. Supplementary experimentation would be needed to verify the existence of the phases identified by the model predictions.

11.2 Solution Compositions and Model Input

The chemical compositions of emergency cooling water were taken from the ICET report (Dallman et al. 2006). The data for the chemicals added to the water are from Table 4-1 (Dallman et al. 2006) and are shown in Table 11. The solution compositions at the end of the 30-day ICET experiments (based on Figures 4-1 through 4-16; Dallman et al. 2006) are presented in Table 12. The conditions of the ICET experiments are outlined in Table 13.

Table 11: Compounds Added to ICET Cooling Solution

Compound Added	Test Number and Concentration, mg/liter				
	1	2	3	4	5
NaOH	7677	0	0	9600	0
$Na_3PO_4 \cdot 12H_2O$	0	4000	4000	0	0
H_3BO_3	16000	16000	16000	16000	6848
$Na_2B_4O_7 \cdot 10H_2O$	0	0	0	0	10580
HCl	100	100	100	100	43
LiOH	0.7	0.7	0.7	0.7	0.3

Table 12: Components Analyzed in ICET Cooling Solution

Component Analyzed	Measurement Unit	Test Number and Concentration or Value				
		1	2	3	4	5
Alkalinity	pH	9.4	7.3	8.0	9.8	8.2
Turbidity	NTU (1)	1	1	1	2	1
Total Suspended Solids	mg/liter	23	11	10	39	12
Al		350	BD (2)	BD	BD	49
Ca		10	6	109	42	32
Cu		0.8	0.2	0.1	0.3	0.7
Zn		BD	BD	BD	BD	BD
Mg		BD	4.8	2.3	BD	0.9
Na		4500	1000	1000	10700	1200
Si		5	85	85	170	7

(1) NTU is nephelometric turbidity units.
(2) BD means below detection.

Table 13: Experimental Conditions in the ICET Tests

Test #	Boron Added, mg/L	NaOH Added, mg/L	TSP Added, mg/L	Test pH Range	pH Buffering Agent	Insulation Material	
						Fiberglass	Cal-sil
1	2800	7677	–	9.3–9.5	Borate	100%	–
2	2800	–	4000	7.1–7.4	Borate and phosphate	100%	–
3	2800	–	4000	7.3–8.1	Borate and phosphate	20%	80%
4	2800	9600	–	9.5–9.9	Borate	20%	80%
5	2400	–	–	8.2–8.5	Borate	100%	–

From Dallman and colleagues (2006) and Klasky and colleagues (2006). Further details on solution composition are given in Table 11 and Table 12 of the present report.

The concentrations from Table 11 and Table 12 were entered into the StreamAnalyzer program and reconciled to balance charges and calculate pH. The values shown in Table 11 were entered as neutral compounds and the values in Table 12 as ions, except Si, which was added as the neutral species, amorphous SiO_2. The hydroxide ion concentration value was adjusted to obtain charge neutrality, and the NaOH or $Na_3PO_4 \cdot 12H_2O$ amounts were adjusted until the

calculated pH approximated the measured pH. One exception was for ICET #5, which was charge-balanced with hydroxide without pH adjustment.[11]

Adjustments in sodium ion concentrations also were necessary and resulted in model compositions differing slightly in sodium concentration from those obtained from chemical analyses for sodium or calculated from the experimental NaOH or $Na_3PO_4 \cdot 12H_2O$ additions. This adjustment is required when as-analyzed concentrations have to be reconciled to balance positive and negative ion charges; NaOH quantities were modified to adjust pH. Because sodium is the predominant dissolved species, the relative impact of this required change is lower for sodium than it would be if another ion were selected. The LiOH and the metals with a concentration below 1 mg/liter were not included in the simulations since their concentrations are so low that they would have had no effect on conditions of interest, particularly solids formation.

The compositions resulting from the StreamAnalyzer charge reconciliation were exported to the ESP to simulate the reaction of the emergency cooling water with the air in the containment enclosure. From the data presented in "Principal Attributes of the LOCA Accident Sequence,"[12] it was estimated that the containment volume is about 30 times the volume of the emergency cooling water pool. The average or slightly above average total containment volume is ~3 million ft^3, and the average pool volume is ~100,000 ft^3.

A simple ESP simulation was created in which a nominal 100,000 ft^3 of ICET-simulated emergency cooling water (with entrained solids) was reacted with 3 million ft^3 of air containing 1 vol% water vapor and 375 ppm (volume or mole basis) of CO_2, as would occur during a LOCA, to partition the gaseous constituents to the vapor and solution phases The resulting mixture of emergency cooling water and containment air was then imported as a stream back into the StreamAnalyzer, and temperature surveys were run. For each ICET mixture, the equilibrium composition was determined at temperatures from 140°F to 250°F (60°C to 121°C) in 5°F increments. The output was plotted to show pounds of solids predicted to form as a function of temperature for this typical volume of containment space and the volume of the emergency cooling water pool.

11.3 Simulation Results—Below the Boiling Point

Portions of the ESP output summary reports containing the predicted compositions of the air-cooling water mixture at 140°F (60°C) are shown in

(11) It has been noted that the amounts of cal-sil insulation material (and associated calcium silicate) supplied to the ICET #3 and #4 experiments were extremely high compared with what might be expected in a more realistic post-LOCA situation. As a result of this high-calcium silicate loading, and the affinity of calcium for phosphate, the solution in the ICET #3 test became depleted in phosphate rather than becoming depleted in calcium. A modified ICET #3 experiment with lower cal-sil loading, and associated modeling based on the experimental outcomes to address a lower calcium silicate infusion scenario, may yield useful information, but was not done for the present analysis.

(12) Bruce Letellier presentation, March 27, 2006.

Table 14 for ICET #1. The compositions of the phases are listed in the columns under the phase name. No organic phase is present, so all column values for this phase are zero. Species that have a neutral aqueous form are listed first, then aqueous ions with the ending ION, and then solids that do not have an equivalent aqueous neutral form. Similar ESP calculations were run in 5°F increments from 140°F (60°C) to 250°F (121°C) for all five ICET experiment compositions.

The temperature survey plots from simulations of the five ICET experiments for the 140 to 210°F (60°C to 99°C) temperature interval are shown, respectively, in Figure 4 to Figure 8 with discussion of the significant effects. The 210 to 250°F (99°C to 121°C) range was considered separately from the 140°F to 210°F range to allow a different solid mass scale for the solids formed below the boiling point and those formed from evaporation of the water. The higher range simulates solids that are predicted to form if the emergency cooling water is flashed on hot fuel assemblies or other hot surfaces in the core of the reactor.

The experiment for ICET #1 is representative of plants that use NaOH for pH control in reactor containments and have little calcium silicate insulation (Table 13). The formation of about 180 lb (82 kg) of $CaCO_3 \cdot H_2O$ (hydrocalcite) and 95 lb (43 kg) or less of the sodium aluminosilicate natrolite ($Na_2Al_2Si_3O_{10} \cdot 4H_2O$) from the soluble or entrained calcium and silicon are predicted for this case (Figure 4). Interestingly, the OLI software predicts that the form of calcium carbonate shifts from calcite to hydrocalcite around 100°F. The hydrocalcite species is contained in the CRMSE databank, designed for studying corrosion phenomena among other things. The hydrocalcite form is generally associated with colder temperatures. This apparently incorrect prediction of the hydrate is discussed further in Section 11.4. Nonetheless, the retrograde solubility of $CaCO_3$ or the hydrate is not manifest in these simulations because essentially all (99%) of the calcium is predicted to be precipitated within this temperature range.

Table 14: ESP Output for ICET #1 at 140°F

```
STREAM: ICET#1+Air
FROM  : ICET#1-Air Mixer

Phases----------->  Aqueous       Solid         Vapor         Organic
Temperature, F      140.          140.          140.          140.
Pressure, atm       1.            1.            1.            1.
pH                  9.38983
Total lmol          338787.       81.87373      8438.281      0.0
------------------  lb -----------lb -----------lb -----------lb ---------
H2O                 6.06206E+06   0.0           29932.74      0.0
CO2                 0.01582458    0.0           1.366679      0.0
BOH3                18664.37      0.0           0.7221629     0.0
HCL                 1.21427E-13   0.0           3.44155E-12   0.0
N2                  52.34492      0.0           149966.       0.0
O2                  28.54927      0.0           45546.33      0.0
SIO2                9.329865      0.0           0.0           0.0
ALOH3               0.0129071     6247.641      0.0           0.0
CACL2               1.71779E-08   0.0           0.0           0.0
NABOH4              16031.99      0.0           0.0           0.0
CACO3               0.09165912    0.0           0.0           0.0
ALO2H2CL            1.18431E-25   0.0           0.0           0.0
OHION               32.53833      0.0           0.0           0.0
ALOH2ION            2.71548E-07   0.0           0.0           0.0
ALOH4ION            36.82693      0.0           0.0           0.0
ALOHION             7.61751E-13   0.0           0.0           0.0
B2OOH5ION           3614.747      0.0           0.0           0.0
B3O3OH4ION          12483.81      0.0           0.0           0.0
B4O5OH4ION          4795.054      0.0           0.0           0.0
B5O6OH6ION          123.1697      0.0           0.0           0.0
BOH3CLION           6.729215      0.0           0.0           0.0
BOH4ION             58511.18      0.0           0.0           0.0
CAION               1.092315      0.0           0.0           0.0
CAOHION             0.01297687    0.0           0.0           0.0
CLION               604.589       0.0           0.0           0.0
CO3ION              20.06105      0.0           0.0           0.0
H2SIO4ION           0.01888412    0.0           0.0           0.0
H3OION              6.09689E-05   0.0           0.0           0.0
HCO3ION             41.07034      0.0           0.0           0.0
HSIO3ION            18.23164      0.0           0.0           0.0
NAION               21340.89      0.0           0.0           0.0
ALION               1.46170E-16   0.0           0.0           0.0
CACO3.H2O           0.0           180.6157      0.0           0.0
NATROLITE           0.0           95.17759      0.0           0.0
                    ============= ============= =============
=============
Total lb            6.19847E+06   6523.434      225447.       0.0
Volume, ft3         99496.95      42.87554      3.68950E+06   0.0
Enthalpy, Btu       -4.19010E+10  -4.59754E+07  -1.68750E+08  0.0
Density, lb/ft3     62.29811      152.1476      0.06110499
Osmotic Pres, atm   9.94169
Ionic Strength      0.00281952
```

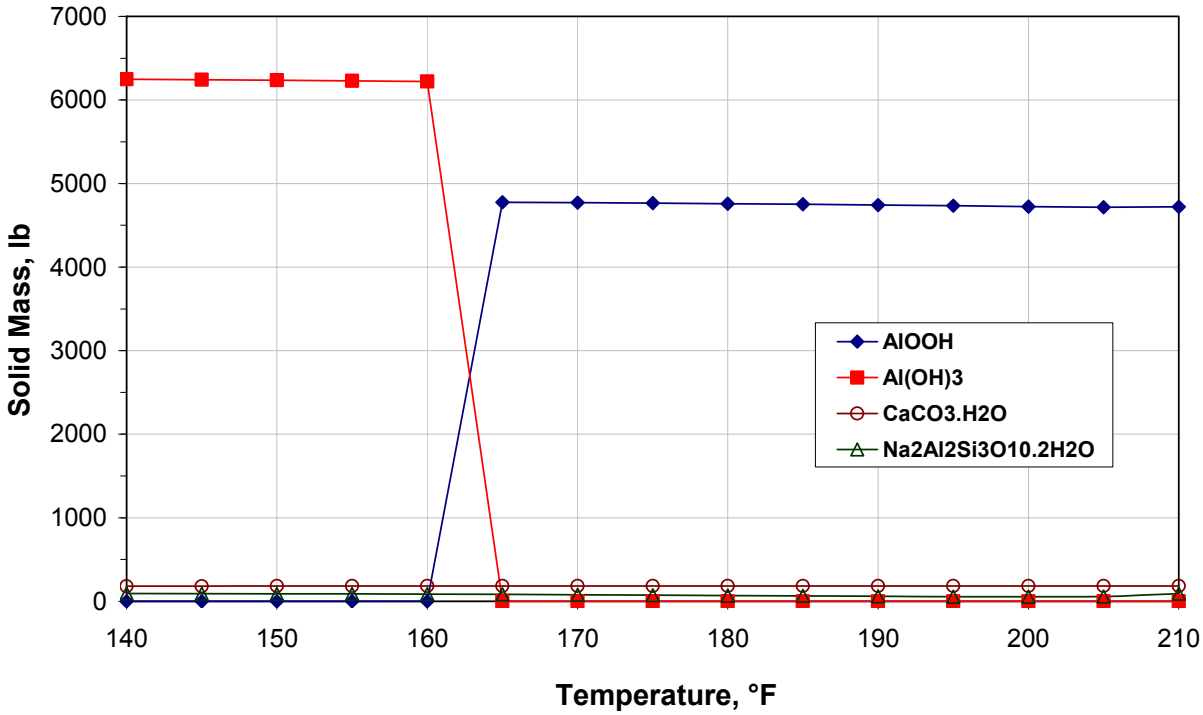

Figure 4: Solids Predicted to Form from ICET #1 Fluids Below Boiling

The result of major significance is the predicted precipitation of aluminum as $Al(OH)_3$ (gibbsite or amorphous) at lower temperatures and as AlOOH (boehmite) at higher temperatures. In the ICET experiment, the aluminum did not precipitate unless cooled or allowed to dwell for some time at temperature. The comparison of the predicted and observed outcomes indicates that the aluminum is likely supersaturated or colloidal in the ICET experiment, a situation not uncommon for aluminum. The apparent aluminum supersaturation may be abetted by surface complexation by borate and other anions (Klasky et al. 2006).

If it is possible that a change in conditions could cause the aluminum to precipitate (achieve thermodynamic equilibrium) or the precipitates to coalesce during a post-LOCA period, then large amounts of $Al(OH)_3$ or AlOOH (~6000 to 5000 lb or ~2700 to 2300 kg, respectively, depending on temperature) could form. The transition from $Al(OH)_3$ to AlOOH would occur between 160 and 165°F (about 72°C). Although predicted, the reverse conversion of AlOOH to $Al(OH)_3$ as the solution cools below 165°F is not expected because of the low solubilities of AlOOH and $Al(OH)_3$ and the observed slow kinetics of aluminum hydroxide and oxide hydroxide interconversions (Wefers and Misra 1987). The ICET #1 experiment found an aluminum-rich solid post-precipitated when the sample was cooled from 60°C.

The ICET #2 experiment represents plants that use TSP for pH control in reactor containments and have little calcium silicate insulation (Table 13). The amount of solids predicted to be present is relatively small. The measured calcium is predicted to be completely precipitated as the phosphate (hydroxylapatite), with little change in amount (92 lb; 42 kg) over the temperature range studied (Figure 5). The measured silica and magnesium is predicted to be completely soluble at lower temperatures (over 1100 lb or 500 kg of amorphous SiO_2), but solid magnesium silicate [chrysotile; $Mg_3Si_2O_5(OH)_4$] is predicted to form starting at about 155°F (68°C), increasing to as much as 90 lb (41 kg) at 205°F (96°C). This is not enough material to cause

concern, but could become significant if larger amounts of magnesium were present. Magnesium oxide and hydroxide are used to remove silica from water and wastewater because silica is adsorbed by the precipitate and because insoluble magnesium silicates form in accordance with this prediction. Calcium and sodium silicates are not nearly as insoluble as magnesium silicate. No solids were observed to precipitate within the ICET #2 solution.

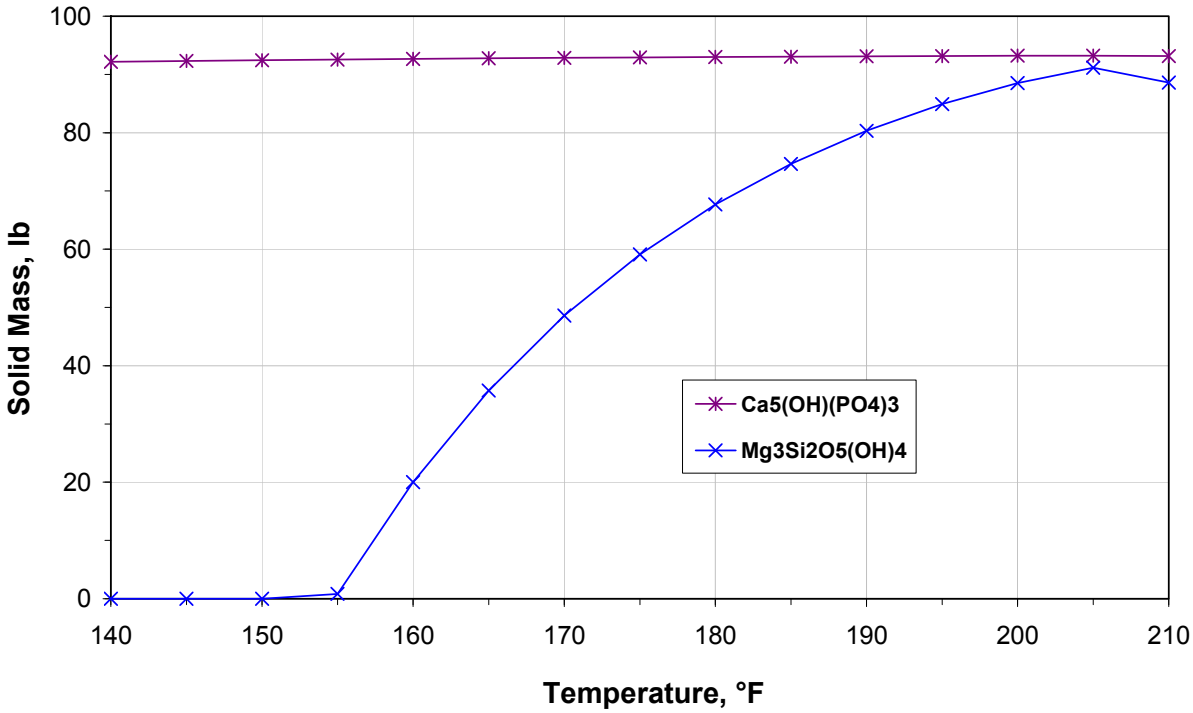

Figure 5: Solids Predicted to Form from ICET #2 Fluids below Boiling

The ICET #3 experiment represents plants that use TSP for pH control in reactor containments and have substantial calcium silicate insulation (Table 13). The measured pH of 8 could not be obtained in a simulation with the compositional data in Table 11 and Table 12. The composition is nearly the same as ICET #2, and the predicted pH is the same, i.e., near neutral. After considering the high level of calcium and silica found in the ICET #3 samples, and the increase in pH from the same initial value as ICET #2, it was concluded that the calcium silicate insulation must have dissolved, releasing hydroxide anions. Therefore, $Ca_5Si_6O_{17}{\cdot}5.5H_2O$ (tobermorite, the main mineral in the calcium silicate insulation) was added to the StreamAnalyzer input composition.[13]

It was found that with 3,000 mg/liter of tobermorite added to the initial composition, the equilibrium pH was predicted to be 8.0.[14] This is due to the dissolution of the tobermorite and precipitation of $Ca_5(OH)(PO_4)_3$ and amorphous SiO_2 by the reaction:

$$Ca_5Si_6O_{17} + 3\ Na_3PO_4 + 5\ H_2O \rightarrow Ca_5(OH)(PO_4)_3 + 6\ SiO_2 + 9\ NaOH$$

(13) Note that tobermorite has the ideal composition $Ca_5Si_6O_{16}(OH)_2{\cdot}4H_2O$; the formula used is that found in the OLI database.

(14) Adding 3 g of tobermorite per liter of solution, about 0.3 wt%, is minor compared to the ~11 volume percent of cal-sil (compared with water), about 25 wt%, added to the ICET #3 experiment.

As the tobermorite dissolves, it is expected that the pH will continue to increase. The calcium precipitates until all of the phosphate and carbonate are consumed; the concentration of soluble calcium then increases as the tobermorite dissolves. The silica will continue to precipitate as the tobermorite dissolves, maintaining equilibrium with dissolved silica. These trends were observed in the ICET #3 experiment, in which the relatively large initial increase in pH was paralleled by the increases in calcium and silicon measured in the samples. As time progressed, the silica concentration leveled off while the calcium concentration continued to increase.

As shown in Figure 6, large amounts of hydroxylapatite and silica are predicted to precipitate, with the silica amount in general decreasing with temperature. At 140°F (60°C), 10,717 lb (4,866 kg) of apatite and 288 lb (131 kg) of hydrocalcite are predicted to form, with 1,378 lb (625 kg) of calcium remaining in solution as Ca^{2+}. At the same temperature, 8613 lb (3910 kg) of amorphous SiO_2 is predicted to precipitate, with 1,546 lb (701 kg) remaining dissolved. The phase $Ca_2Si_3O_7(OH)_2 \cdot 1.5H_2O$ (gyrolite, similar to tobermorite) is predicted to partially replace silica at the higher temperatures. Based on element analysis of solids deposited on clean surfaces in the ICET #3 experiments (which showed only calcium, oxygen, and phosphorus), the precipitation of a calcium phosphate occurred during ICET #3. According to the thermodynamic modeling, apatite is the favored calcium phosphate phase. However, other calcium phosphates have such low solubilities at neutral pH that their conversion to apatite would be kinetically hindered. The practical difference with respect to solids loading and precipitation is negligible, however.

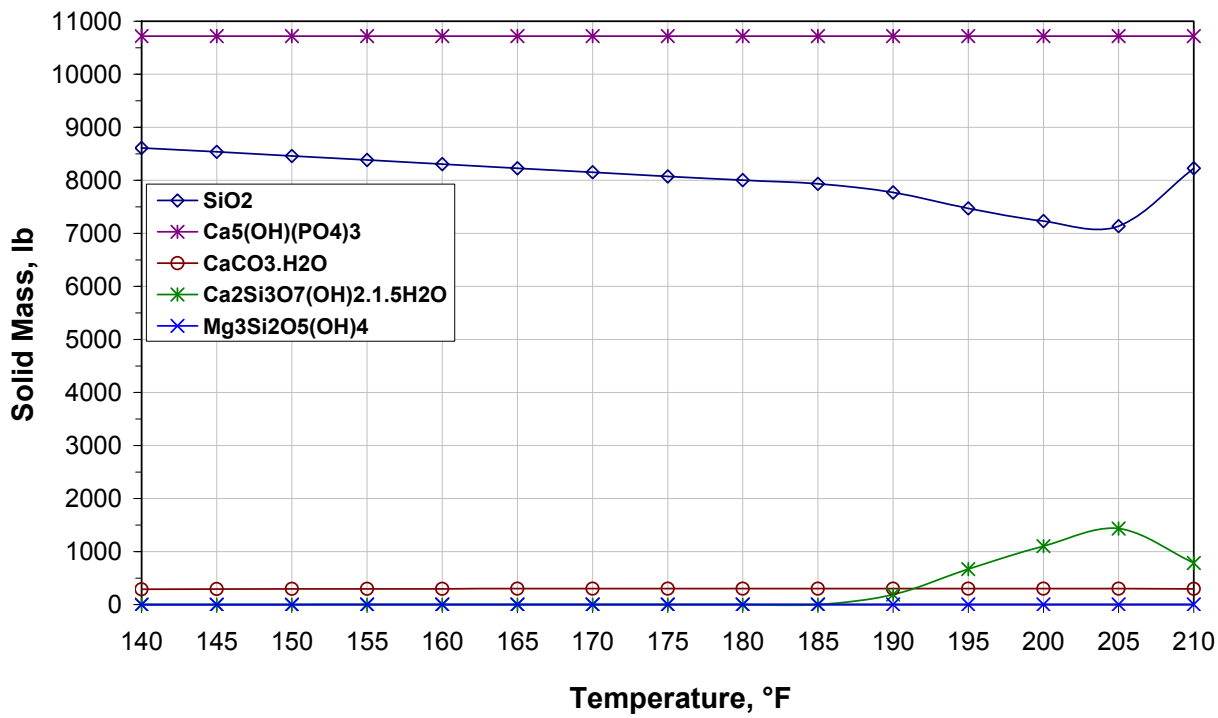

Figure 6: Solids Predicted to Form from ICET #3 Fluids Below Boiling

If the large amounts of hydroxylapatite and silica predicted to precipitate actually existed in the ICET #3 experiment, they apparently settled out during the test and were not observed in the sampled water. A calcium phosphate precipitate deposit was observed on corrosion coupons

and the coupon rack (Section 3.6 of the ICET #3 report; Dallman et al. 2006). There was also substantial evidence that calcium phosphate precipitate had formed, precipitated, and settled out during the ICET #3 experiment. The total amount of solid phase in the cooling system pool would increase because of the conversion of tobermorite solids from the calcium silicate insulation to hydroxylapatite and calcite, converting soluble phosphate and carbonate to precipitated solids, and the accompanying precipitation of SiO_2.

In the OLI simulations, the 18,700 lb (~8,500 kg) of tobermorite added to achieve the target pH was predicted to be converted to 19,600 lb (~8,900 kg) of apatite and silica, an increase of 900 lb (~400 kg). It would be expected (and was observed in the ICET #3 experiment by the distribution of solids within the test vessel) that the freshly precipitated solids would be more mobile than the source tobermorite insulation, increasing the risk of plugging the containment sump strainers and blocking water flow to the RHR pumps.

The ICET #4 experiment represents plants that use NaOH for pH control in reactor containments and have substantial amounts of calcium silicate insulation (Table 13). Even though the same amount of calcium silicate insulation was used in ICET #4 as in #3, no evidence of secondary precipitates was described in the test findings (Dallman et al. 2006). The simulation results agreed with the test observations and also gave no indication of large amounts of precipitates (Figure 7). This is logical because no phosphate was available to react with the insulation to precipitate apatite, as in ICET #3. The simulations predicted that only hydrocalcite will form, apparently by the following tobermorite decomposition reaction:

$$Ca_5Si_6O_{17} + 5\ CO_2 + H_2O \rightarrow 5\ CaCO_3{\cdot}H_2O + 6\ SiO_2$$

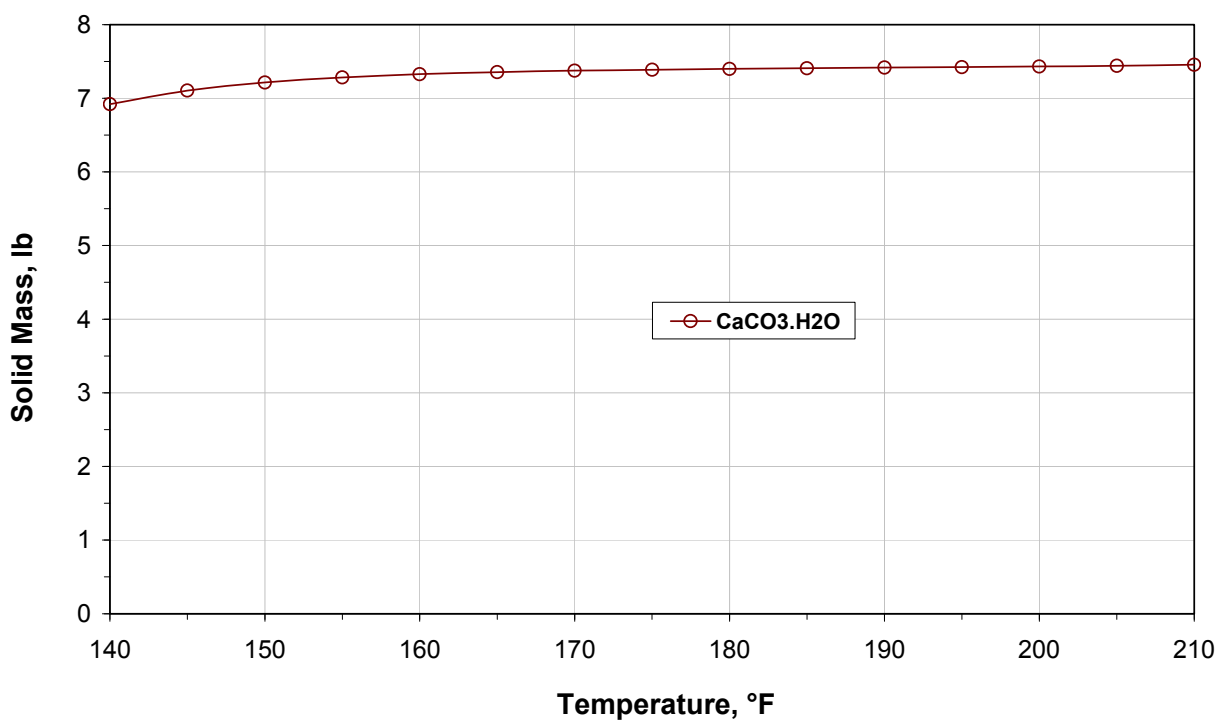

Figure 7: Solids Predicted to Form from ICET #4 Fluids Below Boiling

As discussed above, calcite rather than hydrocalcite is likely the actual product. Silica is much more soluble than calcite or hydrocalcite (particularly at the temperature and pH of the test), so precipitated silica was not predicted. No tobermorite was added to the input composition, however, as in the simulation of ICET #3, so that only the calcium concentration analyzed in the ICET #4 water samples was available to precipitate. If all of the 86 lb (39 kg) of carbonate ion predicted to form in the simulations were reacted with calcium, 143 lb (65 kg) of calcite could form. This is still not a significant amount of precipitate for 100,000 ft^3 (~2.8×10^6 liters) of cooling water. Though not significant, the retrograde solubility of hydrocalcite is shown in Figure 7.

The ICET #5 experiment was designed to represent plants that use $Na_2B_4O_7{\cdot}10H_2O$ (borax) for pH control in reactor containments and have little calcium silicate insulation (Table 13). This composition behavior is similar to that of ICET #1, except that the sample aluminum concentrations were about 13% of those in the ICET #1 experiment. As in the ICET #1 simulations, essentially all of the aluminum is predicted to precipitate (Figure 8). The same explanation is offered; the aluminum is probably supersaturated or in suspended colloidal form. If this condition existed in the cooling water, the precipitation or agglomeration of relatively large amounts of amorphous aluminum hydroxide is likely. As was observed in ICET #1, aluminum-rich post-precipitate was observed in the ICET #5 experiment.

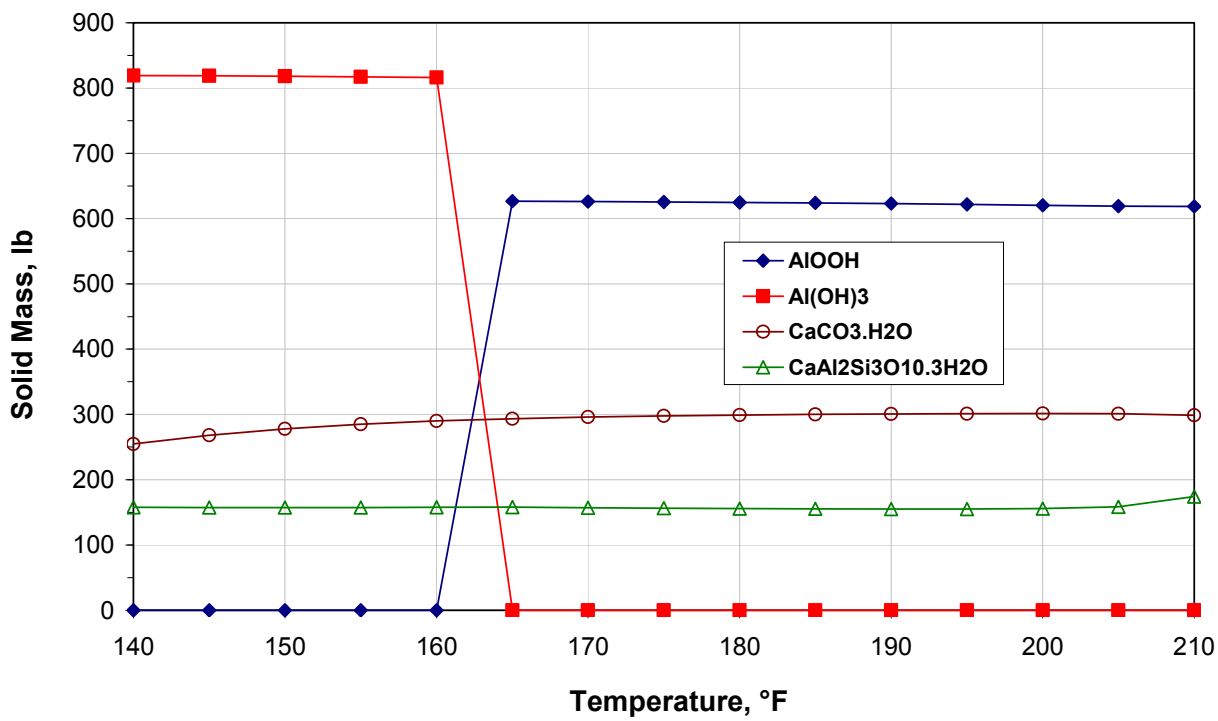

Figure 8: Solids Predicted to Form from ICET #5 Fluids Below Boiling

The concentration of calcium measured in the ICET #5 samples is high considering that no calcium silicate insulation was included. Consequently, the OLI simulations (which used the measured values as input) predict significant amounts of hydrocalcite and $CaAl_2Si_{10}{\cdot}3H_2O$ (scolecite) precipitation (Figure 8). The retrograde solubility of calcium compounds is apparent in the plot of the results. Although scolecite was not observed in the ICET #5 experiment

(Dallman et al. 2006), the amounts of solids predicted from this source are less abundant than those from other sources.

11.4 Simulation Results—Above the Boiling Point

If the cooling water contacts surfaces that are hot enough and have enough thermal mass (heat capacity) to flash part or all of the water to steam, various solids will form that may enhance corrosion of the heated reactor vessels or fuel. The water evaporation will leave solids deposited on the hot surfaces. Initially, these solids will be amorphous or glassy due to the rapid precipitation rate induced by the rapid water evaporation. However, dynamic re-wetting and drying could enhance crystal growth in these solids. Because of dissolved salts, the bubble point of the solution rises to 250°F (121°C) or more before all of the water is vaporized.

The compounds that are predicted by the OLI software to result from solution evaporation are shown in Figure 9 to Figure 13 for the ICET #1 through #5 experiments, respectively. Again, the predictions are made based on thermodynamic modeling, reflecting equilibrium conditions, and do not include the effects of reaction rates (kinetics), which could be important but require experimentation to determine. As will be shown, at high enough temperatures, molten borate salts could form, which can be quite corrosive, possibly generating more solids by corroding the underlying metal that would eventually be carried away by the cooling water. The predicted compounds do not include any of these possible corrosion products, however.

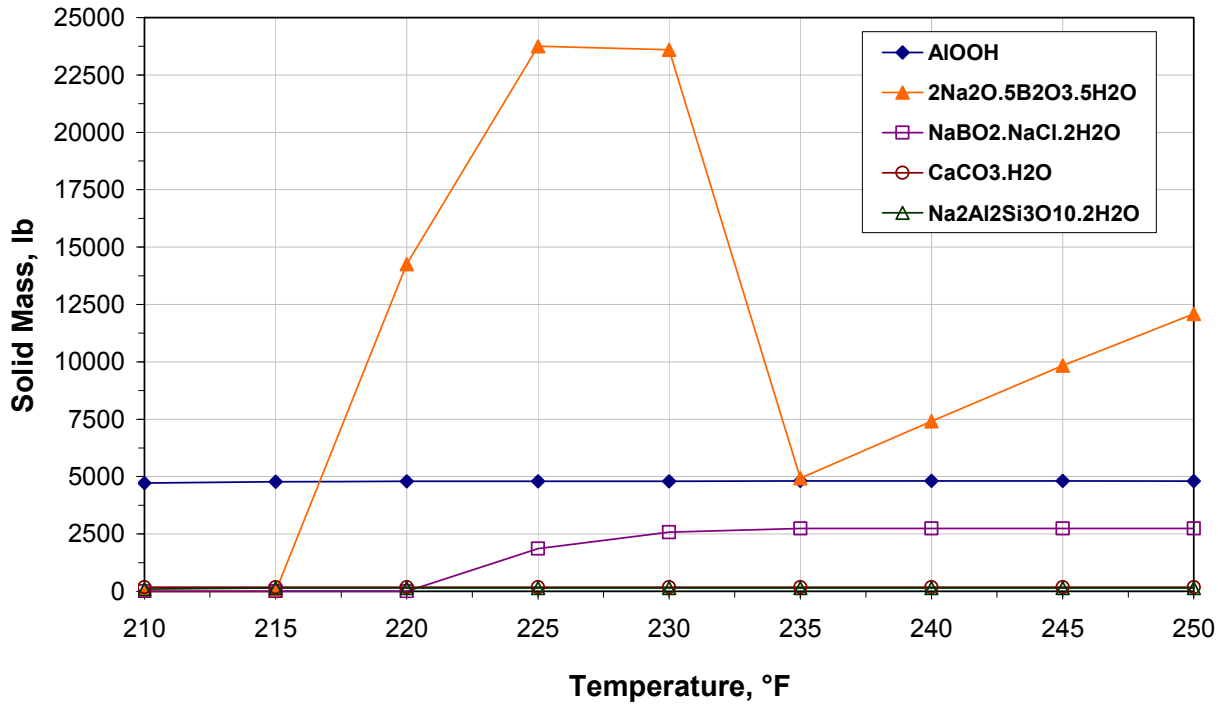

Figure 9: Solids Predicted to Form from ICET #1 Fluids above Boiling

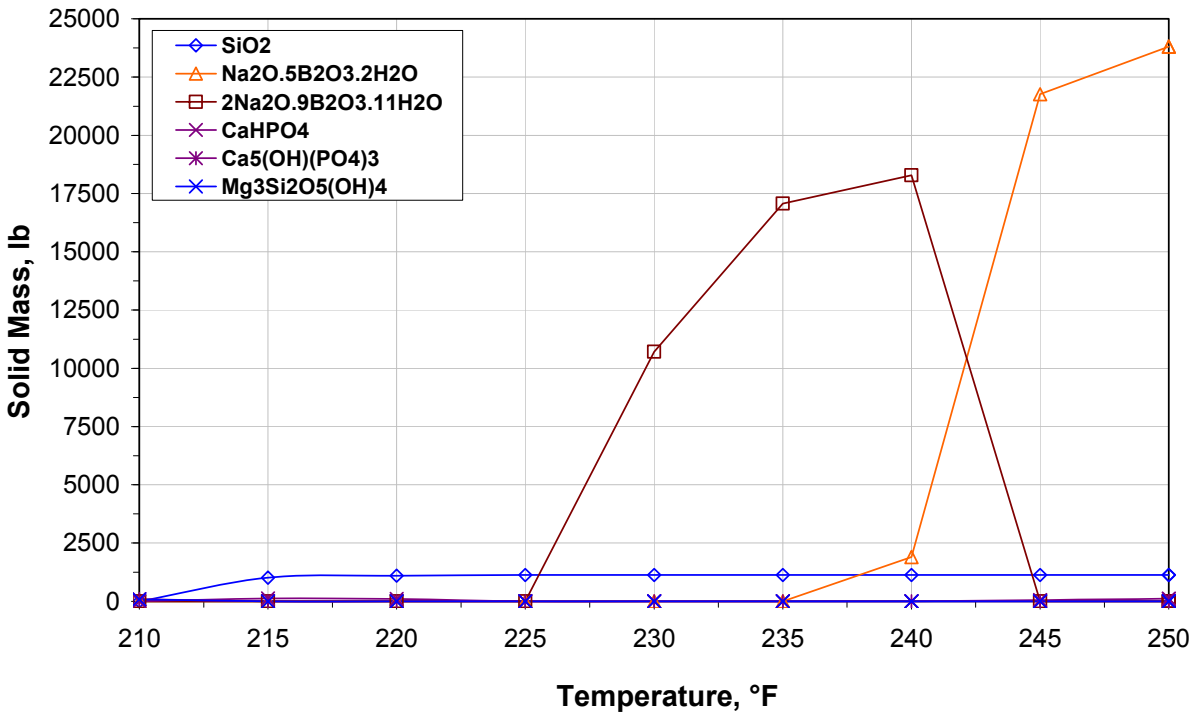

Figure 10: Solids Predicted to Form from ICET #2 Fluids above Boiling

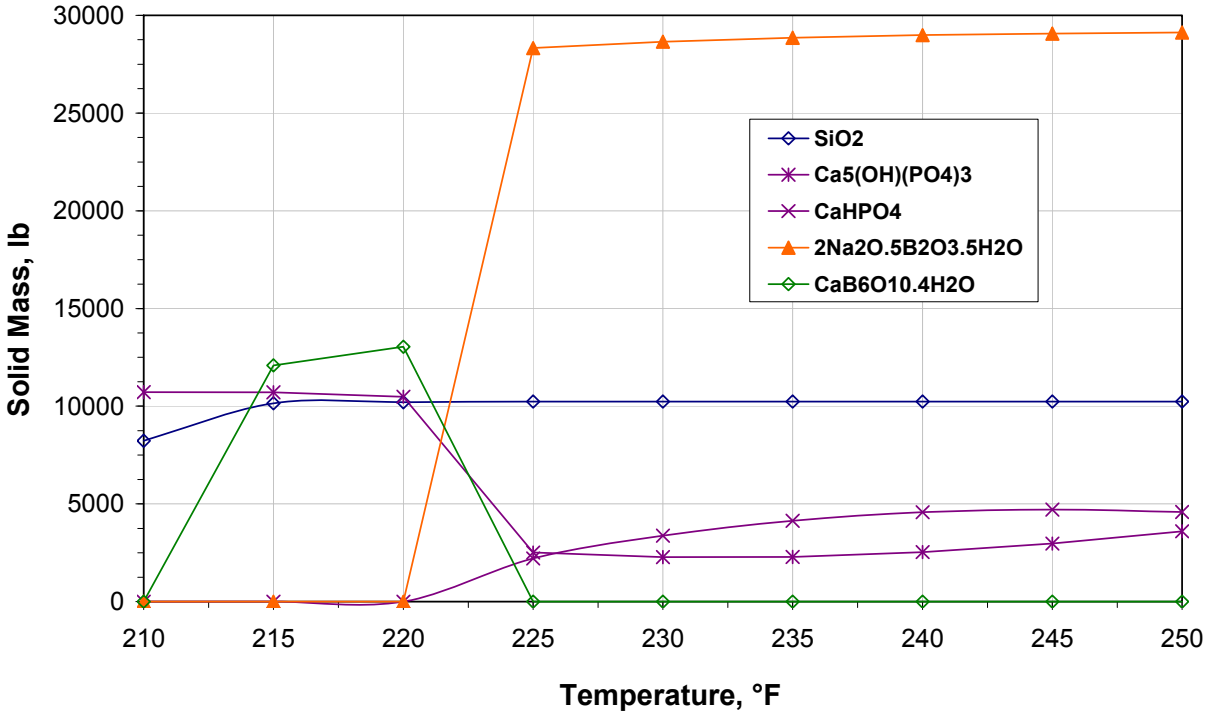

Figure 11: Solids Predicted to Form from ICET #3 Fluids above Boiling

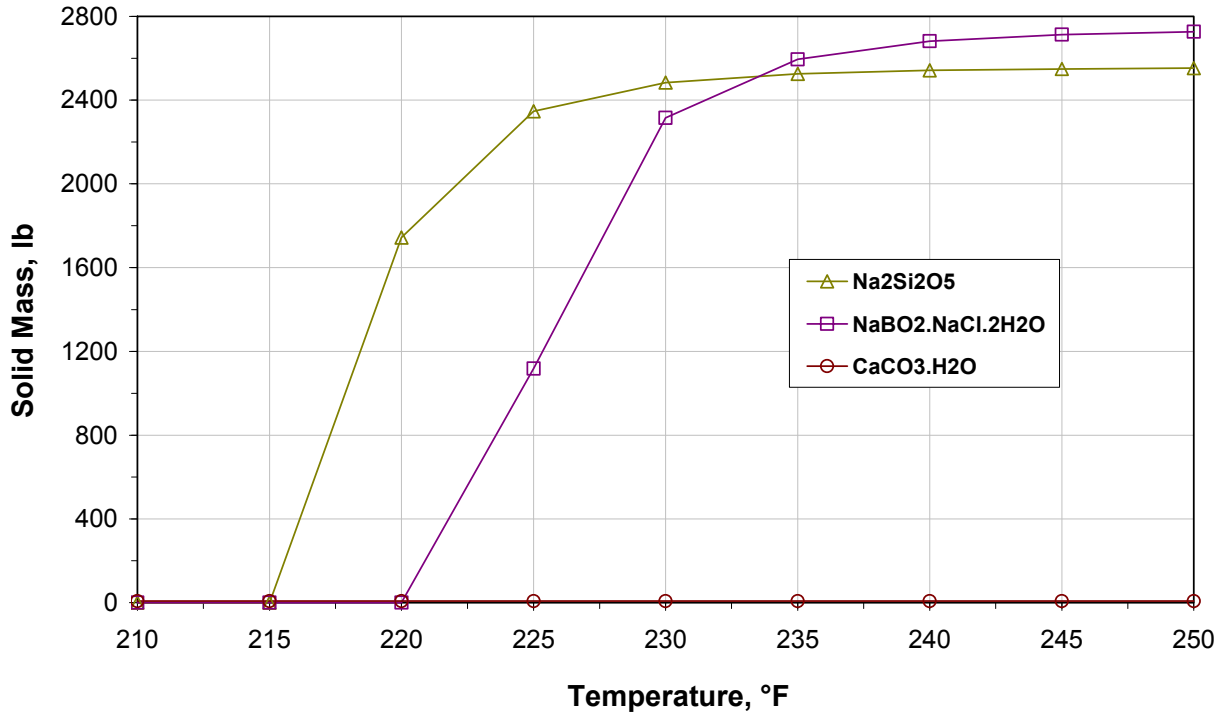

Figure 12: Solids Predicted to Form from ICET #4 Fluids above Boiling

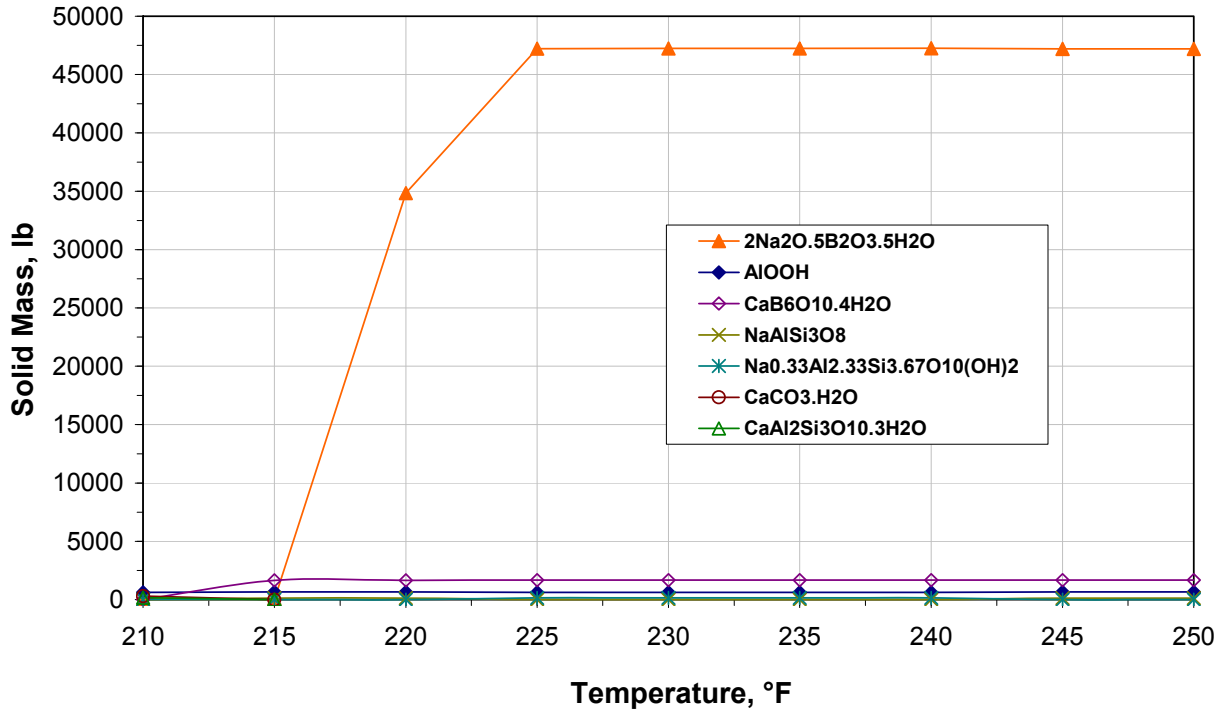

Figure 13: Solids Predicted to Form from ICET #5 Fluids above Boiling

To illustrate the evolution of the solid phases that arose at 140 to 210°F (Figure 4 to Figure 8), the y-axes of Figure 9 to Figure 13 are expanded in Figure 14 to Figure 18, respectively.

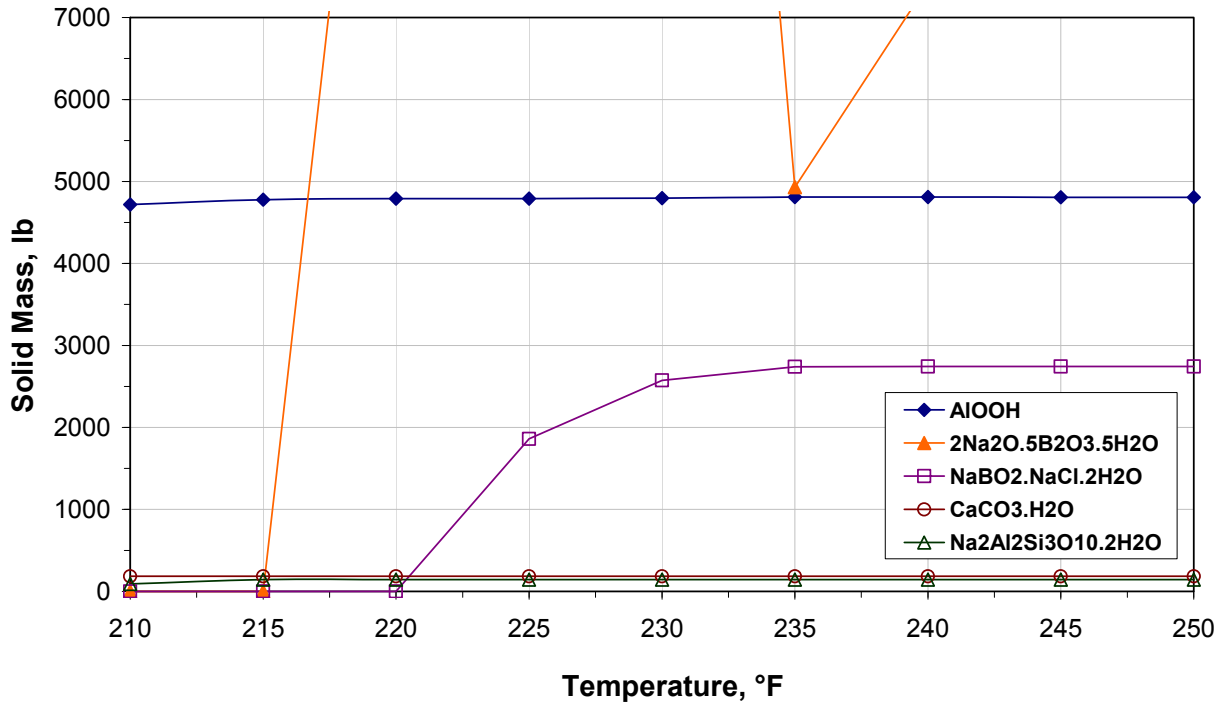

Figure 14: Minor Solids Predicted to Form from ICET #1 Fluids above Boiling

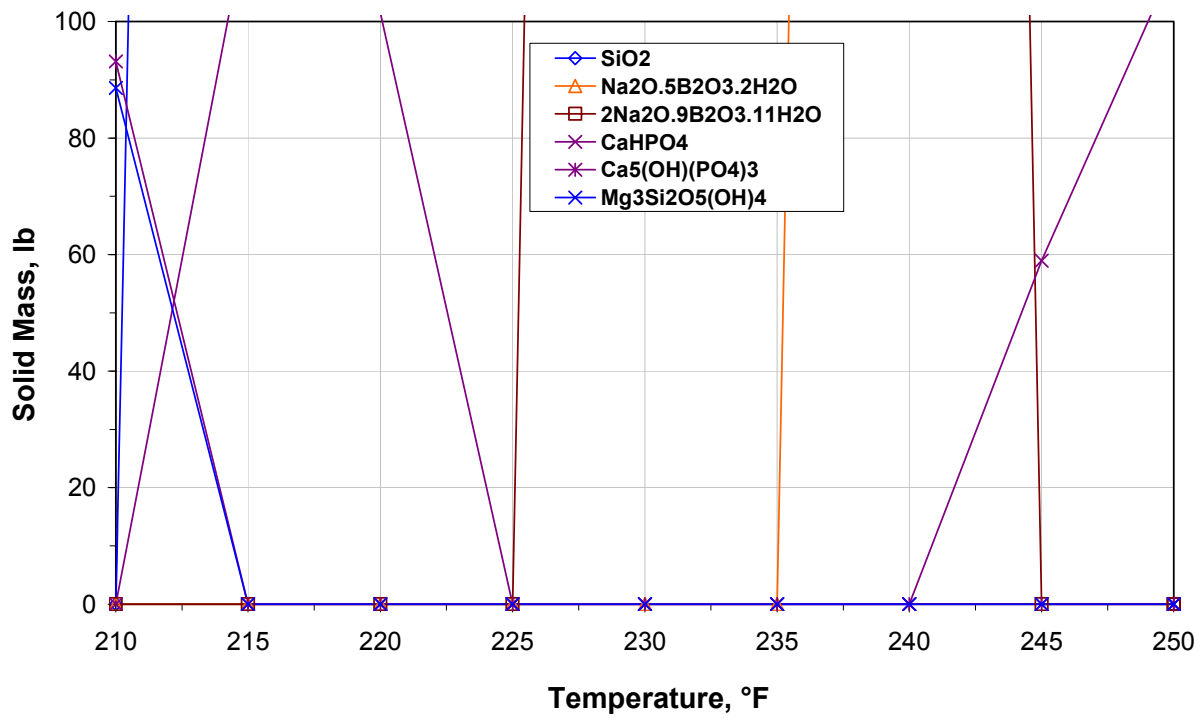

Figure 15: Minor Solids Predicted to Form from ICET #2 Fluids above Boiling

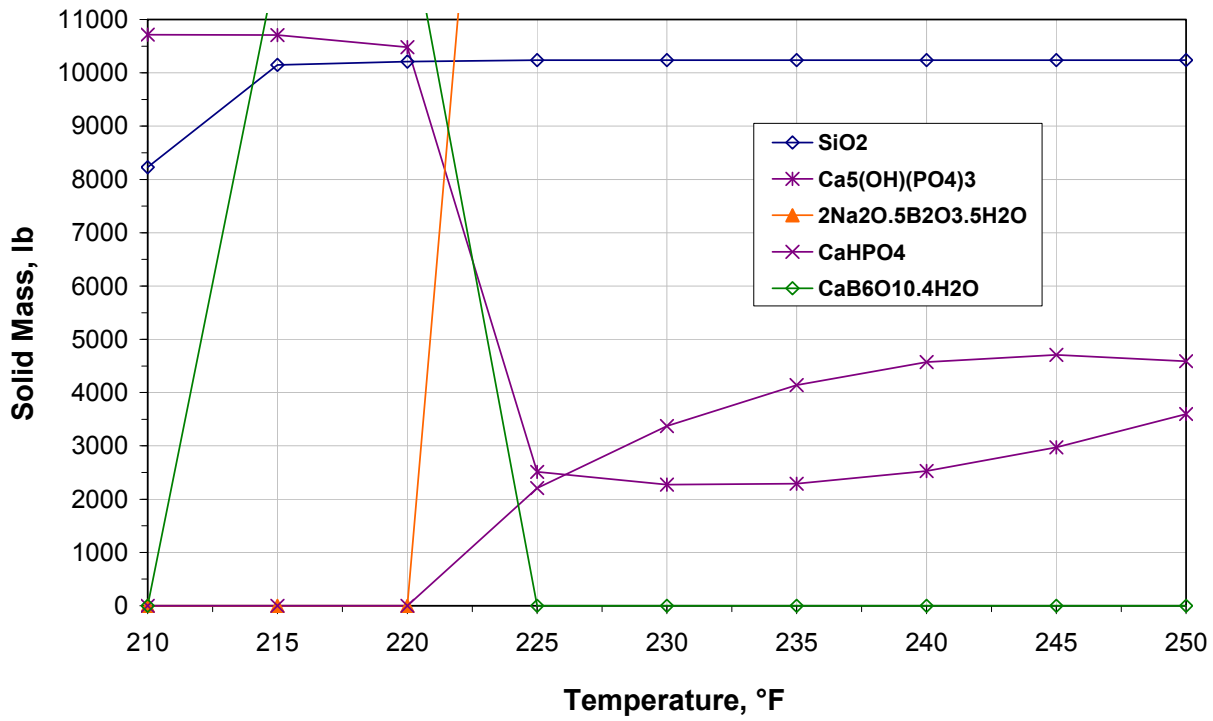

Figure 16: Minor Solids Predicted to Form from ICET #3 Fluids above Boiling

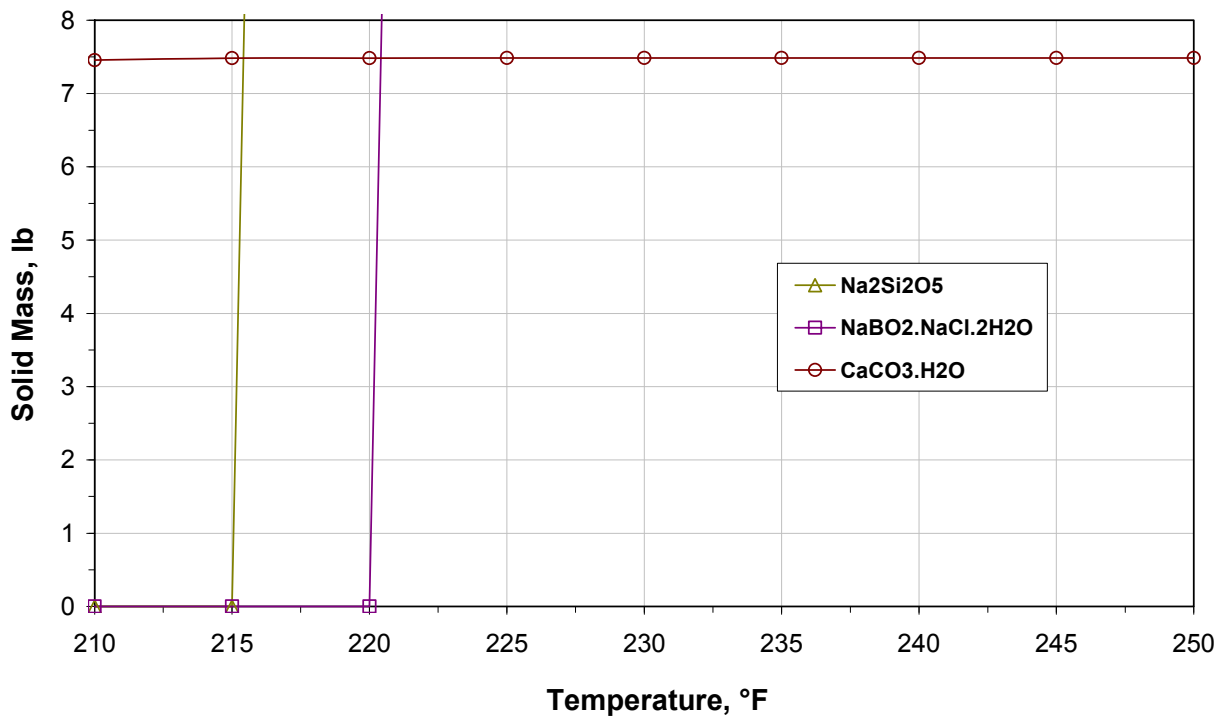

Figure 17: Minor Solids Predicted to Form from ICET #4 Fluids above Boiling

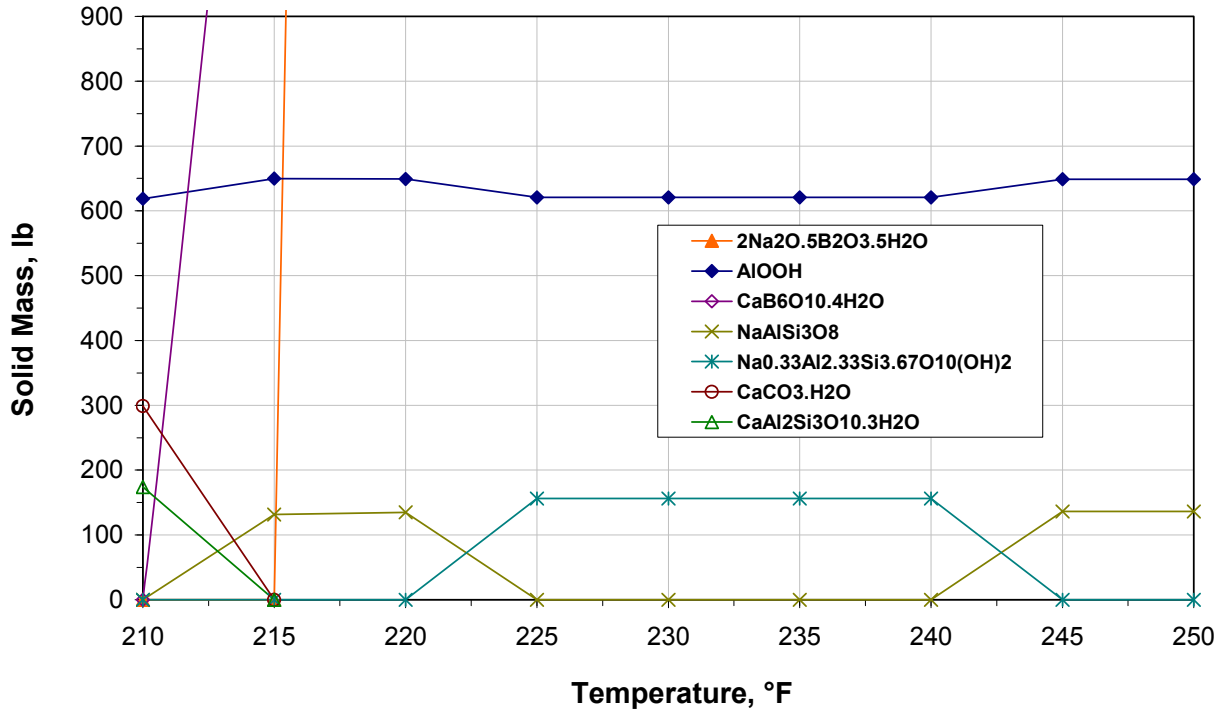

Figure 18: Minor Solids Predicted to Form from ICET #5 Fluids above Boiling

As shown in Figure 9 through Figure 13, since boric acid and borax are the main chemicals dissolved in the cooling water, the major solids that are formed are borate salts. The borate salts predicted to form are $2Na_2O{\cdot}5B_2O_3{\cdot}5H_2O$, $NaBO_2{\cdot}NaCl{\cdot}2H_2O$, and $2Na_2O{\cdot}9B_2O_3{\cdot}11H_2O$. The phase $CaB_6O_{10}{\cdot}4H_2O$, predicted for ICET #3 and #5 compositions in lesser amounts, is controlled by the amount of calcium in solution. The other predicted solids carry over from the lower temperature precipitates (Figure 14 through Figure 18) and include sodium silicates, calcite, hydroxylapatite, boehmite, silica, and minor amounts of calcium and magnesium silicates. The various borate salts are expected to be readily redissolved upon their re-immersion into hot water. The reversibilities of the dissolution of the lower solubility precipitates such as hydroxylapatite (and calcium hydrogen phosphate, $CaHPO_4$), boehmite, silica, the sodium, calcium, and magnesium silicates, and the aluminosilicates, however, are expected to be poor because of their low solubilities and the low solubilities of their constituent silicates, aluminates, and phosphates. For example, $NaAlSi_3O_8$ (albite, a framework-type aluminosilicate mineral) and $Na_{0.33}Al_{2.33}Si_{3.67}O_{10}(OH)_2$ (sodium beidellite, a sheet-type aluminosilicate mineral) are shown in Figure 18 to interconvert from albite to beidellite and back to albite as the temperature is raised from about 220°F and 245°F. However, the formation, dissolution, and re-formation of these highly structured three-dimensional aluminosilicates are kinetically slow even under optimum conditions. Thus, the predicted interconversions between albite and sodium beidellite are highly unlikely within the 30-day post-LOCA time of interest and, rather, a sodium aluminosilicate gel may even form.

Hydrocalcite, $CaCO_3{\cdot}H_2O$, is also predicted to be present in the 210°F to 250°F range. However, as mentioned previously, this is an obvious error in the thermodynamic model. The literature on hydrated calcite indicates that it only exists at low temperatures (e.g., air conditioning systems) whereas the anhydrous form is dominant in most systems. The ESP model predicts that hydrocalcite solubility decreases with temperature faster than that of calcite,

$CaCO_3$, making calcite more stable at low temperatures and hydrocalcite more stable at higher temperatures. This trend is in direct opposition to what is found in the technical literature. This result indicates that hydrocalcite should be replaced by calcite in all of the simulation results.

Water will be boiling at atmospheric pressure in the PWR core and pressure vessel under post-LOCA conditions. Therefore, further insight into solids deposition might be found in BWR experience. For example, the "evaporation and dry-out" model describes the deposition of precipitated hydroxides such as FeOOH and $Ni(OH)_2$ followed by their dehydration to form ferrite spinel phases found in crud (see Topic 8, crud release effects) such as magnetite, Fe_3O_4, and nickel ferrite, $NiFe_2O_4$ (Chen 2000; work of Asakura such as Asakura et al. 1978). Similar or identical phenomena could be expected in the post-LOCA PWR where not only solid phase recirculating steel or high nickel alloy corrosion products would be expected, but also finely particulate debris from concrete, shredded fiberglass, and cal-sil insulation.

11.5 Conclusions

Retrograde solubility is a topic of concern in considering the behaviors of the fluids transiting the reactor vessel and fuel. The software predicts an increasing activity coefficient for the Ca^{2+} ion with temperature, characteristic of retrograde solubility, as shown in Table 15. Of the important solute species [Na^{+1}, Ca^{+2}, CO_3^{-2}, $B_3O_3(OH)_4^{-1}$, $Al(OH)_4^{-1}$, $H_2SiO_4^{-2}$, OH^{-1}, and Cl^{-1}], only Ca^{+2} has increasing activity coefficients by increasing the temperature from 140°F to 210°F, meaning that only calcium-bearing solids will increase in quantity as the temperature increases.(15)

The role of retrograde solubility in increasing the quantity of calcium precipitation in the post-LOCA system is not predicted to be significant relative to the total amounts of solids. The total quantities of calcite predicted to form from suspended or dissolved species in the cooling water are as high as 300 lb (136 kg; of which only ~50 lb or 22 kg is from retrograde solubility). This total quantity is only about 50 mg/liter for a 100,000 ft^3 cooling water pool. When hydroxylapatite was predicted to form because of the apparent phosphate-induced dissolution of calcium silicate insulation, the solubility is so low that little or no retrograde solubility effect was predicted in the range of 140°F to 210°F.

The amount of hydroxylapatite that may form from the dissolution of calcium silicate insulation, however, is very large for those systems using phosphate buffers. It was predicted by the simulation of ICET #3 that approximately 18,000 lb (~8,200 kg) of the insulation could dissolve and be precipitated as hydroxylapatite and silica. These solids would be very fine in particle size and gelatinous (owing to hydroxylapatite's exceedingly low solubility and the propensity of silicate minerals to form silica gels when the parent silicate minerals are dissolved; Iler 1979). In practice, calcium phosphate precipitates at lower temperatures, as shown in the ICET experimentation, and re-crystallization to form hydroxylapatite would be slow. In the presence of circulating dissolved phosphate salt, the calcium phosphate precipitation would occur on or near the dissolving calcium silicate insulation as the calcium ion is released.

---

(15) Activity coefficients are not given for higher temperatures because solvent water evaporates and because the activity coefficient only has meaning for dissolved species. However, even with evaporative loss of water, the new MSE model developed by OLI allows the thermodynamic transition from terms of aqueous solution activity coefficients to solid- and molten-phase Gibbs-free energies expressed in the mole fraction. Note also that the model predicts $H_2SiO_4^{-2}$, although H_4SiO_4 and $H_3SiO_4^{-1}$ might be predicted at lower temperatures.

Table 15: Water Activity and Activity Coefficients for Soluble Species in Post-LOCA Coolant

Temp. °F	Activity H_2O	Activity Coefficient							
		Na^{+1}	Ca^{+2}	CO_3^{-2}	$B_3O_3(OH)_4^{-1}$	$Al(OH)_4^{-1}$	$H_2SiO_4^{-2}$	OH^{-1}	Cl^{-1}
140	0.9959	0.7952	0.6030	0.3958	0.7952	0.7998	0.4129	0.7759	0.8492
145	0.9958	0.7942	0.6199	0.3940	0.7945	0.7986	0.4109	0.7758	0.8468
150	0.9958	0.7931	0.6372	0.3922	0.7937	0.7974	0.4089	0.7757	0.8443
155	0.9958	0.7920	0.6549	0.3903	0.7928	0.7961	0.4068	0.7755	0.8417
160	0.9958	0.7908	0.6730	0.3882	0.7919	0.7948	0.4046	0.7752	0.8392
165	0.9958	0.7896	0.6915	0.3860	0.7909	0.7935	0.4023	0.7748	0.8365
170	0.9957	0.7882	0.7104	0.3837	0.7898	0.7920	0.3999	0.7743	0.8339
175	0.9957	0.7868	0.7296	0.3813	0.7886	0.7906	0.3974	0.7737	0.8311
180	0.9957	0.7853	0.7492	0.3786	0.7874	0.7890	0.3947	0.7730	0.8283
185	0.9956	0.7836	0.7691	0.3757	0.7860	0.7873	0.3918	0.7721	0.8254
190	0.9956	0.7816	0.7894	0.3724	0.7843	0.7854	0.3885	0.7710	0.8223
195	0.9955	0.7793	0.8100	0.3683	0.7822	0.7831	0.3844	0.7694	0.8189
200	0.9954	0.7760	0.8308	0.3625	0.7793	0.7799	0.3788	0.7668	0.8149
205	0.9952	0.7696	0.8514	0.3512	0.7735	0.7739	0.3681	0.7611	0.8089
210	0.9932	0.7342	0.8373	0.2922	0.7406	0.7411	0.3136	0.7263	0.7845

Such materials may create serious plugging problems on the pump strainers or other places in the pumping circuit if they release from the parent calcium silicate insulation. Overall, it appears that phosphate, and the higher pH, abets the dissolution of the calcium silicate insulation, leading to the formation, with the dissolved calcium, of the highly insoluble calcium phosphate or hydroxylapatite, leaving the dissolved silica to quickly exceed its solubility and form gels.

Another phenomenon of concern is aluminum corrosion with apparent supersaturation or formation of stable colloidal suspensions in the systems, having little calcium silicate insulation. As mentioned in the ICET reports, it appears that calcium silicate insulation dissolves to provide the corrosion protection to aluminum that is characteristic of silicates. Indeed, sodium silicate solutions are commercially used as aluminum corrosion inhibitors, and silicate is particularly effective at alkaline pH (Figure 9, page 39, of Davis 1999). Phosphate also has been found to be effective (Troutner 1957). But in the absence of silicate, the corrosion of aluminum is severe. If the supersaturated solution or colloidal suspension becomes unstable, severe plugging could result from aluminum hydroxide precipitation.

For temperatures at or above the boiling point, high concentrations of dissolved borate salts and other solids could form because of flashing of the cooling water on the hot stainless steel reactor vessel liner or fuel cladding surfaces. This may result in significant deposits that could be corrosive to the vessel and cladding, indirectly adding corrosion products to the solids load in the coolant circuit. The outcome is more severe to the hotter fuel cladding, threatening its integrity and possibly contaminating the coolant circuit with the contained fuel. Deposits also will impair heat transfer from the fuel to the coolant, increasing the fuel cladding temperature.

The corrosion resistance of stainless steel to 100°C ~0.4 mole/liter ammonium tetraborate solution is ≤1 μm/year (Belous et al. 1965). However, the interactions of borate salt deposits in hot dry-out conditions with the reactor vessel materials and the fuel cladding at higher temperature may deserve additional investigation. This is because molten sodium borate salts are aggressive towards refractory metal oxides, making them useful as fluxing agents to break down minerals for chemical analysis (Bock 1979). One type of mineral susceptible to molten

sodium tetraborate is zirconium dioxide, ZrO_2, the protective layer on zirconium metal. Boric acid/carbonate salt mixtures are used to break down chromium oxide, the protective layer on stainless steel. Although these analytical fusions are conducted at ~1000°C to decrease analysis times, the high temperatures attained on reactor vessel or fuel surfaces may be sufficient to initiate breakdown of these protective layers on the pressure vessel and fuel, leading to more rapid corrosion of the underlying metal.

The corrosion of carbon steel by a hot and evaporatively concentrated boric acid leak near the CRDM of the Davis-Besse plant shows the aggressiveness of this medium. Although the boric acid attack was directed to the low alloy steel, leaving only the stainless steel vessel cladding material as the vessel coolant pressure boundary, the temperature was kept relatively cool by the fully functional heat exchange system (NRC 2004b). The corrosion of low alloy steel, 308 stainless steel, and Alloy 600 in boric acid systems at 150°C, 260°C, and 300°C has been tested (Park et al. 2005). In dry environments, the boric acid exists as a dry powder of HBO_2/H_3BO_3 at 150°C, molten HBO_2 at 260°C, and as a molten mixture of HBO_2 and B_2O_3 at 300°C; negligible corrosion is found for all three metals tested under dry conditions at these three temperatures. However, the low-alloy steel corroded significantly (150 mm/y at 150°C) in boric acid with water present while no corrosion was observed for 308 stainless steel or Alloy 600. The low-alloy steel corrosion rate decreased with increasing temperature.

No information was found on the corrosion rates of stainless steel or zirconium alloys in molten HBO_2/B_2O_3 under the oxidizing higher temperature (>300°C) conditions that might exist in dry-out locations in or near the core. If prior laboratory studies of the interactions of hot mixed borate salt with zirconium and stainless steel do not exist, a program of laboratory study is recommended, given the use of boric acid or borates for fusion digestions. The deposition of solids on core and reactor vessel surfaces by various drying mechanisms that have been described for BWR experience also might be extended and expanded to post-LOCA PWRs.

12 TOPIC 10—ORGANIC MATERIAL IMPACTS

Questions regarding the impacts of organic materials on the post-LOCA coolant environment and in sump strainer blockage were raised in Section 5.6 of the PIRT report (Tregoning et al. 2007). These issues are addressed in the following discussion. The impacts of organics on co-precipitation and other synergistic effects (Topic 6) and on inorganic agglomeration (Topic 7) have been previously discussed. An introduction to the topic of organic materials, primarily as coatings, is given in Section 12.1. Stabilities of the coatings by vapor-phase and aqueous-phase processes are addressed in Sections 12.2 and 12.3, respectively. The transport of organic coatings as fragments and as flakes is discussed in Section 12.4. The leaching of organics from coatings is discussed in Section 12.5. Estimates of the maximum organic concentration in competition with the loss of organic concentration from solution by radiolysis are provided in Section 12.6. Conclusions drawn from these considerations are presented in Section 12.7 followed by suggestions for further study in Section 12.8.

12.1 Introduction—Coating Application and Failure Modes

The largest inventory of organics likely to be released in the post-LOCA environment comprises degraded coatings used within containment and solvents leached from these coatings. The coating types include epoxies, alkyds, vinyl, and inorganic zinc (IOZ) (Natesan et al. 2006). A search was conducted for qualified and unqualified coating stability data for conditions up to the severity encountered during a LOCA event. The survey focused on reports of coating degradation and failure. Degradation and failure modes included dissolution, blistering, flaking, cracking, and delamination. While solvent leaching into the aqueous phase can occur and is considered below, it is not considered here to be a degradation mode since the integrity of the film typically is not compromised by this process alone. Reports found for Service Level I coatings used in the nuclear industry and reports for closely related coatings were used to reach the conclusions discussed in this Section. If a failure was noted under conditions less harsh than the LOCA event, it was assumed that failure could also occur under the more severe LOCA conditions.

A key issue related to the integrity of a qualified coating under any condition is whether the coating was properly applied. To verify proper crosslinking under test conditions, epoxies need to be cured at a temperature consistently above 50°F for at least 3 days for atmospheric use and for at least 7 days for immersion conditions consistent with a LOCA DBA. Coatings intended for use and cured adequately for nominal atmospheric service are expected to also be sufficient for immersion conditions, assuming that they are not immersed within several weeks of application. In addition, the majority of DBA-qualified coatings were documented to be applied in accordance with the plant specifications and in compliance with ANSI N101.2 and N101.4 paint testing and quality assurance standards.

The topcoat applied to a cured epoxy film needs to be done within an “overcoating window” to allow proper bonding to the base coat. Beyond this time limit, poor adhesion may result in cracking, peeling, and delamination of the topcoat. Topcoat adhesion may also be reduced by “amine blush,” a surface coating of unreacted polyamines, often caused by improper humidity or poor ventilation during curing. Unreacted amines and retained solvents can also cause blistering upon immersion.

The topcoat can delaminate from IOZ coatings if there is insufficient moisture when the zinc coating was applied. A full cure requires a relative humidity of at least 40% or misting of the primer film. An experienced applicator is required to minimize excessive dry film thickness, which can cause mudcracking. The IOZ coatings react with both acids and bases and are not recommended for pH below 5.5 or above 8.5; the susceptibility of IOZ to failure caused by post-LOCA fluids being outside this pH regime therefore is of concern.

The Plant Support Engineering center within the Electric Power Research Institute (EPRI) has surveyed nuclear plants to gather data on the condition of service level 1 coatings used within primary containment (PSE 2007, p. 5). The primary conclusions drawn from this survey were that modified phenolic epoxy (MPE) was associated with degradation more frequently and consistently than in other coatings. This was true whether or not the MPE was applied over an IOZ primer onto metal substrates. Though MPE was applied to concrete in only 31% of the surveyed cases, it accounted for 81% of the total instances of degradation. The most common reason for coating failure was attributed to coating application problems in surface preparation, coating thickness, or sufficiency of curing. The degradation was manifest most frequently by delamination. Blistering, cracking, and flaking were the successive secondary manifestations of failure. These failures were symptomatic of coating application problems. The data did not identify aging as a cause of failure.

Several studies have been conducted to investigate coating stabilities under a variety of conditions, including accident scenarios. The findings for vapor phase (non-immersed, but normally sprayed) and aqueous phase (immersed) studies are discussed below.

12.2 Vapor-Phase Processes

Industry-sponsored coating tests have been conducted for different coating types and applications. Testing has been conducted for unqualified original equipment manufacturer (OEM) coatings used in containment (Eckert 2005), for qualified coatings in the zone of influence of the LOCA break (Andreychek 2006), and on qualified coatings in containment (Dupont et al. 2001 and Sindelar et al. 2000).

The report on unqualified OEM coatings (Eckert 2005) summarizes the degradation evident when a non-buffered boric acid solution was sprayed onto several non-nuclear-grade coating samples under simulated DBA conditions using a modified ASTM D3911 procedure (ASTM 2003). ASTM D3911 simulates DBA conditions using a 7-day spray with an initial temperature of 153°C that is decreased to 93°C over the course of the test. Alkyd, epoxy, epoxy ester, urethane, and IOZ coatings were tested. There was a remarkable variation in the coating stabilities observed.

Without radiation pre-treatment, the following range of percent detachments were seen: alkyd, 1 to 95%; epoxy, 1 to 25%; epoxy ester, 0 to 5%; urethane, 0 to 99%; and IOZ, 1 to 95%. Generally, radiation treatment slightly increased detachment, but its effect depended on coating type and sample. Some samples were more stable after radiation treatment. Thus, unqualified coatings were tested on items treated to 3.2×10^8 rad exposure and a DBA temperature curve (up to 307°F; ~153°C) using a borated water spray for a 7-day duration. Seventeen of the 36 samples were alkyd, and about half of them suffered from 20 to 95% delamination. Nine of the samples were epoxies, and two of them suffered 20% or greater delamination. The five

urethane-coated samples had 5% or less delamination. The two acrylic samples showed 0 and 50% delamination. A zinc primer item showed no delamination while two IOZ coatings showed <1% delamination and 95% delamination. In a separate study, alkyds were found to degrade in alkaline environments; their resistance to the alkaline CSS spray thus would be expected to be poor (Alion 2007). These results demonstrate the possible negative effects of high temperatures on certain coatings and just how statistically variable some coatings' performance can be.

Andreychek (2006) evaluated high-temperature and jet-impingement effects of a 30-sec blowdown through a 2-in. nozzle at 277°C and 2200 psia. No failure or significant erosion of epoxy coatings on any substrate was reported, though some erosion of IOZ coatings was found.

The Savannah River Technical Center (SRTC) examined IOZ primer/epoxy phenolic topcoat coatings (Dupont et al. 2001) and polyamide epoxy primer/polyamide epoxy topcoat coatings (Sindelar et al. 2000) on steel substrates using the ASTM D3911 procedure (ASTM 2003) as in the earlier unqualified coatings testing (Eckert 2005). Results were similar for each coating type. Without irradiation, films remained intact, but with irradiation (10^9 rad), blistering was observed. This high level of irradiation is equivalent to about 1.4 years of exposure at 80,000 rad/h (the exposure rate for the circulating coolant) or 114 years at ~1,000 rad/h (the exposure rate at the sump strainer) and thus exceeds the highest range of radiation exposure expected in the containment over the 30-day post-LOCA period.

Based on these studies, properly-applied qualified coatings are not expected to degrade under the post-LOCA pressure and temperature transient environment. Aging is also not expected to significantly affect the qualified coatings' ability to perform. Unqualified coatings, however, exhibit highly variable performance, and a number of them may fail in the post-LOCA interval.

12.3 Aqueous-Phase Processes

Findings for aqueous-phase testing and case studies are discussed by coating type.

12.3.1 Epoxy Coatings

Polyamide epoxies are usually recommended for fresh and salt water immersion uses. However, there are examples of these epoxies blistering when immersed in fresh water. For example, a steel water tank was coated with a polyamide epoxy primer and topcoat and had weeks to cure before being put into service (Weldon 2002). It is unknown (but unlikely) that the epoxy coatings were rated for nuclear service. Within 6 months, the interior coating was extensively blistered below the waterline. An examination found that residual glycol ether solvent in the coating led to osmotic blistering, indicating that, even after several weeks, the cure was incomplete. Correspondingly, most of the blistering occurred in regions where the coating was thickest. The author noted that it is possible for solvents to remain trapped in coatings for years. It was also suggested that the coating was improperly formulated for the intended use because it contained water-soluble solvents that can facilitate blistering.

At least two epoxies rated for nuclear use contain water-soluble solvents. Whether these coatings hold up during a LOCA with weeks-long immersion could be a matter of speculation without additional evaluation. If a coating was specified to be in an immersion zone, DBA tests

would have been performed per ANSI N101.2 and/or ASTM D3911 to qualify it for the expected service.

Similarly, degradation tests of Service Level I coatings under LOCA conditions found that epoxy coatings on metal coupons formed blisters when heated to 90°C in water for up to 1 month (Wren et al. 1999 and 2000a). Blistering did not occur below 90°C.

Two common Service level I epoxy coatings have been qualified for potable water use in accordance with NSF/ANSI Standard 61 which tests coatings, in part, for leachable organics. The results of the tests showed the total leachable organic concentrations to be very low, < 1.0 mg/L (1.0 ppm), for the test conditions, pH 5, 8 and 10 in 23° C water temperature. In addition, paint chip samples of another Service Level I coating were tested in an autoclave to determine debris degradation characteristics in a simulated loss of coolant environment (TXU 2006). The liquid residue from the test was analyzed using Infrared Spectroscopy. Trace amounts of aliphatic hydrocarbon material was evidenced by a small band near 2900 cm^{-1}. However, epoxy resin was not detected in either of the filter sample extracts nor the liquid residue. These test results taken together, would indicate that DBA qualified Service Level 1 epoxy coatings would not contribute significantly to the organic source term in a post LOCA sump.

12.3.2 Alkyd Coatings

It is widely recognized that alkyds are not stable under alkaline conditions. Consequently, their use on concrete is not recommended. A commercial study (Alion 2007) demonstrates that the polyester bonds in the alkyd are cleaved under LOCA-relevant conditions. In this study, oils and particulates were produced, and coatings were completely removed from the coupons. These results suggest that, during a LOCA, alkyd coatings below the waterline after buffering are likely to fail. Although not explicitly tested (e.g., with respect to time, temperature), the above findings, which show the instability of alkyds to alkaline environments, suggests that their exposure to the alkaline spray of the CSS also could cause their failure.

12.3.3 Vinyl Coatings

Wren and colleagues (2000a) report that many Service Level I vinyl paint samples form blisters at 90°C but not at lower temperatures. Although vinyl paint Service Level I usage in U.S. nuclear power plants is rare, vinyl paint may be used in OEM equipment. Vinyl applied to carbon steel delaminated at the coupon edges. While it appears that coatings are not dissolved by hot aqueous solutions, they do have the potential to separate from the surface and form particulates that could affect sump operation, especially in combination with other debris that collects at sump strainers.

12.3.4 Inorganic Zinc Coatings

Some testing indicates that non-topcoated IOZ coatings are possibly subject to failure under alkaline (pH >10) conditions that occur under a LOCA (Pinney 1988). The manufacturer of Carbozinc 11SG (Service Level I), Carboline, does not recommend it for non-topcoated use at pH <5.5 or pH >8.5. The Material Safety Data Sheet for Keeler and Long's Kolor-Zinc (not Service Level I) similarly states that these coatings cannot withstand direct contact with acids and alkalis and should be topcoated. There are many square feet of non-topcoated zinc primer in nuclear facilities (Andreychek 2005), many with estimated sump pH near or above pH 10 (some as high as 11 and some as low as 4.5).

The ICET experiments were conducted on IOZ coatings under a variety of conditions simulating possible LOCA scenarios for a period of 30 days (Dallman et al. 2006). Testing at pH 9.5 (NaOH) and 60°C (ICET #1) resulted in weight increases for both submerged and unsubmerged IOZ-coated steel coupons, indicating water uptake or zinc corrosion. Similar results were observed in the ICET #4 experiment at pH 9.8 (NaOH) and 60°C. However, only trace amounts of zinc were found in the test solution for the ICET #4 experiment (i.e., little zinc dissolution as zincate, $Zn(OH)_4^{2-}$, in this ICET experiment having the highest pH). Weight gains were also noted in ICET experiment #5 at 60°C in pH 8 to 8.5 borate solution.

It would appear that in ICET experiments, the IOZ coatings remain attached to the surface of the coupons. However, some plants expect pH ranges higher than those evaluated during ICET, and the post-LOCA temperatures, for relatively short durations (i.e., ranging from a few hours to a day), are also higher than the 60°C evaluated in ICET.

Based on these findings, some degradation of immersed IOZ coatings could be expected in the post-LOCA environment, particularly for alkaline conditions.

12.4 Coating Particle Transport

The Naval Surface Warfare Center (NSWC) studied transport properties of paint chips with equivalent diameters down to approximately 0.4 mm in quiescent and moving water (Fullerton et al. 2006). Five paint systems were studied. The lowest bulk tumbling velocity observed (the velocity needed to transport a chip) was 0.08 m/s. At 0.06 m/s, only the lightest alkyd chips transported with most remaining submerged near the release point. Most of the modified sump strainer designs are expected to have approach flows that are much less than 0.06 m/s; replacement sump strainers for 15 different PWRs have approach velocities ranging from 0.0006 to 0.007 m/s (Alion 2006). Therefore, the transport of similarly-sized and larger paint chips than evaluated in this study are not expected unless localized transport flow velocities approach the transport velocities determined from the NSWC study. The transport of paint particles attached to inorganic solids, including fiberglass insulation, has not been studied, but it seems unlikely that the denser inorganic solids, even as fibers, would enhance paint-chip transport. Therefore, the transport of coating fragments to the sump strainers under post-LOCA flow may occur but is of low likelihood.

Degraded coatings may also be present as equant particles (i.e., particles whose dimensions along the three axes are approximately equal) as well as flakes. The particles will be about the thickness of the applied paint (~0.3 to 0.5 mm) and will be even less subject than paint chips to transport by flowing water. Overall, the transport of coating debris is not expected within containment pools where the bulk transport velocity or localized velocity near the strainer is much less than 0.06 m/s. However, finer coating particles (down to 50 μm diameter) may be transportable.

12.5 Leaching of Organics from Coatings

Iodine interactions with organics within containment during a LOCA scenario have been studied (Wren et al. 1999 and 2000a). Leaching and radiolysis of organics from Service Level I coatings also have been investigated as part of these studies. Four different paints used in the industry were examined—zinc primer and epoxy (which can be used as Service Level I

coatings) and vinyl and polyurethane (which are not used as Service Level I coatings). Some of the main conclusions for these four coating types are:

- Iodine volatility increases because of the presence of paints.
- Organic impurities in the aqueous phase arose from leaching organic solvents out of paints.
- Soluble organics did not come from failure of paints or decomposition of other organic polymers, such as cable insulation.
- MIBK, acetone, heptan-2-one, toluene, and xylene all had very similar dissolution kinetics, and the organic release rate was nearly the same for epoxy, vinyl, and polyurethane coatings. It appeared that the dissolution was dependant on the rate of diffusion of water into the coatings.
- Coatings held solvents for many years. A 5-year-old polyurethane sample contained solvent that was readily released when immersed in water.
- Radiolysis (~47,000 rad/h for up to 20 days) of the dry solid phases was not observed to affect the release of organics from these materials into solution.
- Under the test conditions, radiolysis of the soluble organics was faster than their leach rates. Toluene and xylene were not observed because they were oxidized to phenolics. Other solvents gave organic acids, which decreased the solution pH and eventually formed CO_2.
- There was a strong temperature relationship for organic dissolution from vinyl paints. From coupon tests at 20°C and pH 10, and after 20 h, the MIBK concentration was found to be 1×10^{-5} M. At 60°C, under otherwise similar conditions, the MIBK concentration was about 2.5×10^{-4} M. As the temperature increased, the gas-phase concentration increased.
- The maximum MIBK concentration decreased as the vinyl coating paints aged due to evaporative loss with time. A precise relationship was not obtained, but for a painted area/aqueous volume ratio of 5.25 cm^{-1}, a 2-month-old surface gave 2×10^{-4} M MIBK, while a 5 to 6 year-old sample gave 2.5×10^{-5} M MIBK. These concentrations are far below the solubility limit.
- Solution pH had no effect on organic leaching.

Indications from Wren and colleagues' papers are that organics will be leached from the paints, but that the 10^5- to 10^6-rad/h dose rates expected in the reactor core during the post-LOCA period will readily oxidize those organics that pass through the core to products that are more soluble in water (i.e., phenolics and carboxylic acids) and then eventually to CO_2.

12.6 Estimation of Maximum Leachable Organic Concentration and Radiolysis Rates

Some conservative estimates of the total amount of leachable organics can be made using the results of Wren and colleagues (2000a) and the known characteristics of PWRs (Tregoning et al. 2007). In addition, radiolysis rates can be estimated to give an indication of whether soluble organics are expected to build up or be destroyed over the 30-day period following the LOCA.

Wren and colleagues (2000a) estimate the maximum cumulative organic molecule concentration in their tests as about 1×10^{-3} M for epoxy, the most prevalent coating in nuclear power plants, with concentrations highest at 40°C in the studied range of 25°C to 90°C. With a test volume of 60 milliliters and a coupon area of 5.7 cm^2, the leachable organic per unit area was 1.05×10^{-5} moles of organic/cm^2 or 9.78×10^{-3} moles of organic/ft^2. Coating thicknesses in these studies were about 0.025 cm, or about 10 mils, which falls in the mid-range of coating thicknesses expected within containment (Natesan 2006).

The average low-pool and high-pool liquid volumes have been estimated to be 43,000 ft^3 and 74,000 ft^3, respectively. For the purposes of calculating soluble organic concentrations in containment, these two figures were averaged to a mean liquid volume of 58,500 ft^3 (~1.66×10^6 liters).

The mean painted area within containment is 3.16×10^5 ft^2 (calculated from PWR plant survey data in Table 7 of Andreychek 2005). Not all of this area will be submerged during a LOCA since the mean maximum pool height is about 8 feet (Tregoning et al. 2007), and lower submersion depths are possible, depending on the magnitude of the LOCA. Although the painted surface area at 8 feet is not well defined, the painted surfaces above the mean pool height still will be subject to washing by the CSS as well as subject to ongoing condensation. Therefore, the mean painted area was used with the mean liquid volume to conservatively estimate the mean organic concentration from paint leaching at 1.87×10^{-3} M (about 3,100 moles of organic). This aqueous concentration, though relatively low, is still much higher than the dissolved contributions from RCS pump or other lubricating oils that might be discharged during the LOCA event.

Radiolysis of paint-leached organics, using MEK as a model compound, has also been studied by Wren and colleagues (1999, 2000b). The proposed mechanism of MEK decomposition is by the reaction of hydroxyl radical (OH) arising from water radiolysis to form 3-hydroxy-2-butanone, 2,3-butanedione, and acetaldehyde. The butanone and butanedione products further react with the hydroxyl radical to form acetaldehyde and acetic acid. The 2,3-butanedione also reacts with electrons to give the same products. Acetaldehyde and acetic acid then react with hydroxyl radical to form CO_2. Each step is pseudo-first order, and an overall rate constant for MEK disappearance of 5.1×10^{-5} sec^{-1} is reported.

The detailed model proposed by Wren and colleagues (1999, 2000b) could be used to determine the time required to decompose 99% of the organics, as modeled by MEK. Since conservative assumptions were used to estimate the maximum possible organic concentration, a simpler model using a few assumptions will give an approximate indication of the time scales involved with decomposition. One simplification would be to consider the decomposition as a series of irreversible first-order reactions, i.e.:

$$A \xrightarrow{k_1} B \xrightarrow{k_2} C \xrightarrow{k_3} P$$

where A is MEK, B represents the butanone and butanedione products, C is the acetaldehyde and acetic acid products, and P is CO_2. The rates of decomposition are largely controlled in this solution by the hydroxyl radical concentration, which in turn is a function of the dose rate. The rates of reaction of hydroxyl radical with MEK and its degradation products are all about the same, with the exception of acetic acid, which reacts about an order of magnitude slower (Wren et al. 2000b). A further simplification, therefore, might be that $k_1 \cong k_2 \cong k_3 = 5.1\times10^{-5}$ sec^{-1}, with the possibility that k_3 is less than the other rates. The use of Wren's rate constant for k_1 in the present situation may underestimate the constant in the post-LOCA environment by about a factor of 2 since the average dose rate during a LOCA was estimated to be 8×10^4 rad/h, whereas Wren used a dose rate of about 4.3×10^4 rad/h. The k_1 during a LOCA therefore likely is higher than the k_1 reported by Wren and used here because the rate-controlling hydroxyl radical organic oxidant concentration would be proportionately higher with the higher dose rate.

Using the known solution to this sequential first-order decay problem (Schmid and Sapunov 1982, p. 19) and a maximum concentration of 1.87×10^{-3} M, MEK is calculated to be 99% consumed in about 1 day, and MEK and all of its decomposition products are 99% consumed to CO_2 in about 2 days. If k_3 were an order of magnitude slower at 5×10^{-6} sec^{-1}, the organics would be 99% consumed to CO_2 in about 11.5 days, still well within the 30-day period of concern. In reality, therefore, the organic concentration will never reach the maximum 1.87×10^{-3} M since radiolysis will occur as leaching takes place.

In contrast to the mean organic concentration from paint leaching being 1.87×10^{-3} M (~22 ppm), the solubility of lubricating oil in water is ≤1 ppb at 20°C (Cole 1994, p. 63). A typical RCS pump contains about 200 gallons of lubricating oil. The lubricating oil is synthetic (rather than mineral) and has a viscosity of 68 centistokes, similar to SAE 20-30 automotive crankcase oil. A <1-ppb concentration in a pool water volume of 1.66×10^6 liters corresponds to <1.66 milliliter of dissolved lubricating oil from an initial volume of ~750 liters (i.e., <0.0002% of the oil dissolves), and the concentration of the dissolved oil in the water is $<2.5\times10^{-9}$ moles/liter. Therefore, practically all of the lubricating liquids would form a second phase floating on the aqueous solution. The concentration of dissolved oil in water is trivial and is not expected to change appreciably with higher ionic strength, changed pH, and increased temperature. As a result, the effect of the oil itself as a complexant to affect metal ion complexation (addressed under Topic 6) or surfactant by inorganic agglomeration (addressed under Topic 7) is small. The major effect will be in its interaction with inorganic solids to form OMAs (see Topic 6).

The dissolved or suspended oil, or that oil entrained with solids in OMAs and not collected on the sump strainer or other sites, will be transported to the core while the floating oil may or may not reach the core, depending on whether it reaches the sump intake through turbulence or whether the sump strainer is higher than the pool surface. For any oil transported to the core, rapid radiolytic degradation as modeled for MEK would occur to produce CO_2.

While the radiolysis rate estimates are admittedly crude, they demonstrate that radiolysis is sufficient to reduce the water-transported organic concentration to very low levels over the course of the LOCA event, likely within the first few days. Until decomposed by radiolysis, the impacts of the dissolved organics are limited by the low bleed rates from coatings and the low solubilities of the lubricating oil. For those organics that escape high radiolysis by not passing the core, the primary impact remains their capability to form OMAs and contribute to sump strainer blockage as described in Topic 6, co-precipitation, or other synergistic solids formation.

12.7 Conclusions

The main conclusion of this study regarding organic coatings is that all of the coatings identified by Natesan and Natarajan (2006) as being used in the nuclear industry could undergo failure under post-LOCA conditions under both vapor-phase conditions (often subject to spray and condensation) and aqueous phase conditions. This conclusion is supported by a number of individual studies by industry groups and technical institutions. While certain classes of coatings, such as alkyds, have a higher probability of failure, broad generalizations describing the conditions leading to failure for all coating classes do not appear possible. Even coatings generally recognized as having good stability could be susceptible to failure because of improper application or insufficient curing. This situation could arise through no fault of the applicator and may only become apparent under extreme post-LOCA conditions.
Coatings intended for in-air service also may fail because they are sprayed or become immersed under post-LOCA conditions. Variations in how coatings are applied make it more challenging to predict *a priori* which coatings fail and which remain intact. However, recent *in situ* pull tests have been performed for coatings in four operating plants (Cavallo 2007). It was found that aged, DBA-qualified coatings from various manufacturers that exhibited no visual anomalies continue to exhibit system pull-off adhesion at, or in excess of, the originally specified minimum value of 200 psi, suggesting that visual observations of coating integrity may be a sufficient monitoring program.

With a decrease in approach velocities in more advanced sump strainer designs, transport of floating particle flakes to the sump strainers is not expected. Smaller coating particles of dimensions on the order of the coating thickness are expected to sink as well. Smaller coating particles would increasingly be transported to sump strainers as suspensions by coolant flow.

Even without coating failure, organics that are dissolved or miscible in water could be transported past the reactor core and undergo high radiation fields. Simplified calculations of radiolysis rates of the water-transported organics show that conversion to CO_2 will occur in a matter of days and prevent significant build-up of organic concentrations in solution provided that the intermediate products are not retained by interactions on non-mobile solids surfaces.

12.8 Areas for Further Work

The following are key areas could be investigated to more fully understand post-LOCA coating integrity within containment:

- An *in situ* wet test that simulates LOCA conditions on relatively small test areas in a plant would be germane to the GSI-191 issues. Part of the rationale for such testing is that a common failure mode of epoxies is osmotic blistering caused by water being drawn into coatings by water-soluble salts or solvents that remain embedded in the coatings. This type of failure mode would not be detected by a dry pull test. However, such testing would be difficult to implement as little or no painted surface is routinely immersed in PWRs.

- The interaction of paint solids with inorganic debris (e.g., Nukon, cal-sil) formed during a LOCA is not currently well-known. Early results indicate that interactions occur with alkyd paints (Alion 2007). However, the effects of paint solids and mixtures of paint solids and inorganic debris on sump operation and methods to prevent or mitigate those effects also may be studied.

- The dynamics of floating liquid organics in the sump strainer area and their ability to be drawn past the fuel in the core is a consideration. Floating organics have been noted in paint testing (Alion 2007). If lubricating oil or other floating organics can pass through to the reactor core, they will be subjected to high radiolysis rates to undergo decomposition to carbon dioxide.

- Further calculations of the decomposition time of dissolved or miscible organics in the cooling water would help substantiate the expectation that these organics will radiolytically decompose to CO_2 during the 30-day post-LOCA time period.

- Dissolved paint breakdown products such as phenolics or carboxylic acids, may survive mild radiolysis (i.e., not in the core) and be captured on the surfaces of inorganic solids before they can be re-transported past the core fuel to be destroyed radiolytically. The effects of paint breakdown products on inorganic agglomeration (Topic 7) therefore are currently unknown.

The studies identified in this section would be best pursued in light of the associated inorganic materials (latent debris, cal-sil and fiberglass insulation, metallic corrosion products, and crud) to understand the interactions between organic and inorganic materials as outlined in Topics 6 and 7.

13 SUMMARY AND RECOMMENDED TOPICS FOR FURTHER EVALUATION

This report addresses questions associated with 10 topics that had been raised earlier (Tregoning et al. 2007) which potentially impact ECCS performance in a post-LOCA scenario. To address these questions, technical literature associated with NRC and industry-sponsored efforts to resolve GSI-191 and relevant open technical literature studies were reviewed. Scoping calculations have also been performed as appropriate. The objective of this study was to determine whether sufficient information already exists to sufficiently understand the impact of these questions or whether additional literature and laboratory studies may be useful to increase understanding.

The results of this evaluation have been summarized in Sections 3 through 12 in this report. It has been determined that sufficient information exists to properly address the questions raised for Topics 2 and 3 on concrete carbonation and on alloy corrosion. However, for the remaining eight topics, further evaluation would allow more confident prediction of their effects. The supplemental investigations may entail continued scrutiny of the abundant technical literature, bench- or engineering-scale laboratory testing, and/or additional modeling. The rationales used to support these findings and subsequent recommendations are also presented in the relevant sections of the report.

The topics, approach, and findings from this study are summarized in Table 16. Table 16 also provides the qualitative rankings of the perceived importance of the open technical questions. The rankings are given as low, medium, and high in increasing order of importance with respect to their perceived impacts on sump strainer and ECCS performance.

The interactions of organic materials with inorganic solids were accorded the highest priority, primarily because of the potential high impact that OMAs could have in transporting additional materials (both organic and inorganic) to load the sump strainers. Because organic contributions affect three of the technical topics (Topic 6 on co-precipitation and other synergistic effects, Topic 7 on inorganic agglomeration, and Topic 10 on organic material impacts), additional evaluation of these effects might be pursued in combination. However, the ability of organics to alter inorganic agglomeration raised under Topic 7 have been judged to have low priority.

Medium priority topics for further study include mixed potential modeling of the redox properties of the post-LOCA coolant (Topic 1 on radiation effects), laboratory tests of the viability of microorganisms to grow in post-LOCA conditions (under Topic 5 on biological fouling), and literature or laboratory studies of the attack of pressure vessel and fuel cladding by hot dried borate salts (Topic 9 on retrograde solubility and solids deposition).

In addition to altering inorganic agglomeration by organics (Topic 7), low priority was assigned to understanding the effects of anodic reversal (Topic 4 on galvanic corrosion) and crud release (Topic 8).

Table 16: Research Topics, Approach, Findings, and Importance and Recommended Scope of Further Studies

Topic	Approach	Current Findings	Scope of Further Study & Importance Rank
1. Radiation effects	Evaluate coolant water radiolysis to form H_2O_2, ClO_3^-, ClO^-, HOCl, HNO_3, H^+, and H_2 and silica and insulation debris radiolysis for effects on pH and reduction/oxidation (redox) potential.	Radiation effects on pH were found to be minor in comparison with pH buffering. Knowledge of radiation influence on redox potential is limited and complicated by multiple reactions. Assessment of redox effects requires mixed potential modeling.	Mixed potential modeling, similar to that performed for Boiling Water Reactors (BWRs) and perhaps confirmed by experiment, could be used to assess radiolysis effects on redox potential in post-LOCA coolant. *Medium rank*.
2. Carbonation of concrete	Evaluate whether integrated chemical effects testing (ICET) findings would have been affected if aged (more fully carbonated) rather than new (3 to 11 months old) concrete had been used in testing.	The extent of carbonation in the tested concrete coupons are sufficient to have a negligible effect on ICET outcomes compared with outcomes expected had aged coupons been used.	No additional evaluation required.
3. Alloy corrosion	Evaluate whether use of different metal alloys would have affected ICET findings for post-LOCA system.	Aluminum dominated metal corrosion products found in ICET experiments. Variability of aluminum-alloy corrosion behaviors in two different studies and in general overview of aluminum corrosion suggests little change in outcome likely if other aluminum alloys are tested.	Further evaluations of aluminum alloy variation effects are not recommended.
4. Galvanic corrosion	Evaluate whether galvanic corrosion would affect the amounts and types of corrosion products in post-LOCA system.	Galvanic corrosion (between copper and low alloy steel) only affected limited metal surface area to yield negligible additional corrosion product quantities. Anodic reversal at elevated temperature may cause enhanced steel corrosion of limited quantities of galvanized parts.	Additional literature and laboratory evaluation of anodic reversal phenomenon for galvanized steel under post-LOCA conditions could be performed. *Low rank*.
5. Biological fouling	Evaluate whether growth of biota in post-LOCA coolant waters with low-light, low-nutrient, high-boron, high-temperature, and radiation-field stressors may occur, fouling sump strainers.	Many microbes can grow under one or more post-LOCA biological stressors, but growth and rates under stressor combinations are not known. Low light inhibits algal growth. Green flocculent solids found in Three Mile Island waters provide evidence for growth over long periods.	Inoculation tests of various microorganisms under post-LOCA coolant conditions (composition, lighting, temperature, nutrients, inorganic supports) are suggested. If microbes grow, later tests of their interactions with inorganic solids may be considered. *Medium rank*.

Table 16: Research Topics, Approach, Findings, and Importance and Recommended Scope of Further Studies

Topic	Approach	Current Findings	Scope of Further Study & Importance Rank
6. Co-precipitation and other synergistic solids formation	Determine how co-precipitation, organic complexation, and inorganic/organic agglomeration affect solids formation in the post-LOCA system.	No net effect of solids quantity is anticipated solely from inorganic constituents. Organic complexation is expected to have limited influence because of low complexation strength compared with hydrolysis and the chemical masking afforded by the calcium in post-LOCA waters. Physical interactions akin to organic-mineral-aggregates (e.g., tidal oil spills) are expected of inorganic solids with organic paint and lubricants to mobilize solids to sump strainers. Sump strainer heights greater than the upper pool level may allow floating organics to pass through core to undergo radiolysis to CO_2.	Could increase transportability of solids to sump strainers by interactions between floating organics (lubricants, paint, and plastic decomposition products) and inorganic solids. Consider effects in combination with Topics 7 and 10. *High rank*.
7. Inorganic agglomeration	Predict the roles of soluble organics and their decomposition products on inorganic agglomeration.	The contributions of organics and organic break-down products on inorganic agglomeration are not reliably predicted. The effects likely are small as most of the soluble/miscible organics will pass by water circulation to the core to be destroyed by radiolysis.	Consideration of inorganic agglomeration is best pursued in combination with higher priority issues under Topic 6 on synergistic (inorganic/organic) solids formation and in light of studies under Topic 10 on organic degradation. *Low rank*.
8. Crud release effects	Evaluate the quantities and availabilities of crud from RCS (steam generator tubes and piping), fuel, and core structures.	"Crud burst" conditions of increased oxygen concentration, physical shock, and abruptly altered pH and temperature will prevail in LOCA events, potentially mobilizing crud inventories. Crud solids, mostly from fuel, are projected to be ~1000 kg. Quantities are small compared with cal-sil insulation solids but could be significant for systems with limited particulate.	Crud solids contribute to fine solids loading from other sources [$Al(OH)_3$ from Al corrosion, Ca silicates and phosphates and silica from cal-sil reactions]. *Low rank*.
9. Retrograde solubility and solids deposition	Evaluate effects of retrograde solubility and solids deposition on hot core and fuel structures.	Thermodynamic modeling of ICET solution systems is performed at sub-boiling and above boiling to determine retrograde solubility and salt solids depositions on hot core and fuel structures. Retrograde solubility is observed for calcium-bearing solids, but the effect on solids loading is small because of already low calcium solubilities. Extensive borate salt depositions on fuel or component surfaces above boiling temperatures may be corrosive, based on use of borates as mineral fluxing agents in chemical analysis, will add to the solids load,	High-temperature dried borate salts on pressure vessel and fuel cladding may be corrosive. Further literature or laboratory study (e.g., "evaporation and dry-out" in BWRs) would help determine magnitude of this effect. *Medium rank*.

Table 16: Research Topics, Approach, Findings, and Importance and Recommended Scope of Further Studies

Topic	Approach	Current Findings	Scope of Further Study & Importance Rank
		and may impair heat transfer from the fuel.	
10. Organic material impacts	Evaluate effects of physical and radiolytic degradation of organic materials from coatings (paints) and from lubricants.	Many paints undergo hydrolytic decomposition and loss of adherence under LOCA and post-LOCA conditions to contribute to load in coolant. Dissolved and suspended organics undergo radiolysis by passing through the core and fuel. Radiolysis is likely sufficient to fully decompose continually recirculating organics to CO_2 within days. Organics floating above sump strainers or retained behind strainers will survive radiolysis and can interact with solids as described in Topics 6 and 7.	Movement of floating organic past sump strainer and fuel/core for radiolytic destruction depends on strainer design. Effects of organics from paints and from lubricants to enhance sump screen loading should be considered in combination with Topics 6 and 7. *High rank*.

14 REFERENCES

10 CFR Part 50. 2008. "Domestic Licensing of Production and Utilization Facilities." *Code of Federal Regulations*, U.S. Nuclear Regulatory Commission.

Alion. 2006. *ECCS PWR Sump Screen Qualification and Testing Information*. Alion Science and Technology, NRC presentation May 24, 2006, U.S. Nuclear Regulatory Commission, Washington, D.C., ADAMS Accession # ML062080738.

Alion. 2007. *Alkyd Coatings Chemical Testing*. Alion Science and Technology, NRC presentation August 22, 2007, U.S. Nuclear Regulatory Commission, Washington, D.C., ADAMS Accession #ML072420578.

Allen E, P Smith, and J Henshaw. 2001. *A Review of Particle Agglomeration*. AEAT/R/PSEG/0398, Issue 1, AEA Technology Engineering Services, Inc., Sterling, Virginia.

Andreychek TS. 2005. *Test Plan: Characterization of Chemical and Corrosion Effects Potentially Occurring Inside a PWR Containment Following a LOCA*. Westinghouse Electric Company, Revision 13, Monroeville, Pennsylvania; see also Appendix C of Dallman et al. 2006.

Andreychek TS. 2006. *Coatings Jet Impingement Tests*. Presentation to GSI-191 Public Meeting – PWR Sump Debris Blockage, February 9, 2006, U.S. Nuclear Regulatory Commission, Washington, D.C., ADAMS Accession #ML060410490.

Andreychek TS, MD Coury, AE Lane, KF McNamee, RB Sisk, D Mitchell, PV Pyle, WA Byers, KJ Barber, DP Crane, ME Nissley, DJ Fink, G Wissinger, H Dergel, BG Lockamon, and PA Sherburne. 2007. *Evaluation of Long-Term Cooling Considering Particulate and Chemical Debris in the Recirculating Fluid*. WCAP-16793-NP, Rev. 0, Westinghouse Electric Company LLC, Pittsburgh, Pennsylvania.

Asakura Y, M Kikuchi, S Uchida, and H Yusa. 1978. "Deposition of Iron Oxide on Heated Surfaces in Boiling Water." *Nuclear Science and Engineering* 67(1):1–7.

ASTM. 2003. *Standard Test Method for Evaluating Coatings Used in Light-Water Nuclear Power Plants at Simulated Design Basis Accident (DBA) Conditions*. D3911-03, American Society for Testing and Materials, West Conshohocken, Pennsylvania.

ASTM. 2007. *Standard Specification for Aluminum and Aluminum-Alloy Sheet and Plate*. B209-07, American Society for Testing and Materials, West Conshohocken, Pennsylvania.

Barrer RM. 1982. "Synthesis and Some Properties of Salt-bearing Tectosilicates." Chapter 7 of *Hydrothermal Chemistry of Zeolites*, Academic Press, London, United Kingdom.

Barton M, MR Conqueror, K Garbett, MA Mantell, ME Phillips, MV Polley, and WA Westall. 2001. "Corrosion Product Measurements at the Sizewell B PWR," pp 391-398 in Volume 2 of *Water Chemistry of Nuclear Reactor Systems 8*, British Nuclear Energy Society, London, United Kingdom.

Bary B and A Sellier. 2004. "Coupled Moisture – Carbon Dioxide – Calcium Transfer Model for Carbonation of Concrete." *Cement and Concrete Research* 34:1859–1872.

Bates JK, WL Ebert, DF Fischer, and TJ Gerding. 1988. "The Reaction of Reference Commercial Nuclear Waste Glasses during Gamma Irradiation in a Saturated Tuff Environment." *Journal of Materials Research* 3(3):576–597.

Beahm EC, RA Lorenz, and CF Weber. 1992. *Iodine Evolution and pH Control*. NUREG/CR-5950, U.S. Nuclear Regulatory Commission, Washington, D.C.

Belous VN, AI Gromova, ZT Shapovalov, and VV Gerasimov. 1965. "Corrosion Resistance of Structural Materials in Boron-Containing Solutions." *Atomic Energy* 19:1532–1535.

Bergmann CA, J Roesmer, and DW Perone. 1983. *Primary Side Deposits on PWR Steam-Generator Tubes*. EPRI-NP-2968, Electric Power Research Institute, Palo Alto, California.

Bertsch PM, WP Miller, MA Anderson, and LW Zelazny. 1989. "Coprecipitation of Iron and Aluminum During Titration of Mixed Al^{3+}, Fe^{3+}, and Fe^{2+} Solutions." *Clays and Clay Minerals* 37(1):12–18.

Blesa MA, AD Weisz, PJ Morando, JA Salfity, GE Magaz, and AE Regazzoni. 2000. "The Interaction of Metal Oxide Surfaces with Complexing Agents Dissolved in Water." *Coordination Chemistry Reviews* 196:31–63.

Bock R. 1979. Pages 88-92 of *A Handbook of Decomposition Methods in Analytical Chemistry*, International Textbook Company, Glasgow, Scotland.

Booth W. 1987. "Postmortem on Three Mile Island." *Science* 238:1342–45.

Bojinov M, T Buddas, M Halin, M Helin, R Kvarnström, P Kinnunen, T Laitinen, E Muttlainen, K Mäkelä, A. Reinvall, T Saario, P Sirkiä, and K Tompuri. 2002. "Correlating Activity Incorporation with Properties of Oxide Films Formed on Material Samples Exposed to BWR and PWR Coolants in Finnish Nuclear Power Plants." International Conference Water Chemistry in Nuclear Reactors System, Avignon, France.

Brooks BW and RGE Murray. 1981. "Nomenclature for *Micrococcus-radiodurans* and Other Radiation Resistant Cocci Deinococcaceae New Family and Deinococcus New-Genus Including 5 Species." *International Journal of Systematic Bacteriology* 31:339–360.

Cavallo JR. 2007. "Containment Coatings Adhesion Data Collection." Corrosion Control Consultants and Labs, Inc., NRC presentation June 19, 2007, U.S. Nuclear Regulatory Commission, Washington, D.C., ADAMS Accession #ML071840313.

Cloutier CR, A Alfantazi, and E Gyenge. 2007. "Physicochemical Properties of Alkaline Aqueous Sodium Metaborate Solutions." *Journal of Fuel Cell Science and Technology* 4:88–98.

Cole GM. 1994. *Assessment and Remediation of Petroleum Contaminated Sites.* CRC Press, Boca Raton, Florida.

Cookson LJ and K Pham. 1995. "Relative Tolerance of Twenty Basidiomycetes to Boric Acid." *Material und Organismen* (Berlin) 29(3):187–196.

Craig BD, and DB Anderson (editors). 1995. *Handbook of Corrosion Data*, ASM International, Materials Park, Ohio.

Cummins WE, MM Corletti, and TL Schulz. 2003. "Westinghouse AP1000 Advanced Passive Plant." Westinghouse Electric Company, LLC, Pittsburgh, Pennsylvania; paper 3235 presented in the *Proceedings of ICAPP '03*, Cordoba, Spain.

Dacquait F, C Andrieu, M Berger, J-L Bretelle, and A Rocher. 2002. "Corrosion Product Transfer in French PWRs during Shutdown." International Conference Water Chemistry in Nuclear Reactors System, paper 113, Avignon, France.

Dallman J, B Letellier, J Garcia, J Madrid, W Roesch, D Chen, K Howe, L Archuleta, F Sciacca, and BP Jain. 2006. *Integrated Chemical Effects Test Project: Consolidated Data Report and Test #1 - #5 Data Reports*. NUREG/CR-6914, Volumes 1-6, U.S. Nuclear Regulatory Commission, Washington, D.C. Available at: http://www.nrc.gov/reading-rm/doc-collections/nuregs/contract/cr6914/. Accessed 05/16/2008.

Davis JR (editor). 1999. *Corrosion of Aluminum and Aluminum Alloys*, ASM International, Materials Park, Ohio.

DOE. 1993. *DOE Fundamentals Handbook*, "Chemistry." Volume 1 of 2, DOE-HDBK-1015/1-93, U.S. Department of Energy, Washington, D.C.

DOE. 2004. Pages 200-204 of *DOE Hydrogen Program – 2004 Annual Progress Report*, U.S. Department of Energy, Washington, D.C. Available at: http://www.hydrogen.energy.gov/annual_progress04.html. Accessed 05/16/2008.

Dupont ME, NC Lyer, PS Lam, RL Sindelar, TE Skidmore, FR Utsch, and PE Zapp. 2001. *Degradation and Failure Characteristics of NPP Containment Protective Coating Systems (U) Interim Report No. 3*. WSRC-TR-2001-00067, Savannah River Technology Center, Aiken, South Carolina.

Eckert T. 2005. "OEM Unqualified Coatings Testing," presentation April 12-13, 2005, at Washington D.C. and Rockville, Maryland, Electric Power Research Institute, Palo Alto, California, ADAMS Accession # ML051100483.

El-Alaily NA and LS Ahmed. 2002. "Effects of Acid/Alkaline Strength, Temperature and Gamma-Irradiation on the Durability of Fibreglass." *Glass Technology* 43(2):80–88.

EPRI. 1999. "PWR Primary Water Chemistry Guidelines: Volumes 1 and 2." TR-105714-V1R4 and TR-105714-V2R4, Volumes 1 and 2, Rev. 4, Electric Power Research Institute, Palo Alto, California. Copyright © 1999. Electric Power Research Institute TR-105714-V1R4, PWR Primary Water Chemistry Guidelines: Vol. 1: Revision 4 and Electric Power Research Institute TR-105714-V2R4, PWR Primary Water Chemistry Guidelines: Vol. 2: Revision 4. Used with Permission. Available at: http://www.epriweb.com/public/TR-105714-V1R4.pdf and http://www.epriweb.com/public/TR-105714-V2R4.pdf). Accessed 05/16/2008.

Fellers B, J Barnette, J Stevens, and D Perkins. 2002. "Optimization of Reactor Coolant Shutdown Chemistry Practices for Crud Inventory Management." International Conference Water Chemistry in Nuclear Reactors System, paper 113, Avignon, France.

Frattini PL, J Blok, S Chauffriat, J Sawicki, and J Riddle. 2001. "Axial Offset Anomaly: Coupling PWR Primary Chemistry with Core Design." *Nuclear Energy* 40(2):123–135.

Fullerton A, T Fu, D Walker, and J Carneal. 2006. *Hydraulic Transport of Coating Debris*. NUREG/CR-6916, The Naval Surface Warfare Center, Carderock Division, West Bethesda, Maryland.

Ghosh AK, KJ Howe, AK Maji, BC Letellier, and RC Jones. 2007. "Head Loss Characteristics of a Fibrous Bed in a PWR Chemical Environment." *Nuclear Technology* 157:196–207.

Giannakopoulou F, C Haidouti, A Chronopoulou, and D Gasparatos. 2007. "Sorption Behavior of Cesium on Various Soils under Different pH Levels." *Journal of Hazardous Materials* 149:553–556.

Griess JC and AL Bacarella. 1971. "The Corrosion of Materials in Reactor Containment Spray Solutions." *Nuclear Technology* 10:546–555. See also JC Griess and AL Bacarella. 1969. *Design Considerations of Reactor Containment Spray Systems – part III. The Corrosion of Materials in Spray Solutions*. ORNL-TM-2412, Part III, Oak Ridge National Laboratory, Oak Ridge, Tennessee.

Guzonas D, and D Webb. 2002. *Adsorption of Boric Acid on Synthetic Fuel Crud Oxides*. 1003384 NP, Electric Power Research Institute, Palo Alto, California.

Hakem N, B Fourest, R Guillaumont, and N Marmier. 1996. "Sorption of Iodine and Cesium on Some Mineral Oxide Colloids." *Radiochimica Acta* 74:225–230.

Haq Z, GM Bancroft, WS Fyfe, G Bird, and VJ Lopata. 1980. "Sorption of Iodide on Copper." *Environmental Science and Technology* 14:1106–1110.

Hart GH. 2004. "A Short History of the Sump Clogging Issue and Analysis of the Problem." *Nuclear News*.

Hazelton RF. 1987. *Characteristics of Fuel Crud and Its Impact on Storage, Handling, and Shipment of Spent Fuel*. PNL-6273, Pacific Northwest Laboratory, Richland, Washington.

Henshaw J, JC McGurk, HE Sims, A Tuson, S Dickinson, and J Deshon. 2006a. "A Model of Chemistry and Thermal Hydraulics in PWR Fuel Crud Deposits." *Journal of Nuclear Materials* 353:1–11.

Henshaw J, JC McGuire, HE Sims, A Tuson, S Dickinson, and J Deshon. 2006b. "The Chemistry of Fuel Crud Deposits and Its Effect on AOA in PWR Plants." *International Conference on Water Chemistry of Nuclear Reactor Systems,* Jeju Island, Korea, ADAMS Accession #ML063390145.

Iler RK. 1979. *The Chemistry of Silica*. John Wiley & Sons, New York.

Jain V, L Yang, and K Chiang. 2004. *Chemical Speciation Using Thermodynamic Modeling During a Representative Loss-of-Coolant Accident Event*. Center for Nuclear Waste Regulatory Analyses (CWNRA) Report 2004-07 (Revision 1), Southwest Research Institute, San Antonio, Texas. Published as Appendix C to NUREG/CR-6873.

Jain V, X He, and YM Pan. 2005. *Corrosion Rate Measurements and Chemical Speciation of Corrosion Products Using Thermodynamic Modeling of Debris Components to Support GSI-191*. NUREG/CR-6873. U.S. Nuclear Regulatory Commission, Washington, D.C.

Johns RC, BC Letellier, KJ Howe, and AK Ghosh. 2005. *Small-Scale Experiments: Effects of Chemical Reactions on Debris-Bed Head Loss*. NUREG/CR-6868, US Nuclear Regulatory Commission, Washington, D.C.; also as LA-UR-03-6415, Los Alamos National Laboratory, Los Alamos, New Mexico.

Kabakchi SA, VN Shubin, and PI Dolin. 1967. "Influence of pH on Stationary Concentrations of the Radiolysis Products of Aqueous Oxygen Solutions." *High Energy Chemistry* 1:127-131.

Kelm M and E Bohnert. 2004. *A Kinetic Model for the Radiolysis of Chloride Brine, Its Sensitivity against Model Parameters and a Comparison with Experiments*. FZKA-6977, Institut für Nukleare Entsorgung, Karlsruhe, Germany.

Kashefi K and DR Lovley. 2003. "Extending the Upper Temperature Limit for Life." *Science* 301:934.

Klasky M, J Zhang, M Ding, B Letellier, D Chen, and K Howe. 2006. *Aluminum Chemistry in a Prototypical Post-Loss-of-Coolant-Accident." Pressurized-Water-Reactor Containment Environment*, NUREG/CR-6915, U.S. Nuclear Regulatory Commission, Washington, D.C.; also as LA-UR-05-4881, Los Alamos National Laboratory, Los Alamos, New Mexico.

Lagaly G. 2005. "Colloids." In: *Ullman's Encyclopedia of Industrial Chemistry*. Wiley-VCH GmbH & Co., KGaA, Weinheim, Germany.

Lagerblad B. 2001. *Leaching Performance of Concrete Based on Studies of Samples from Old Concrete Constructions*. SKB-TR-01-27, Svensk Kärnbränslehantering AB, Stockholm, Sweden.

Lagerblad B. 2006. *Carbon Dioxide Uptake During Concrete Life Cycle – State of the Art*. ISBN 91-976070-0-2/ISSN 0346-8240, Nordic Innovation Centre, Oslo, Norway. Available at: (http://www.nordicinnovation.net/_img/03018_carbon_dioxide_uptake_during_concrete_life_cycle_-_state_of_the_art.pdf. Accessed 05/16/2008.

Lanning DR. 2005. "FRAPCON-3 Corrosion Models for M5™and ZIRLO™ PWR Cladding." *American Nuclear Society Transactions* 93:759–760.

Li, Z, P Kepkay, K Lee, T King, MC Boufadel, and AD Venosa. 2007. "Effects of Chemical Dispersants and Mineral Fines on Crude Oil Dispersion in a Wave Tank under Breaking Waves." *Marine Pollution Bulletin* 54:983–993.

Lide DR (Editor). 2007. *CRC Handbook of Chemistry and Physics, Internet Version 2007*, 87th edition, Taylor and Francis, Boca Raton, Florida.

Linacre JK and WR Marsh. 1981. *The Radiation Chemistry of Heterogeneous and Homogeneous Nitrogen and Water Systems*. AERE-R-10027, Atomic Energy Research Establishment, Harwell, United Kingdom.

Litman R. 2006. *Evaluation of Integrated Chemical Effects Testing*, Appendix D, U.S. Nuclear Regulatory Commission, Washington, D.C., ADAMS Accession #ML063630498.

Liu, X and FJ Millero. 1999. "The Solubility of Iron Hydroxide in Sodium Chloride Solutions." *Geochimica et Cosmochimica Acta* 63:3487–3497.

Macdonald DD, and M Urquidi-Macdonald. 2006. Chapter 9, "The Electrochemistry of Nuclear Reactor Coolant Circuits." In Volume 5, *Electrochemical Engineering*, DD Macdonald and P Schmuki (editors), in *Encyclopedia of Electrochemistry,* AJ Bard and M Stratman (Editors), Wiley-VCH, Verlag GmbH & Co. KGaA, Weinheim, Germany.

MacLaren DC and MA White. 2003. "Cement: Its Chemistry and Properties." *Journal of Chemical Education* 80(6):623–635.

McMurry J, V Jain, X He, D Pickett, R Pabalan, and Y-M Pan. 2006. *GSI-191 PWR Sump Screen Blockage Chemical Effects Tests: Thermodynamic Simulations*. NUREG/CR-6912, U.S. Nuclear Regulatory Commission, Washington, D.C.

Moore RT. 2001. "Hot Fungi from Chernobyl." *Mycologist* 15:63–64.

Natesan K, and R Natarajan. 2006. *Survey on Leaching of Coatings Used in Nuclear Power Plants: Letter Report*. Argonne National Laboratory, Argonne, Illinois, ADAMS Accession #ML062560368.

Nies NP, and RW Hulbert. 1967. "Solubility Isotherms in the System Sodium Oxide-Boric Oxide-Water Revised Solubility-Temperature Curves of Boric Acid, Borax, Sodium Pentaborate, and Sodium Metaborate." *Journal of Chemical and Engineering Data* 12(3):303–313.

Noshita K, T Nishi, T Yoshida, H Fujihara, N Saito, and S Tanaka. 2001. "Categorization of Cement Hydrates by Radionuclide Sorption Mechanism." In: *Scientific Basis for Nuclear Waste Management*, Vol. 663, KP Hart and GR Lumpkin (Editors), Materials Research Society, Warrendale, Pennsylvania.

NRC. 2004a. *Potential Impact of Debris Blockage on Emergency Recirculation during Design Basis Accidents at Pressurized-Water Reactors*. NRC Generic Letter 2004-02, U.S. Nuclear Regulatory Commission, Washington, D.C., ADAMS Accession #ML042360586.

NRC. 2004b. "Note to Editors: NRC Issues Preliminary Risk Analysis of the Combined Safety Issues at Davis-Besse." *NRC News*, No. 04-117, U.S. Nuclear Regulatory Commission, Washington, D.C. Available at: http://www.nrc.gov/reading-rm/doc-collections/news/2004/04-117.html. Accessed 05/16/2008.

NRC. 2007. *Safety Evaluation by the Office of Nuclear Reactor Regulation Topical Report (TR) WCAP-16406-P, Revision 1.* "Evaluation of Downstream Sump Debris Effects in Support of GSI-191." Pressurized Water Reactor Owners Group Project No. 694, U.S. Nuclear Regulatory Commission, Washington, D.C., ADAMS Accession #ML073520295.

NSF International Standard/American National Standard, NSF/ANSI 61-2007a, "Drinking water system components; Health effects".

NSF 61 test report for Amerlock 400 DCC Number/Tracking ID PM01488 dated March 12, 2008.

NSF 61 test report for Amercoat 90HS Tracking ID PM00111 dated October 27, 2003

Nuclear Engineering International. 2006. *World Nuclear Industry Handbook*. Wilmington Publishing, Sidcup, Kent, United Kingdom.

Oconee. 2007. "Oconee Nuclear Station Corrective Actions for Generic Letter 2004-02." Oconee Nuclear Power Station, Seneca, South Carolina.

Owens EH, and K Lee. 2003. "Interaction of Oil and Mineral Fines on Shorelines: Review and Assessment." *Marine Pollution Bulletin* 47:397–405.

Pade C, and M Guimaraes. 2007. "The CO_2 Uptake of Concrete in a 100 Year Perspective." *Cement and Concrete Research* 37:1348–1356.

Park J-H, OK Chopra, K Natesan, and WJ Shack. 2005. *Boric Acid Corrosion of Light Water Reactor Pressure Vessel Materials*. NUREG/CR-6875, U.S. Nuclear Regulatory Commission, Washington, D.C., ADAMS Accession #ML052360563.

Parker BJ, RG Veness, and CS Evans. 1999. "A Biochemical Mechanism Whereby *Paecilomyces variotii* Can Overcome the Toxicity of the Wood Protectant, Borate." *Enzyme and Microbial Technology* 24:402–406.

Parrott LJ and DC Killoh. 1989. "Carbonation in a 36 Year Old, In-Situ Concrete." *Cement and Concrete Research* 19:649–656.

Pastina B, and JA LaVerne. 2001. "Effect of Molecular Hydrogen on Hydrogen Peroxide in Water Radiolysis." *Journal of Physical Chemistry A* 105:9316–9322.

Pikuta EV, RB Hoover, and J Tang. 2007. "Microbial Extremophiles at the Limits of Life." *Critical Reviews in Microbiology* 33:183–209.

Pinney SG. 1988. "Correctly Select Tank Linings for Immersion Service." *Chemical Engineering Progress* 94(12):65–68.

Plodinec MJ, GG Wicks, and NE Bibler. 1982. *An Assessment of Savannah River Borosilicate Glass in the Repository Environment*. DP-1629, Savannah River Laboratory, Aiken, South Carolina.

Polley MV and ME Pick. 1986. "Paper 21. Iron, Nickel, and Chromium Mass Balances in Westinghouse PWR Primary Circuits." In: *Water Chemistry of Nuclear Reactor Systems 4*. pp 63–70 in Volume 1. British Nuclear Energy Society, London, United Kingdom.

Porter F. 1991. *Zinc Handbook: Properties, Processing, and Use in Design,* Dekker Mechanical Engineering, p 112, CRC Press, Cleveland, Ohio. Available at: http://books.google.com/books?id=LCixI0TZ-D4C&printsec=frontcover&dq=anodic+reversal+zinc+steel#PPA112,M1). Accessed 05/16/2008.

PSE. 2007. "Ongoing Research in Aging and Degradation of Coatings." In: PSE Perspectives, Winter 2007, Electric Power Research Institute, Palo Alto, California. Used with permission and

copyright approval, May 14, 2008, to the U.S. Nuclear Regulatory Commission from the Electric Power Research Institute, Palo Alto, California.

Reid RD, KR Crytzer, AE Lane, and TS Andreychek. 2006. *Evaluation of Alternative Emergency Core Cooling System Buffering Agents*. WCAP-16596-NP, Rev. 0, Westinghouse Electric Company, Pittsburgh, Pennsylvania.

Reid RD, KR Crytzer, and AE Lane. 2007. *Evaluation of Additional Inputs to the WCAP-16530-NP Chemical Model*. WCAP-16785-NP, Rev. 0, Westinghouse Electric Company, Pittsburgh, Pennsylvania.

Roberts K, and SM Siegel. 1967. "Experimental Microbiology of Saturated Salt Solutions and Other Harsh Environments. 3. Growth of Salt-Tolerant *Penicillium notatum* in Boron-Rich Media." *Plant Physiology* 42(9):1215–1218.

Roberts WL, TJ Campbell, GR Rapp, and WE Wilson. 1990. *Encyclopedia of Minerals*, 2nd Edition. Van Nostrand Reinhold, New York.

Romanovskaya VA, PV Rokitko, AN Mikheev, NI Gushcha, YR Malashenko, and NA Chernaya. 2002. "The Effect of Gamma-Radiation and Desiccation on the Viability of the Soil Bacteria Isolated from the Alienated Zone around the Chernobyl Nuclear Power Plant." *Mikrobiologiya* 71:705–712.

Sandler YL. 1979. "Structure of PWR Primary Corrosion Products." *Corrosion* 35(5):205–208.

Sarro MI, AM Garcia, and DA Moreno. 2005. "Biofilm Formation in Spent Nuclear Fuel Pools and Bioremediation of Radioactive Water." *International Microbiology* 8:223–230.

Sato Y, I Inami, N Suzuki, A Fujimori, and H Wille. 2000. "Full System Decontamination for Dose Reduction at the Preventive Maintenance Work of the Reactor Core Internals." In: *Technologies for Improving Current and Future Light Water Reactor Operation and Maintenance: Development on the Basis of Experience*, pp 91–105. IAEA-TECDOC-1175, International Atomic Energy Agency, Vienna, Austria.

Sawicki JA. 2002. "Nuclear Chemistry Model of Borated Fuel Crud." International Conference on Water Chemistry in Nuclear Reactor Systems, Avignon, France.

Schmid R, and VN Sapunov. 1982. *Non-Formal Kinetics.* Verlag Chemie, Deerfield Beach, Florida.

Shaffer CJ, MT Leonard, BC Letellier, DV Rao, AK Maji, K Howe, A Ghosh, J Garcia, WA Roesch, and JD Madrid. 2005. *GSI-191: Experimental Studies of Loss-of-Coolant-Accident-Generated Debris Accumulation and Head Loss with Emphasis on the Effects of Calcium Silicate Insulation*. NUREG/CR-6874, U.S. Nuclear Regulatory Commission, Washington, D.C.; also as LA-UR-04-1227, Los Alamos National Laboratory, Los Alamos, New Mexico.

Shin-Min S, C-S Ho, Y-S Song, and J-P Lin. 1999. "Kinetics of the Reaction of $Ca(OH)_2$ with CO_2 at Low Temperature." *Industrial and Engineering Chemistry Research* 38:1316–1322.

Shults WD. 1979. Letter (no title, about analytical results of Three Mile Island containment water) to JA Daniel, GPU Service Corporation, Parsipanny, New York. Oak Ridge National Laboratory, Oak Ridge, Tennessee.

Sindelar RL, ME Dupont, NC Iyer, PS Lam, TE Skidmore, FR Utsch, and PE Zapp. 2000. *Degradation and Failure Characteristics of NPP Containment Protective Coating Systems*. WSRC-TR-2000-00079, Savannah River Technology Center, Aiken, South Carolina.

Slegers PA, and PG Rouxhet. 1976. "Carbonation of the Hydration Products of Tricalcium Silicate." *Cement and Concrete Research* 6:381–388.

Tagirov B, J Schott, J-C Harrichoury, and J Escalier. 2004. "Experimental Study of the Stability of Aluminate-Borate Complexes in Hydrothermal Solutions." *Geochimica et Cosmochimica Acta* 68(6):1333–1345.

TXU Power to US Nuclear Regulatory Commission October 20, 2006. "Comanche Peak Steam Electric Station (CPSES) Docket Nos. 50-445 and 50-446 Transmittal of Report on TXU Power Sponsored Coatings Performance Test. ADAMS ML070230384

Tregoning RL (U.S. Nuclear Regulatory Commission), JA Apps, (Lawrence Berkeley National Laboratory), W Chen (Dow Chemical Company), CH Delegard (Pacific Northwest National Laboratory), R Litman (Radiochemistry Laboratory Basics), and DD Macdonald (Penn State University). 2007. *Phenomena Identification and Ranking Table Evaluation of Chemical Effects Associated with Generic Safety Issue 191*. NUREG-1918, Nuclear Regulatory Commission, Washington, D.C.

Troutner VH. 1957. *Uniform Aqueous Corrosion of Aluminum – Effects of Various Ions*. HW-51033, Hanford Atomic Products Operation, Richland, Washington.

Tsai, C-H and S-T Lin. 1999. "Disinfection of Hospital Waste Sludge Using Hypochlorite and Chlorine Dioxide," *Journal of Applied Microbiology* 86:827-833.

Uhlig HH. 1948. *The Corrosion Handbook*. John Wiley & Sons, Inc., New York.

Upsher FJ. 1984. "A Comparison of Fungi on Materials at Jungle and Cleared Sites of a Hot-Wet Tropical Exposure Unit." *International Biodeterioration* 20:157162.

Viallis-Terrisse H, A Nonat, J-C Petit, C Landesman, and C Richet. 2002. "Specific Interaction of Cesium with the Surface of Calcium Silicate Hydrates." *Radiochimica Acta* 90:699–704.

Wainwright M, TA Ali, and F Barakah. 1993. "A Review of the Role of Oligotrophic Microorganisms in Biodeterioration." *International Biodeterioration and Biodegradation* 31:1–13.

Weber CF, EC Beahm, and TS Kress. 1992. *Models of Iodine Behavior in Reactor Containments*. ORNL/TM-12202, Oak Ridge National Laboratory, Oak Ridge, Tennessee.

Wefers K and C Misra. 1987. *Oxides and Hydroxides of Aluminum*. Alcoa Technical Paper No. 19, revised, Alcoa Laboratories, Alcoa Center, Pennsylvania.

Weldon DG. 2002. *Failure Analysis of Paints and Coatings.* John Wiley and Sons, New York.

Wilson W, and RJ Comstock. 1999. "Potential Impacts of Crud Deposits on Fuel Rod Behavior on High Powered PWR Fuel Rods." In: *Water Chemistry and Corrosion Control of Cladding and Primary Circuit Components – Proceedings of a Technical Committee Meeting*. IAEA-TECDOC-1128 International Atomic Energy Agency, Vienna, Austria.

Wren JC, JM Ball, and GA Glowa. 1999. "The Interaction of Iodine with Organic Material in Containment." *Nuclear Technology* 125:337–362.

Wren JC, DJ Jobe, GG Sanipelli, and JM Ball. 2000a. "Dissolution of Organic Solvents from Painted Surfaces into Water." *Canadian Journal of Chemistry* 78:464–473.

Wren JC, and GA Glowa. 2000b. "A Simplified Kinetic Model for the Degradation of 2-Butanone in Aerated Aqueous Solutions Under Steady-State Gamma-Radiolysis." *Radiation Physics and Chemistry* 58:341–356.

Xiangke W, D Wenming, G Zhijun, G Huibin, D Jinzhou, and T Zuyi. 2001. "Adsorption and Desorption of Radioiodine in a Calcareous Soil." *Adsorption Science and Technology* 19(9):711–719.

Ye Q, Y Roh, SL Carroll, B Blair, J Zhou, CL Zhang, and MW Fields. 2004. "Alkaline Anaerobic Respiration: Isolation and Characterization of a Novel Alkaliphilic and Metal-Reducing Bacterium." *Applied and Environmental Microbiology* 70:5595–5602.

Zhang J, M Klasky, M Ding, D Chen, J Dallman, and B Letellier. 2005. "Preliminary Analysis on Chemical Compositions Following a Loss-of-Coolant Accident." *Transactions of the American Nuclear Society* 93:312–313.

Zhang XG. 1996. *Corrosion and Electrochemistry of Zinc*. Plenum Publishing Corp., New York.

Zhdanova NN, VA Zakharchenko, VV Vember, and LT Nakonechnaya. 2000. "Fungi from Chernobyl: Mycobiota of the Inner Regions of the Containment Structures of the Damaged Nuclear Reactor." *Mycological Research* 104:1421–1426.